

Bristol Composites Institute

# POSTGRADUATE RESEARCH SYMPOSIUM

March 2024 University of Bristol

POSTER BOOKLET



Photo credits: cover: Jan Maurycy Uszko



EPSRC Centre for Doctoral  
Training in Composites Science,  
Engineering and Manufacturing



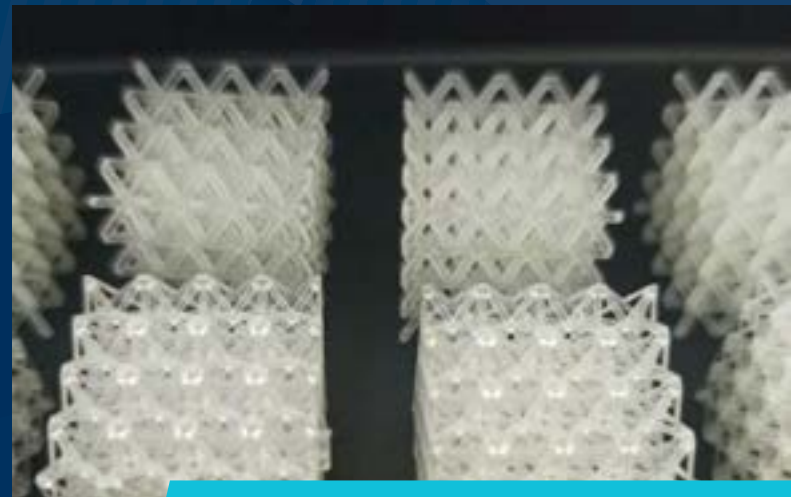
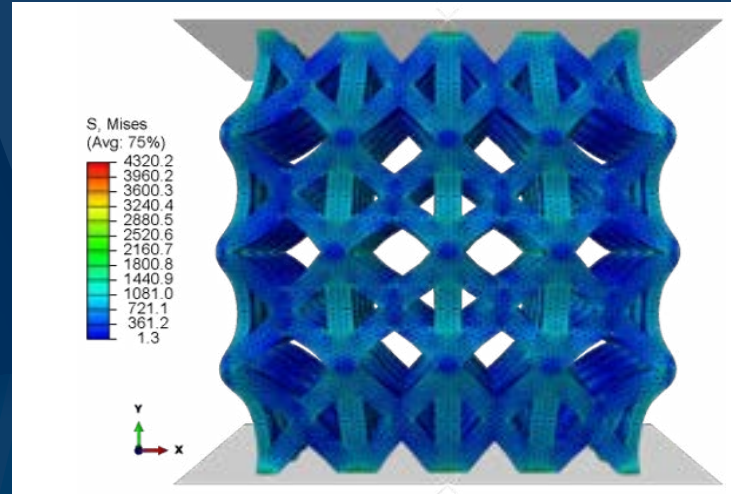
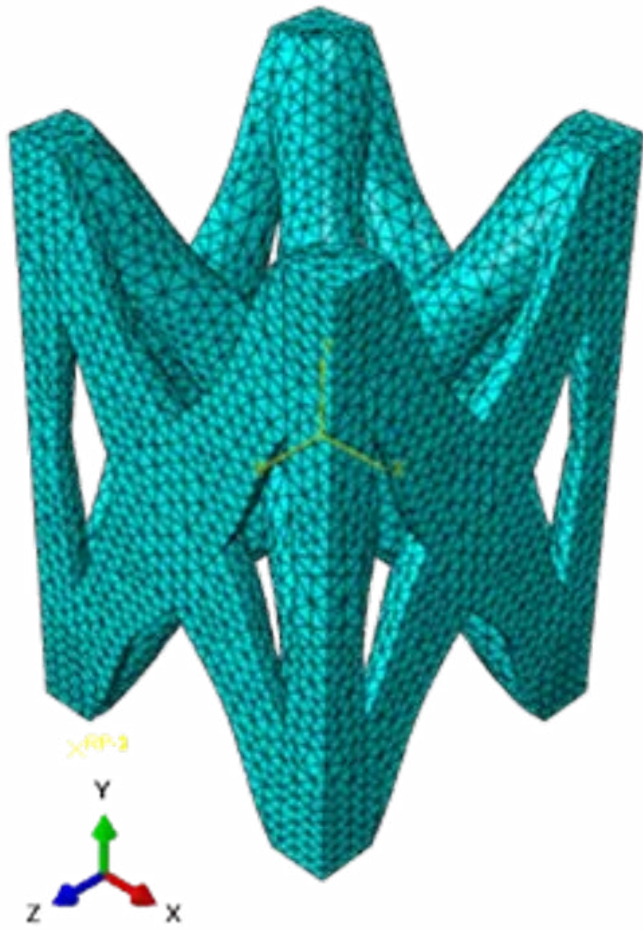
EPSRC Centre for Doctoral Training  
in Advanced Composites  
for Innovation and Science



Bristol Composites Institute



Engineering and  
Physical Sciences  
Research Council



# MATERIALS



# Recycling of FRP wind blade waste material in concrete

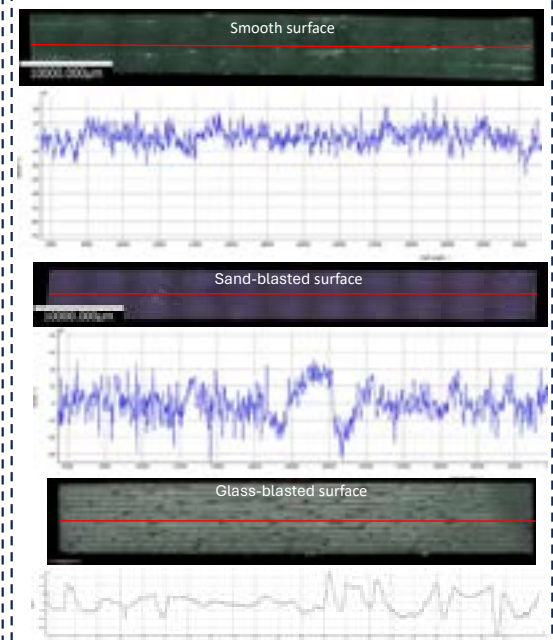
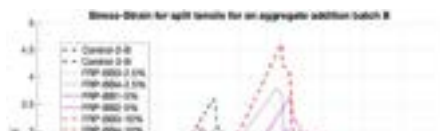
Meiran Abdo, Eleni Toumpanaki, Andrea Diambra, Lawrence C. Bank

**Aim:** The project evaluates the mechanical performance of recycled wind blade waste in structural applications, considering variables such as **FRP needle geometry** and aggregate replacement ratio.



**1. Results:** The results suggest that incorporating FRP Needles into concrete **increases** splitting tensile strength for both batches. However, a **slight decrease in compressive strength** was observed in **batch A**, while **batch B** gradually **increased** compressive strength with increasing FRP needle content.

**2. Surface Analysis:** The **Alicona** machine was utilised to obtain the surface roughness measurements for the FRP Needles with three different surface conditions: smooth, sand-blasted, and glass-blasted

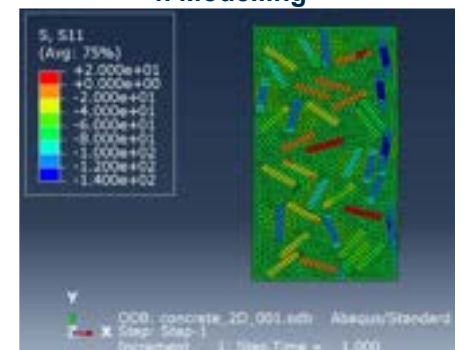


### 3. Pull-out

The **pull-out** test was conducted to determine the **Bond Strength** between fibre-reinforced polymer (FRP) needles and concrete for different needles' surface roughness and bond length.



### 4. Modelling





# Potential Environmental Impact of Mycelium Composites on African Communities

S. Akromah, J. Rowlandson, N. Chandarana, S. J. Eichhorn

1.

## Goal & Scope

- i. To identify the environmental hotspots of mycelium composite (MC) production (i.e., processes that contribute significantly to overall impact).
- ii. To assess the life cycle impact of MCs as compared to concrete within the context of Africa.

## Relevance

Pre-emptively addressing the potential ecological impact of MCs is crucial, particularly for the Global South, as it can lead to cost savings while preserving the ecosystems.

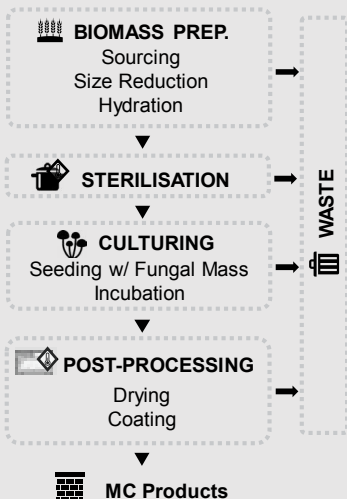
## Method

**Life-Cycle Assessment (LCA)** – A systematic method used to measure environmental impact from

- i. **Cradle-to-Gate**  
Extraction > Manufacture
- ii. **Cradle-to-Grave**  
Extraction > Disposal

2.

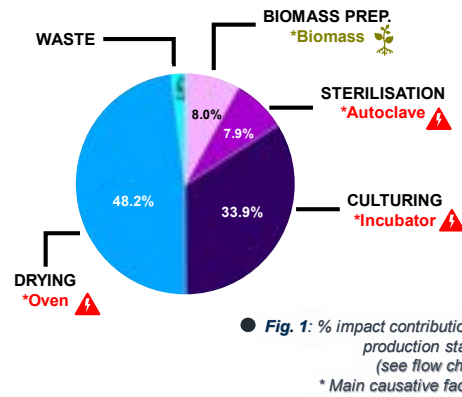
## The MC Manufacturing Process



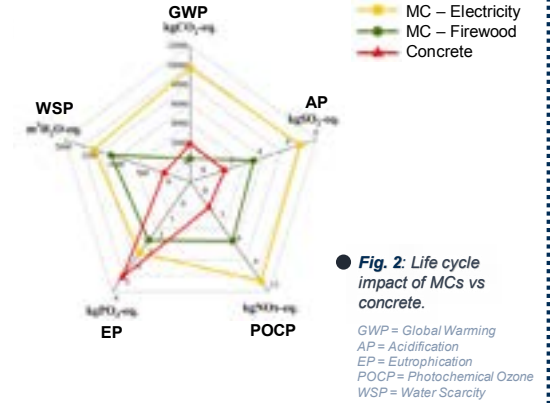
3.

## RESULTS

### Environmental Hotspots (Cradle-to-Gate)



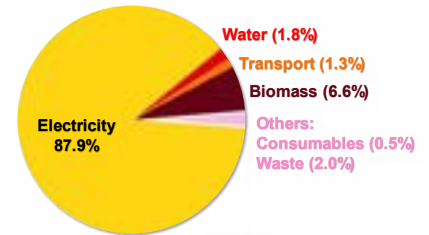
### Life-Cycle Impact (Cradle-to-Grave)



## Key Findings

Total footprint of MCs is mainly influenced by:

- ⚠️ **Electricity** → Heavily used to power equipment
- 🌱 **Biomass** → Main contributor to EP and WSP due to fertilisers and water for cultivation
- 💧 **Water** → Fungi require a lot of water for growth
- 🚚 **Transport** → Impact depends on travel distance & mode

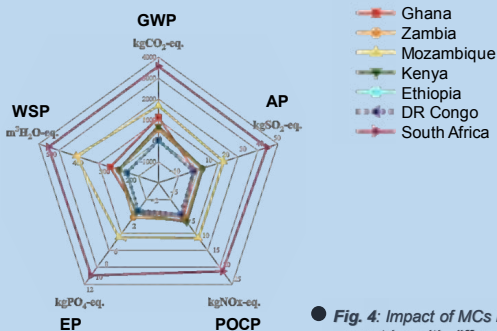


4.

## RECOMMENDATIONS

- ✗ ✗
  - Cost-effective greener fuel alternatives (e.g., wood)
    - Energy-efficient equipment
  - Avoid expendable machinery if possible (e.g., incubators)

(Especially in fossil-fuel dependent countries)



- ✗ ✗ ✓
  - Prioritise lignocellulosic biomass
  - Source biomass from post-harvest, agro-industrial, storage, and post-consumer waste
  - Source biomass from other industrial waste (e.g., wood from construction)
- ✗ ✓
  - Harvest rainwater
- Recycle wastewater from MC production
- ✗ ✓
  - Local sourcing
  - Fuel-efficient vehicles
- Lorries & cargo ships for long-haul distribution



# Hilbert Fractal Acoustic Metamaterials



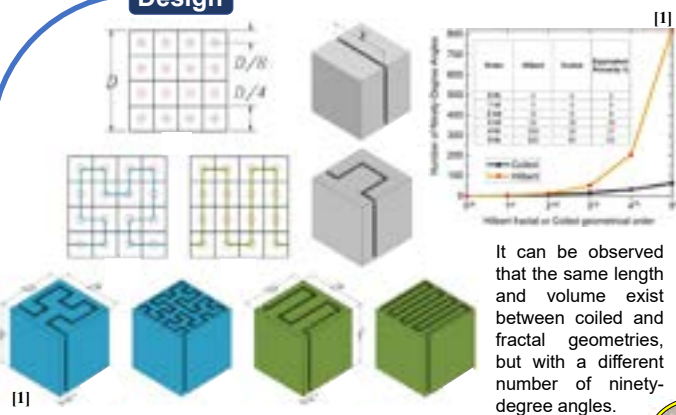
Gianni Comandini, Valeska P. Ting, Fabrizio Scarpa

## Introduction

Sound insulation, particularly within the low-mid frequency range, has long been a complex challenge for engineers and scientists. Traditional methods, employing dense and thick materials, can face critical limitations due to their weight, volume, and space occupancy. The need for bulky layers to manage low-mid frequency sounds often does not keep pace with modern demands for lightweight and space-efficient solutions. These challenges have pushed forward the exploration of new approaches to sound control. A viable solution is offered by acoustic metamaterials, where coiled geometries and, lately, fractal patterns have emerged as effective architectures. Unlike conventional materials, acoustic metamaterials based on fractal patterns can offer precise control over sound waves with relatively low weight and compact dimensions, even in the difficult low-mid frequency spectra.



## Design



## Working Mechanisms

An open-open resonator is used to predict the absorption peaks in the frequency spectrum.

$$f = \frac{c}{2} \sqrt{\left(\frac{l^2}{X^2} + \frac{j^2}{Y^2} + \frac{k^2}{Z^2}\right)}$$

AC

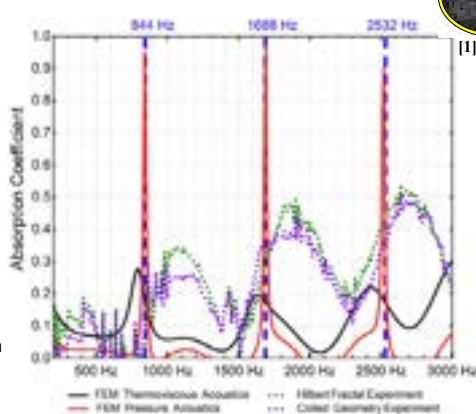
An open-closed resonator is used to forecast the transmission loss peak positions in the frequency domain.

$$f = \frac{rc}{4(L + \Delta L)}$$

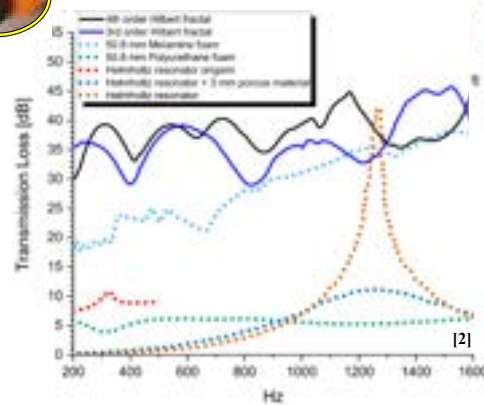
TL

Comparative study of absorption behaviours in Hilbert and coiled geometries via two distinct simulation techniques.

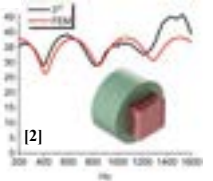
Thermoviscous dissipation plays a pivotal role in the phenomenon of acoustic absorption. The phenomenon is linked to the conversion of sound energy into heat within the used medium.



## Absorption Coefficient



## Transmission Loss



Comparative analysis of transmission loss in various materials of identical thickness using third and fourth-order Hilbert fractal structures.

## Conclusions

- Coiled and Hilbert geometries yield similar absorption coefficients in the investigated frequency range
- Absorption peak positions can be determined using an open-open resonator model
- Transmission loss peak positions can be predicted with an open-closed resonator model

## References

- [1] Comandini, Gianni, et al. "Sound absorption in Hilbert fractal and coiled acoustic metamaterials." *Applied Physics Letters*, doi.org/10.1063/5.0079531 (2022).
- [2] Comandini, Gianni, et al. "Acoustic Transmission Loss in Hilbert Fractal Metamaterials." *Scientific Reports*, doi.org/10.1038/s41598-023-43646-1 (2023).



# Advanced High-Fidelity Modelling of Woven Composites

Ruggero Filippone, Dr. Bassam El Said, Dr. Adam Thompson, Dr. Peter Foster and Prof. Stephen Hallett

This study focuses on advancing the modelling capabilities for meso-scale damage analysis in woven textile composites. An Advanced High-Fidelity Model (AHFM) has been developed to explore the nonlinear behavior resulting from debonding failures following the redistribution of stress and strain and to characterize the mechanical behavior of this class of composites. Exploiting the fabric compaction algorithm of *SimTex*, a *co-penetration preventing algorithm* has been performed to generate nested yarn volumes. This enables the creation of an enhanced realistic representation of the *Representative Unite Cell (RUC)* through a dedicated algorithm that uses structured mesh. Moreover, cohesive elements with finite thickness has been adopted into the interface regions to investigate how the stress and strain state in these areas trigger debonding defects leading to a softening of the material. To validate the model, a comparison against experimental results of a *2x2 Twill Woven fabric* has been carried out. Finally, a study of cohesive element properties and a comparison against voxel mesh model have been conducted.

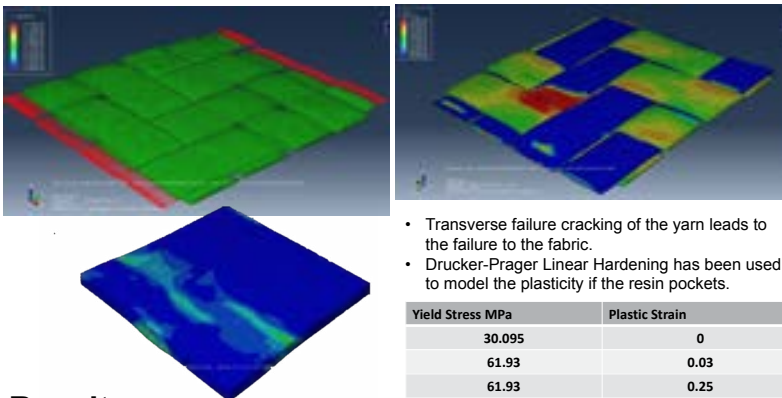
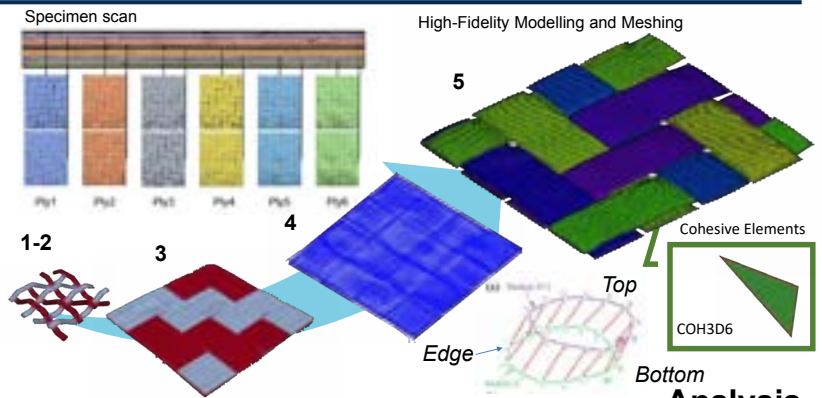
## Advanced H-F Modelling

### Main Steps:

1. Geometry and fabric architecture identification from the specimen scan.
2. SimTex: Compaction simulation of the RUC the Secions.csv and Nodes.csv (Fig.a)
3. Co-Penetration algorithm: It detects intersections and co-penetrations between yarns and subsequently remodel the data to ensure that they do not penetrate each other.
4. High-Fidelity Modelling: the Volume of the yarns and matrix are generated
5. Meshing: Structured mesh and Cohesive elements generation.

### Co-Penetration Algorithm

- The algorithm describes the yarns as splines generated by constrained nodes.
- For each combination of two splines, it checks the points in x-y projection) where the paths of different yarns cross each other. The algorithm assesses yarn positions (top, bottom, or edge) and relative z-coordinates of intersection points to accurately identify co-penetrated segments.
- When co-penetration is detected, the algorithm adjusts the positions of boundary nodes accordingly. It calculates new positions based on the midpoint of the intersection points and moves the boundary nodes to resolve the co-penetration while maintaining the integrity of the fabric structure.



An explicit FEA has been run using CDM for the yarn and cohesive elements. Mass Scale used 1E-06 times the material density.

### Boundary Conditions:

- An exponential ramp of velocity in y (*weft*) direction of the yarns to simulate a tensile test, on the both of sides. Final Velocity = 0.15 mm/s

### Mechanical Properties

- Constant Volume Fraction:  $V_f = 0.71$
- Chamis criterion to homogenize the yarns has been used.
- The material used for the fabric is Solvay's SolvaLite™ 710-1-38%-12KT700-2X2-400-1250g prepreg.

### Continuum Damage Model

- Yarn: Transverse failure cracking

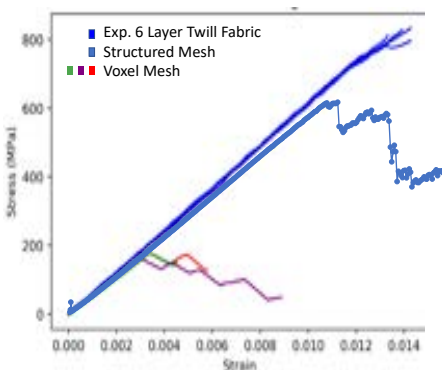
$$\left(\frac{\sigma_T}{S_T - \mu_T \sigma_N}\right)^2 + \left(\frac{\sigma_L}{S_L - \mu_L \sigma_N}\right)^2 = 1$$

- Cohesive: Mixed mode

Initiation of debonding and degradation equations:

$$\sqrt{\left(\frac{\sigma_{I,II}}{S_{I,II}}\right)^2 + \left(\frac{\sigma_{I,II}}{S_{I,II}}\right)^2} = 1$$

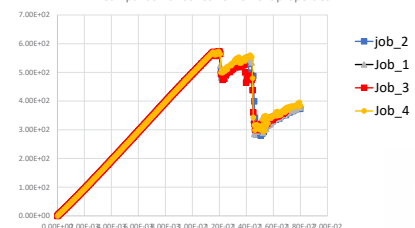
## Results



- The conformal mesh model exhibits enhanced accuracy (of more than 200%) in assessing the stiffness and the strength of the fabric in contrast to the voxel mesh approach.
- The deviation in stiffness observed between the experimental outcomes and the proposed High-Fidelity model may be ascribed to the absence of periodic boundary conditions (BCs) and the absence of the other layers.
- Given the flat geometry of the fabric, the characteristics of the cohesive elements exert minimal influence on fabric failure. The slope of the stress-strain curve remains unaltered, with a discernible decline indicating yarn failure.

	Job_1	Job_2	Job_3	Job_4
$G_{IC}$	0.15	0.15	0.15	0.3
$G_{IIC}$	1.002	0.9	0.8	1.1
$\sigma_I^{MAX}$	50	50	40	70
$\sigma_{II}^{MAX}$	90	70	50	100

Comparison of Cohesive Element properties







# Investigation into testing approaches for material characterisation of filament-wound components for hydrogen storage

## Composite pressure vessel testing

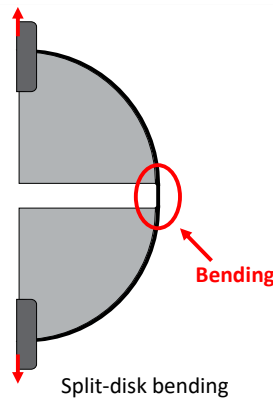
- Most hydrogen pressure vessels today are manufactured using filament wound composite material for their shells to carry the high loads from the pressurized gas.
- Flat coupon tests and whole vessel burst tests are the most common procedures seen in a vessel's design cycle.
- Split-disk testing is a method used for testing ring structures but is not used as commonly by pressure vessel manufacturers.
- **Question:** what is the best way to characterize filament wound material?



Ability composites, Composite overwrapped pressure vessels (COPV), 2014



Flat panel, Y. K. Ökten 2022, MSc Thesis, Middle East Technical University

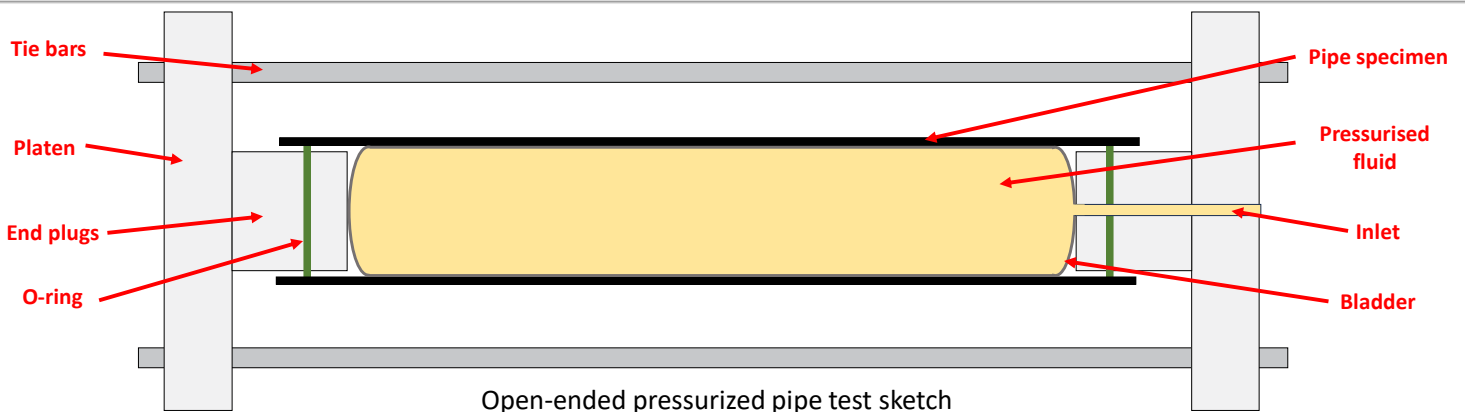


## Challenges of current methods for material characterisation

- Flat coupons are challenging to manufacture by filament winding and unrepresentative of the final manufactured vessel, therefore standard material characterisation approaches, such as ASTM D3039 or ISO-527, are not entirely appropriate.
- The split-disk method induces bending in the ring, therefore measuring the *apparent* tensile strength of the material, not its true tensile strength.

## Open-ended pipe testing

- Open-ended pipe testing is a method that internally pressurises a pipe without any axial constraints. The pipe can deform freely which results in no axial stresses, only pure hoop stress.
- This stress state allows the tensile properties of the material to be measured using a hoop wound pipe.
- Open-ended pipe testing has been demonstrated in literature [1-3], but the methodology has not been standardised.
- The intention of this research is to design a testing methodology based on internal pressurisation that can provide material properties directly from filament wound parts.
- This will improve the accuracy of current design methods, leading to lighter and lower cost pressure vessels.



## References

- [1] D. Hull, *et al*, "Failure of glass/polyester filament wound pipe" (1978)  
 [2] P. D. Soden, *et al*, "Influence of Winding Angle on Strength and Deformation of Filament-Wound Composite Tubes Subjected to Uniaxial and Biaxial Loads" (1993)

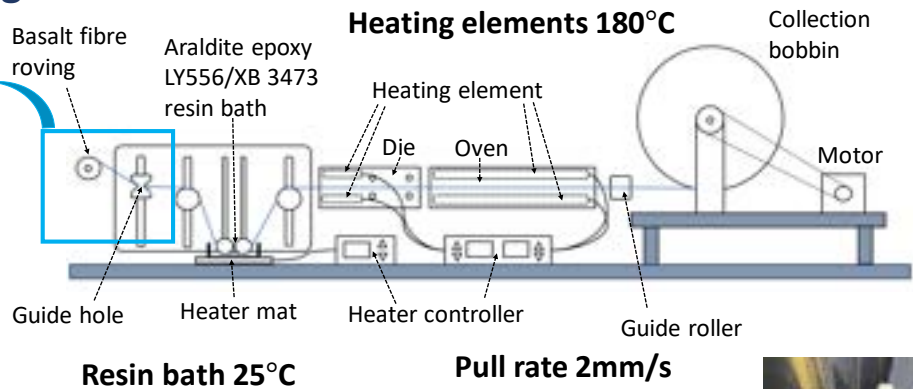
# Pultrusion of basalt fibre composite rods: Towards more sustainable composites for compression

Eleni Georgiou<sup>1</sup>, Gustavo Quino<sup>1,2</sup>, Ian Hamerton<sup>1</sup>, Richard S. Trask<sup>1</sup>

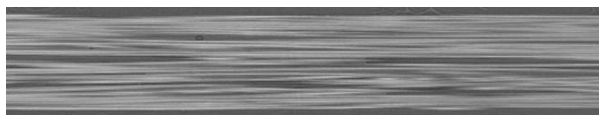
<sup>1</sup>Bristol Composites Institute, University of Bristol <sup>2</sup>Department of Aeronautics, Imperial College London

Continuous fibre reinforced polymers (FRPs) have become increasingly more popular for advanced structural applications in the aerospace, wind energy, marine and automotive sectors. However, longitudinal compression failure is a design limiting factor, with compression strength being up to 60% lower than the tensile strength for a given composite material [1]. With compressive loads arising in structures intentionally and otherwise, the safety margins accounted for at the design stages often result in oversized and inefficient structures [2]. In this study, we consider the manufacture of natural fibre pultruded rods which will be used to fabricate a hierarchical ply-level structure to improve the compressive performance of sustainable constructs. Critically to this investigation, resin-bath pultrusion facilitates the manufacture of composites with a high degree of fibre alignment.

## 1. Pultrusion and Imaging

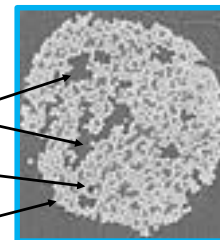


- Pultruded basalt/epoxy composite rods ( $\phi 0.8\text{mm}$ )
- Pultrusion = continuous + cost-efficient method for constant cross-section profiles
- Exploring the influence of various parameters upon material quality



2D orthogonal slice of basalt/epoxy pultruded rod

Resin rich zones  
Voids (black spots)  
Basalt fibre

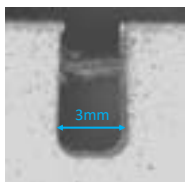


CT imaging

## 2. Compression Testing

Challenges with uniaxial compression tests:

- Stress concentrations at grips
- Need to avoid global buckling
- High variability in results



To ease these challenges, the compression side of a PMMA beam under bending was used to test the basalt composite rods [3].

- Mean failure strain  $-1.8\% \pm 0.37$

## 3. Future Work

Short term:

- Improve field of view of digital image correlation (DIC) cameras
- Improve manufacturing quality of rods
- Explore the effect of resin modification on the compressive strength

Long term:

- Explore effect of different cross-sections on compressive strength
- Consider interlocking of rods within sandwich ply structure for improved compressive performance



## References

- [1] N.A. Fleck, "Compressive failure of fiber composites". *Advances in Applied Mechanics*, Vol. 33, pp. 43-117, 1997  
 [2] G. Idarraga, M. Jalalvand, M. Fotouhi, J. Meza, and M. R. Wisnom, "Gradual failure in high-performance unidirectional thin-ply carbon/glass hybrid composites under bending", *Compos. Struct.*, 2021  
 [3] Quino, G et al., 2022, "Design of a bending experiment for mechanical characterisation of pultruded rods under compression" - Proceedings of the 20<sup>th</sup> European Conference on Composite Materials

# Cryogenic Thermal Shock of Epoxy Nanocomposites

James Griffith<sup>a</sup>, Dr. Karthik Ram Ramakrishnan<sup>a, b</sup>, Dr. Marcus Walls-Bruck<sup>b</sup>, Dr. Sebastien Rochat<sup>c</sup>, Prof. Valeska Ting<sup>a</sup>, Prof. Ian Hamerton<sup>a, b</sup>

## Liquid Hydrogen (LH<sub>2</sub>) for Civil Aviation

Liquid hydrogen (LH<sub>2</sub>) is hydrogen gas cooled down to **20 K (-253°C)**. It is widely considered the best zero carbon emission alternative to kerosene to service the majority of the aircraft market, with a **better payload and range** than:

- Batteries, which have low gravimetric energy efficiency
- Gaseous H<sub>2</sub>, which requires a larger tank mass for lower density and higher pressure storage
- Ammonia, which has environmental concerns and high fuel system mass

However, there are numerous challenges to overcome, with the Aerospace Technology Institutes 2022 Technology Strategy stating "The biggest research and technology challenges concern the safe storage and use of cryogenic hydrogen as a fuel on aircraft..."<sup>1</sup>

## LH<sub>2</sub> Storage Challenges

While composite tanks offer a predicted 43-47% mass saving over metallic tanks, which can translate to considerable lifelong cost savings of \$2000/kg<sup>2</sup>, carbon fibre reinforced polymers (CFRP) are susceptible to matrix microcracking in cryogenic environments.

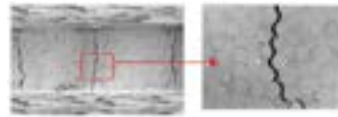


Figure 1: Microcracking in composites due to transverse stress<sup>3</sup>

This can lead to:

- Increasing LH<sub>2</sub> and H<sub>2</sub> permeation
- Decrease in tank stability
- Potential delamination or tank rupture if the LH<sub>2</sub> in cracks boils off during thermal cycling

## Causes of Cryogenic Matrix Microcracking

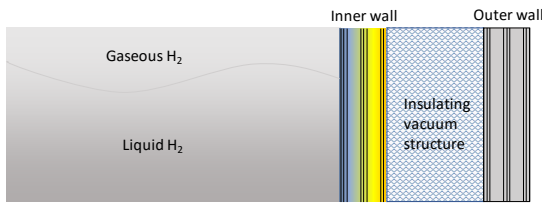


Figure 2: Schematic of inner wall CFRP thermal shock

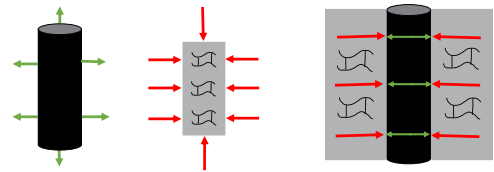


Figure 3: Co-efficient of thermal expansion (CTE) mismatch in constituents

Thermal shock of the composite material through exposure to cryogen

Temperature gradient across material

Build up of transient residual stresses

Micro-cracking

Build-up of compressive stress at the fibre-matrix interface

Opposing expansion and contraction of constituents

Constituent CTE Mismatch<sup>4</sup>

## Research Questions

1. Without the issue of CTE mismatch, will microcracking occur in the epoxy matrix alone due to thermal shock from cryogenic cycling?
2. Can microcracking be prevented by matrix toughening and how do the physical properties of the matrix change during thermal cycling?

## Results

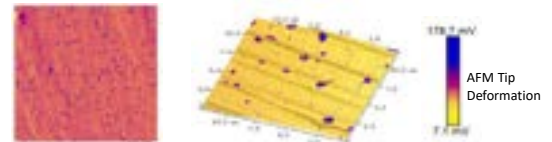


Figure 6: Atomic Force Microscopy (AFM) depicting softer particles within the stiffer matrix of the particle and thermoplastic-particle toughened material after cryogenic cycling

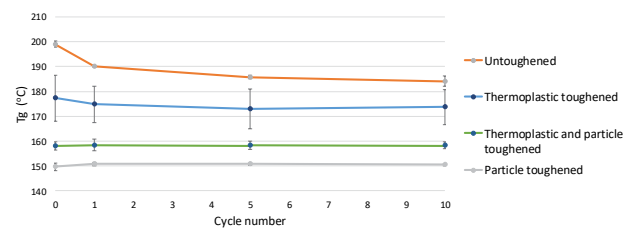


Figure 7: Change in glass transition temperature ( $T_g$ ) with cryogenic cycling

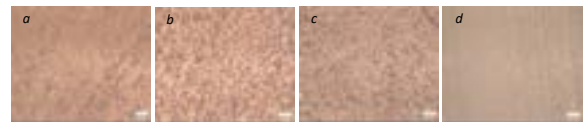


Figure 8: Optical microscopy of a) untoughened b) thermoplastic toughened c) particle toughened and d) thermoplastic and particle toughened epoxies after 10 cryogenic cycles, exhibiting no microcracking

## Materials and Methods

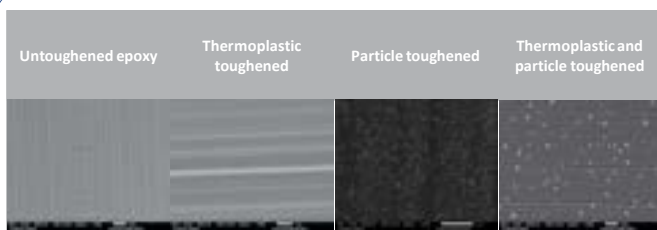


Figure 4: SEM cross-section of matrix materials investigated



Figure 5: Cryogenic cycling method. Liquid nitrogen was used due to availability and safety issues with testing in liquid hydrogen

## Conclusions

- Thermal shock through fast cooling cryogenic cycling did not cause microcracking in toughened and untoughened epoxy resins
- This suggests the fibre-matrix CTE mismatch plays a larger role in composite matrix microcracking than thermal shock during fast cooling
- Elastomeric particle toughening led to better cryogenic performance by maintaining physical properties during thermal cycling




# Multi-Objective Mechanical Optimisation of Lattice Cores

Athina Kontopoulou\*, Bing Zhang\*, Fabrizio Scarpa\*, Giuliano Allegri\*

\*Bristol Composites Institute, University of Bristol.

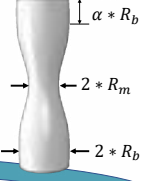
Structural weight can be reduced by substituting conventional monolithic components with sandwich ones. Our work aims to **optimise** the mechanical properties of lattice cores, which can be manufactured through conventional 3D printing techniques. The topology of the lattice unit cell is crucial for the ensuing mechanical performance. Here, we aim to **maximise** the **specific compressive ( $E_2$ ) and out-of-plane shear stiffness ( $G_{23}$ )** of lattice cores using a **multi-objective genetic algorithm (GA)**. A Representative Volume Element (RVE) for parametric lattice designs is used in a finite element (FE) modelling framework, which is incorporated within a GA-driven optimisation loop. **Manufacturing constraints** are accounted for in the optimisation. A **relative density constraint** for the lattice design is also considered.

### Micro-mechanical Optimisation

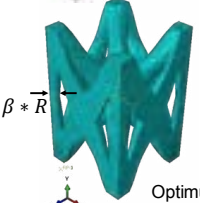


**Objectives:** minimise  $f_1(x) = -\log(E_2/\rho)$   
 minimise  $f_2(x) = -\log(G_{23}/\rho)$   
 Subject to relative density ( $\bar{\rho}_{rel}$ ) constraint:  
 $\bar{\rho}_{rel} = \frac{\rho^*}{\rho_s} = \frac{V_{lat}}{V_{RVE}} \leq 0.30$

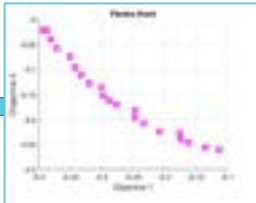
Variable	Lower bound	Upper bound
$R_m, R_b$	0.3 mm	1.2 mm
YRVE	5.0 mm	10.0 mm
$\alpha$	0.1	2.0

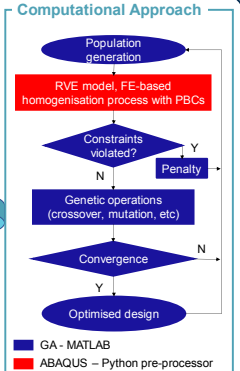


Tapering factor  $\beta = \frac{R_m}{R_b}$




Optimum design

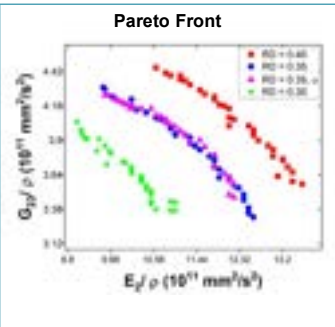




**Computational Approach**

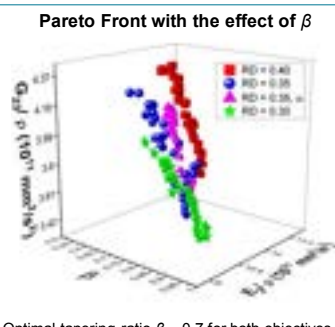
To learn more about our optimisation scan here : 

### Optimisation Results



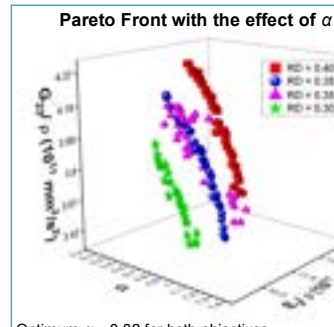
**Pareto Front**

\*RD = Relative Density ( $\bar{\rho}_{rel}$ )



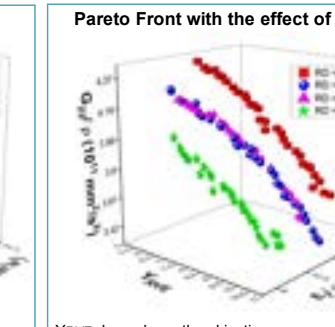
**Pareto Front with the effect of  $\beta$**

Optimal tapering ratio  $\beta \sim 0.7$  for both objectives.



**Pareto Front with the effect of  $\alpha$**

Optimum  $\alpha \sim 0.82$  for both objectives.

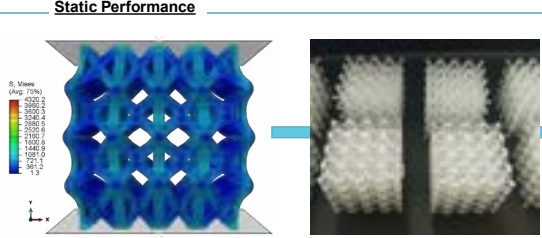


**Pareto Front with the effect of YRVE**

YRVE depends on the objectives.

### Macro-mechanical Validation

#### Static Performance



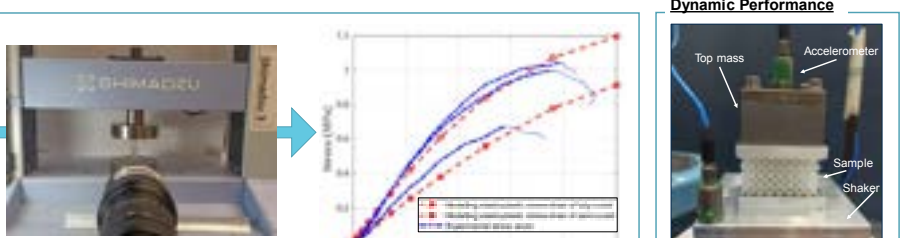
Elasto-plastic full-scale models under quasi-static compression load:

- Solid quadratic tetrahedral (C3D10) elements in ABAQUS.
- Material properties from tensile tests of 3D printed dogbones.

Additive manufactured samples through Stereolithography:

- Form 3+ 3D printer from Formlabs was used.
- Clear resin from Formlabs.
- UV curing at 60°C for 30 minutes.

#### Dynamic Performance



The samples are tested under quasi-static compression load:

- According to ASTM C365, loading speed 1mm/min.
- Strain recorded with video gauge.

Comparison between the experimental results and full-scale modelling predictions of fully- and semi-cured 3D printed material properties.

Vibration Transmissibility test rig:

- The sample is connected with superglue to the plates.
- White noise signals are generated using MATLAB.

### Conclusions

Tapering the struts has a beneficial effect on both compressive and out-of-plane shear stiffnesses, which can be increased up to 11% and 5%, respectively. The optimum tapering ratio  $\beta \sim 0.7$  is independent of the YRVE and relative density, with an optimum  $\alpha$  factor at  $\sim 0.82$ .

### Future work

Investigate the dynamic properties of the optimum lattice structures through numerical predictions and experimental validation with vibration transmissibility tests.

**Affiliations:**

- Bristol Composites Institute, University of Bristol, Bristol, BS8 1TR, U.K.
- School of Chemistry, University of Bristol, Cantock's Close, Bristol, BS8 1TR, U.K.
- Department of Mechanical Engineering, University of Bristol, Bristol, BS8 1TR, U.K.
- Centre for Innovation and Technology in Composite Materials, Department of Mechanical and Production Engineering, Federal University of São João del-Rei, São João del-Rei, 36301-158, Minas Gerais, Brazil

**References:**

- Gama, N., Ferreira, A., & Barros-Timmons, A. (2018). Polyurethane Foams: Past, Present, and Future. In *Materials* (Vol. 11, Issue 10, p. 1841). MDPI.
- Soares, L. F., César dos Santos, J., Araújo de Freitas, V. A., Dutra Pereira, R. B., Panzera, T. H., & Scarpa, F. (2024). Castor-oil based foam: the effect of the composition on the physical and mechanical properties via a statistical mixture design. In *RSC Sustainability*, Royal Society of Chemistry (RSC).
- Trovati, G., Sanches, E. A., Neto, S. G., Mascarenhas, Y. P., & Chierice, G. O. (2009). Characterization of polyurethane resins by FTIR, TGA, and XRD. In *Journal of Applied Polymer Science* (Vol. 115, Issue 1, pp. 263–268). Wiley.
- Rahimidehghan, F., & Altenhof, W. (2023). Compressive behavior and deformation mechanisms of rigid polymeric foams: A review. In *Composites Part B: Engineering* (Vol. 253, p. 110513). Elsevier BV.

# Rigid Polyurethane Foams from Commercial Castor Oil Resins

Jacopo Lavazza<sup>a</sup>, Qicheng Zhang<sup>a</sup>, Charles de Kergariou<sup>a</sup>, Gianni Comandini<sup>a</sup>, Wuge H. Briscoe<sup>b</sup>, Jemma Rowlandson<sup>c</sup>, Tulio Hallak Panzera<sup>d</sup>, Fabrizio Scarpa<sup>a</sup>

## Background

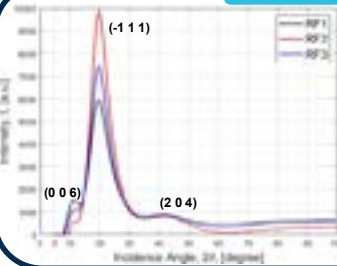
Rigid polyurethane foams (RPUFs) are among the most used polymeric materials due to their tailorable properties. Legislative requirements related to environmental protection and the depletion of petroleum resources lead the industry towards greener and biobased polyol sources. Castor Oil (CO) has also rapidly become one of the most successful alternatives to replace fossil-based polyurethane components because it naturally presents hydroxyl (-OH) functionalities<sup>1</sup>. However, the low hydroxyl number, low reactivity and steric hindrance of CO typically result in poor mechanical properties and low productivity of RPUFs. A great effort has gone into identifying suitable chemical modifications to overcome these drawbacks. The characteristics of CO-based RPUFs are also strongly influenced by their composition and the reagents utilised during production. Commercially available resin systems could solve these limitations<sup>2</sup>.

## Materials

Foam	Composition		
	RDA, [wt%]	RDB, [wt%]	AGTB, [wt%]
RF1	60	40	0
RF2	50	20	30
RF3	50	40	10

Three foam formulations (RF) obtained from different mixing ratios of *isocyanate* (RDA) and *polyols* (RDB, AGTB).

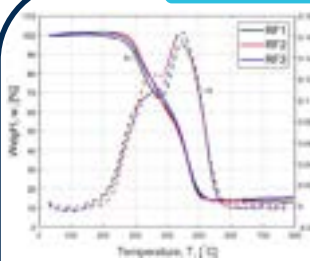
## Nanostructure



X-ray diffraction (XRD) peaks confirm PU structure<sup>3</sup>. No shifts of peak position are observed for the three foams. The (-1 1 1) peak intensity correlates with the foam density (and morphology):

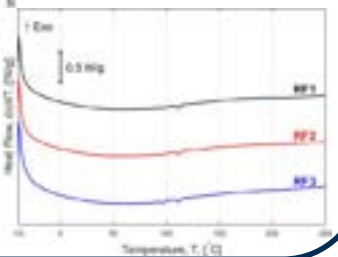
Foam	$\rho$ , [g/cm <sup>3</sup> ]	I, [a.u.]	P, [%]
RF1	0.08 ± 0.01	4838 ± 848	92.6 ± 0.1
RF2	0.14 ± 0.01	8295 ± 1974	85.1 ± 0.2
RF3	0.09 ± 0.01	6192 ± 891	90.8 ± 0.1

## Thermal Characteristics

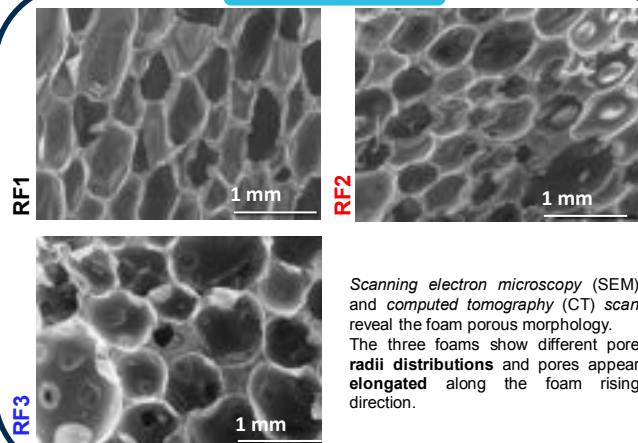


Thermogravimetric analysis (TGA) results present the typical degradation mechanisms of RPUFs. No significant differences are observed among characteristic temperatures and char residue.

Differential scanning calorimetry (DSC) highlights the presence of  $T_g$  and  $T_m$  for all three foams. Also in this case, no significant differences are observed in characteristic temperatures.

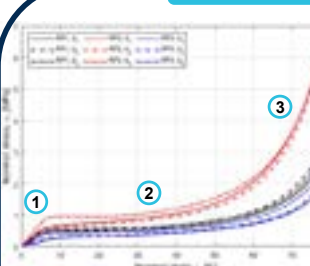


## Morphology



Scanning electron microscopy (SEM) and computed tomography (CT) scan reveal the foam porous morphology. The three foams show different pore radii distributions and pores appear elongated along the foam rising direction.

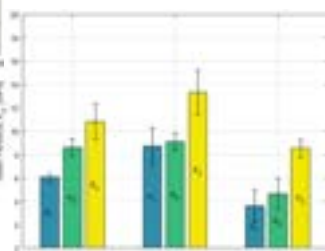
## Mechanical Behaviour



Quasi-static compression tests were employed to investigate the macroscopic mechanical behaviour of the foams. The response presents **three regions**<sup>4</sup>:

- Linear elastic
- Plateau
- Densification

The **static modulus** was determined from the linear elastic region of the response (tangent at  $\epsilon \approx 2.5\%$ ). As expected, the foams present different response, strictly related to the pore radius distribution and **porosity degree**. **Anisotropy** is observed which is a consequence of the elongated pore shape.



## Conclusions

- Three CO-based RPUFs have been extensively investigated:
- The polymeric macromolecular structure (from TGA and DSC) is not affected by the foam formulation.
- The (-1 1 1) XRD peak is related to the foam porosity and mechanical behaviour, highlighting how nano, micro and macro properties are interconnected.
- Anisotropy of the mechanical response is observed and related to the pore elongation during the foam process.

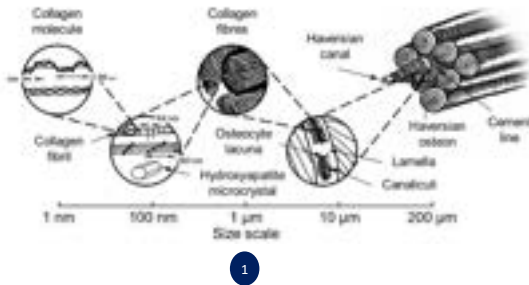
## Future Work

- Investigate the foams' dynamic mechanical response (drop impact, vibration transmissibility).
- Determine the effect of mechanical testing on the (-1 1 1) XRD peak.
- Convert the present CO-based RPUFs into auxetic metamaterials and study the effect of the conversion process.



# Biomimetic hierarchical architectures for enhanced compressive performance

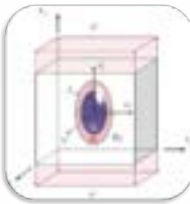
I.R. Lee, L.R. Pickard, I. Hamerton, G. Allegri



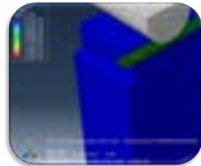
Natural composites such as bone, wood and shell, can exhibit significant compressive strength, despite often being formed from weak constituent materials. Key to this resilience are hierarchical systems of discrete structural elements, which couple mechanistic processes across length scales. This project is investigating the application of such architectures to improve measurable compressive performance within manufactured fibre / polymer composites. Novel system combinations are being developed which integrate constituent elements such as pultruded rods, micro-braided fibres, continuous fibre preregs, and highly aligned discontinuous fibre tapes created using the HiPerDiF process.

## Systems Modelling

Numerical micro-mechanical modelling of discontinuous fibre compressive response, utilising Eshelby inclusion theory



Predictions for lamina system level performance modelled within FEA software



Proposed laminae level system combinations initially rendered in CAD. From simple aligned rod-prepreg laminae, biomimetic architectures such as Bouligand structures can be developed for modelling

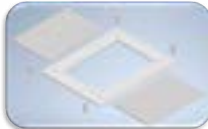


## Design & Manufacture



Material manufacture, inc. HiPerDiF tapes & braided fibre overwound rods

Bespoke tooling has been designed and manufactured for sample production



Tooling for novel cobotic manufacture prototyped using 3D printing methods



Sample material systems processed from hierarchically integrated constituent materials



## Testing & Evaluation

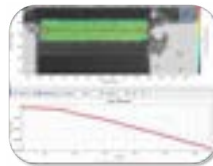
Compressive response characterisation utilising novel 4 Point Bend Test...



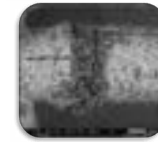
& standard shear-compression test



Mechanical data capture using digital & physical measurement methods



Pre & post failure system imaging at different length scales using techniques inc. SEM, optical microscopy & CT scanning



## Future Work

- Iterative development of more complex hierarchical architectures
- Improved integration of cobotic manufacturing methods
- Design, manufacture and testing of an industrial relevant structural member using biomimetic architectures

## References

- 1: Adapted from Hierarchical structure in human compact bone from Materials with Structural Hierarchy, R Lakes, Nature, Vol. 361, Pages 511-515 (1993), DOI: 10.1038/361511a0
- 2: Adapted from Two-step hierarchical micromechanics model of partially saturated porous composites doped with ellipsoid particles with interface effects, E Garcia-Macias, R Castro-Triguero, F Ubertini, Composites Part B, Vol. 148, Pages 49-60 (2018), <https://doi.org/10.1016/j.compositesb.2018.04.037>.

## Acknowledgements

The authors kindly acknowledge the funding for this research provided by UK Engineering and Physical Sciences Research Council (EPSRC) programme Grant EP/T011653/1, Next Generation Fibre-Reinforced Composites: a Full-Scale Redesign for Compression, a collaboration between Imperial College London and the University of Bristol.





# An assessment framework for the sustainable use of timber in the UK

Matthew Leeder, Eleni Toumpanaki, James Norman, Stephen J Eichhorn, Neha Chandarana

## Where does our timber come from?

There is a persistent disconnect between engineers and the origins of their materials, and this extends to timber.

Not all timber is the same; its range of origins means its embodied carbon, and its local social and ecological impact, can vary greatly.

### Currently:

Engineers are provided with minimal information about their timber's provenance. This conceals the large range of forestry techniques and their varying impacts.



## How can engineers better understand the origins of their timber?

My Project aims to translate the little information engineers have about their timber into the possible impacts. This will then inform the design of timber structures, such as timber frame buildings.

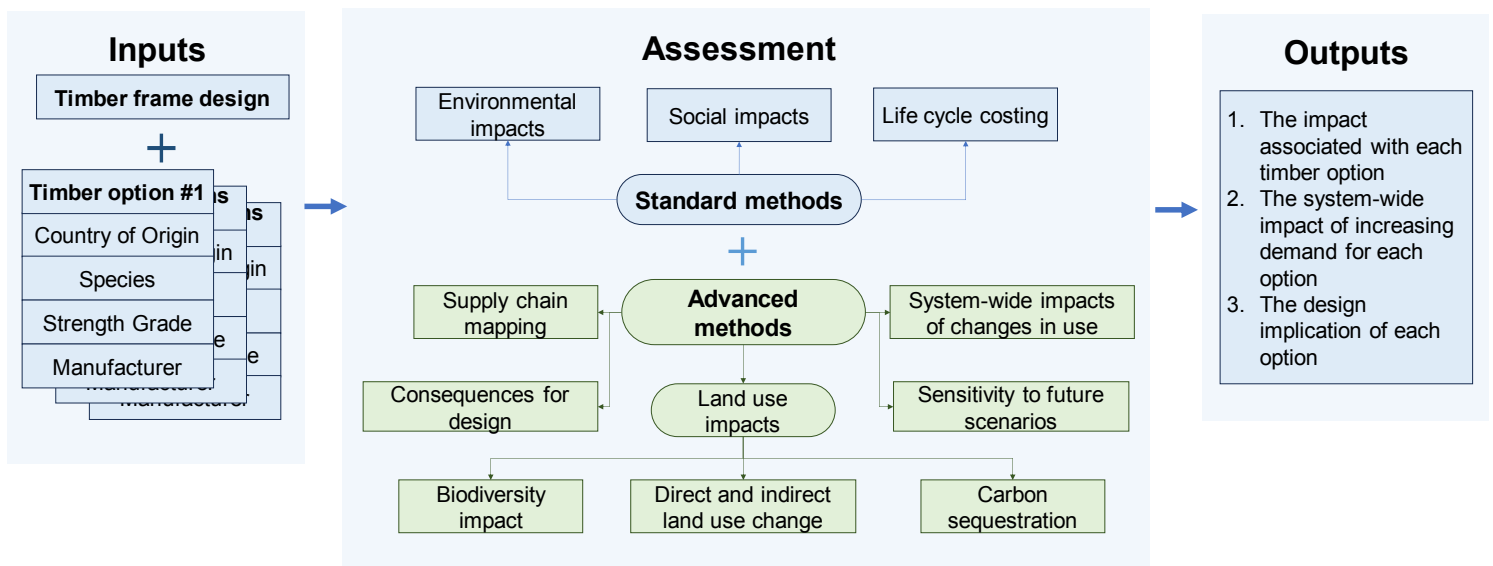
### It will help to answer questions such as:

- What are the consequences of sourcing your timber from the UK?
- Should you source timber from where it is native?
- What are the consequences of sourcing from monoculture plantations?
- Should you design with more lower grade UK timber?



My project will facilitate the consideration of **land use** and **supply chain** impacts by engineers when they use life cycle assessment to inform their timber choices.

This will be done through an assessment framework:



# Polyborosiloxanes as a Platform for Mechanical Memristors

Katherine Nelms, Jemma Rowlandson, Charles de Kergariou, Neha Chandarana, Fabrizio Scarpa

## Background

Polyborosiloxanes (PBS) are a class of polymer which are viscous liquids at slow loading rates but behave as a rigid, crosslinked thermoset at high loading rates. They are typically synthesized by reaction between boric acid and polydimethylsiloxane (PDMS, also known as silicone oil). Their rate-dependent behavior is a result of dynamic bonds between boron atoms incorporated into the polymer backbone and oxygen atoms in adjacent chains. At slow rates, these bonds have time to break and reform, allowing for viscous flow. At high rates, the B-O bonds remain rigid.

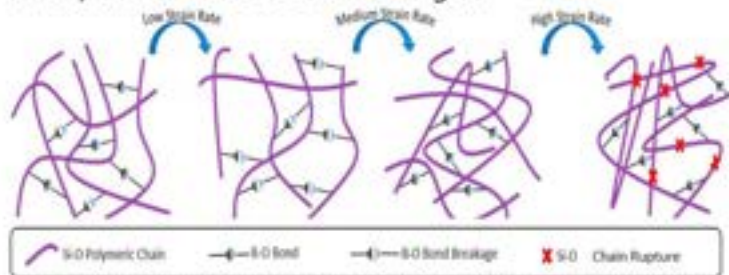


Fig. 1: Rate dependant behavior of dynamic B-O bonds in PBS [1]

Resistors can be considered as a linear  $i/o$  relationship between voltage and current. Memristors are devices which relate charge and flux, and they are characterized by a nonlinear, 'squeezed hysteresis' I-V curve which often evolves with loading. That is, the current output by a memristor ('memristivity') is a function of previous voltage history, thus storing memory of the loading.

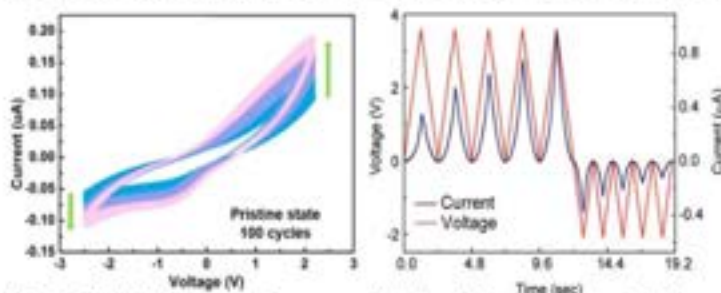


Fig. 2: (left) I-V curves for a memristor for 100 voltage cycles [2]. (right) Cyclic voltage across a memristor overlaid with measured current output [3]

## Research Aims

We aim to develop memristor-inspired materials from PBS whose mechanical properties adapt as a function of their loading history. These 'mechanical memristors' will be a step towards intelligent structures which evolve to become better suited to their environment, or autonomous actuators which learn from their environment and remove need for active control.

## Preliminary Results

My first year has been focused on acquiring background and materials selection. Now, I am focused on characterizing the mechanical behavior of PBS and identifying how the rate-dependent behavior contributes to mechanical memory.

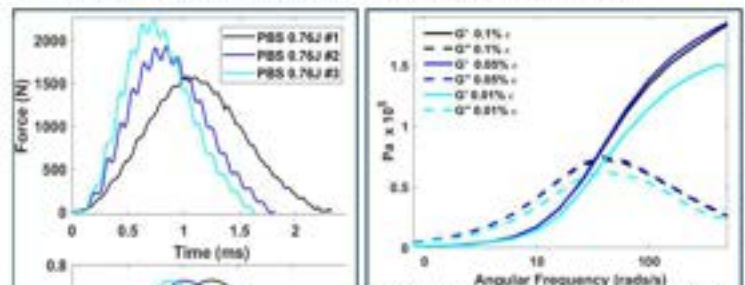


Fig. 3: Rheometry of PBS. Frequency sweeps were measured at different strains. The switch from viscous to rigid occurs when the storage modulus equals the loss modulus



Fig. 4: Repeat impact loading of the same PBS sample with an impact energy of 0.76J shows a shift in response peak. The 'noise' is thought to be mechanical reflection in the sample.

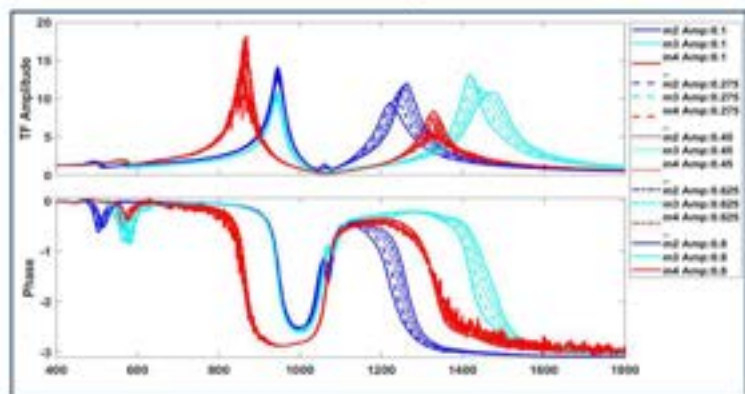


Fig. 5: Vibrational transmissibility of the same sample repeated at different base accelerations by varying mass of shaker and amplitude of vertical displacement. Response for each amplitude was recorded for each mass before changing mass.

## Future Work

- Finish PBS characterization for statistical validation
- Repeat characterization for PBS blended with elastomers
- Assess if repeated loading can be used to tune the mechanical properties of polymer blends
- Ideally, dynamic bonds in the PBS phase enable changes in the blends' phase distribution
- Eventually, we hope to make similar memory-active systems using biomaterials



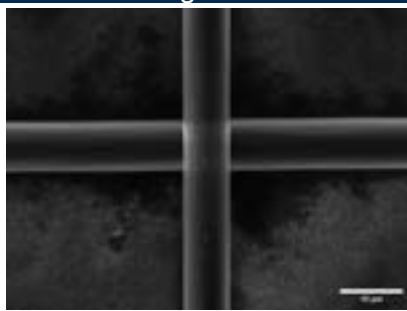
# Searching for excitonic superconductivity using transition metal dichalcogenides and carbon composites.

Rikesh Patel, Prof Simon Hall, Prof Steve Eichhorn, Dr Chris Bell

Superconductors are materials that, below a critical temperature, exhibit 0 DC resistance and expel an applied magnetic field from within itself. Often, the critical temperature is reached through cryogenic cooling. However, a mechanism of superconductivity, known as excitonic superconductivity, has been hypothesised to allow for room temperature superconductivity, through the compositing of transition metal dichalcogenides and carbon. No excitonic superconductor has yet been realised. This project aims to take the existing theory and make it a reality.

## Carbon Fiber Coating

Carbon fibers were functionalised with the metallophilic amine and thiol groups by Prof Luke Henderson's group at Deakin University. These fibers were then dipped in a suspension of WSe<sub>2</sub> Nanoparticles in ethanol.



## WSe<sub>2</sub> Nanoparticle Synthesis

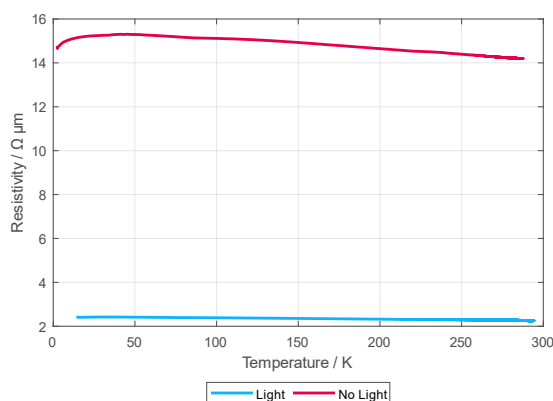
1. Bulk WSe<sub>2</sub> powder was ground in a pestle and mortar (30 minutes).
2. The powder was then mixed in ethanol (50 mg/ml, 3 ml).
3. The mixture was sonicated in an ice bath (6 hours).
4. The resulting suspension is filtered and centrifuged, leaving a light brown supernatant layer.



## Electrical Characterisation

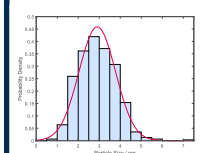


Using an Oxford Instruments OptiStat cryostat, the resistance of the TMD coated carbon fibers was measured in the presence of a broad-spectrum xenon light source. An average drop of 12.53  $\Omega \mu\text{m}$  in resistivity was seen. Whilst superconductivity was not seen, this drop in resistivity may be due to excitonic contributions.



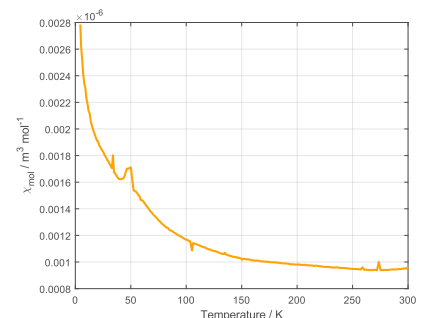
Resistance of the coated fiber was measured using a 4 – point contact method. A voltage of 1 mV was passed through a single fiber and the amperage measured over an 11 mm section of fiber. Then using Ohm's law, the resistance and thus the resistivity was calculated. The resistivity of the material increased with a decrease in temperature.

## WSe<sub>2</sub> Nanoparticle Characterisation



TEM images show round nanoparticles of WSe<sub>2</sub> with an average size of  $2.94 \pm 0.1 \text{ nm}$  with a PDI of 0.958.

SQUID Magnetometry shows the WSe<sub>2</sub> nanoparticles are weakly paramagnetic.



## Conclusions and Further Work

WSe<sub>2</sub> Nanoparticles have been successfully synthesised using a sonication method. A significant drop in resistivity of the system was observed, however, superconductivity not yet observed.



# Dual Mode Shielding Against Space Radiation Using Superconductive Enhanced Composites

Gokhan Sancak<sup>a</sup>, Simon Hall<sup>b</sup>, Tom Scott<sup>c</sup>, Ian Hamerton<sup>a</sup>

a. Bristol Composites Institute, Department of Aerospace Engineering, University of Bristol

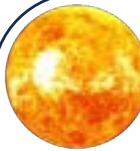
b. School of Chemistry, University of Bristol

c. Southwest Nuclear Hub, School of Physics, University of Bristol, Bristol BS8 1TL, UK

## Space Radiation

Recent advancements in space technology have brought humanity closer to achieving one of its most ambitious goals -manned space exploration. Despite this promising progress, the challenge of mitigating health threats posed by space radiation remains [1]. Thus, beyond the terrestrial magnetic field, ensuring the safety of humans and electronics engaged in extraterrestrial activity has been a compelling research area. This project addresses the critical need for innovative materials to effectively protect human health and essential equipment during extraterrestrial activities, marking a pivotal step toward the actualisation of the plan of manned space exploration.

The extensive range of ionising radiation encountered in space encompasses Solar Particle Events (SPEs) and Galactic Cosmic Rays (GCRs) originating from the sun and outside the solar system. These two radiation sources exhibit distinct energy spectra and radiation compositions, necessitating separate consideration.



### Solar Particle Event

- Characterised by,
- abrupt and extremely intense,
  - low-energy particles,
  - Sun-origin

SPE consists of primarily protons and a minor presence of alpha particles (helium ions).

### Galactic Cosmic Ray

- Characterised by,
- continuous,
  - high energy particles,
  - Supernova-origin

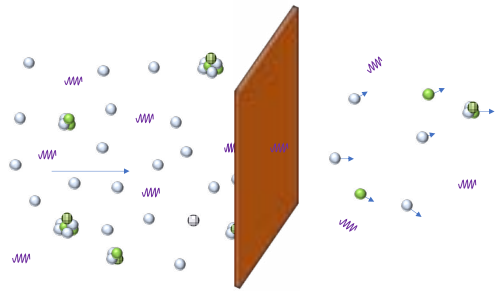
Approximately 87% of GCRs are protons, followed by 12% of He ions and 1% of high atomic number ( $Z > 2$ ) and energy particles (HZE) [2].

## Radiation Shielding

Various shielding methods have been explored to address the challenges posed by space radiation and can broadly categorised as active and passive shielding.

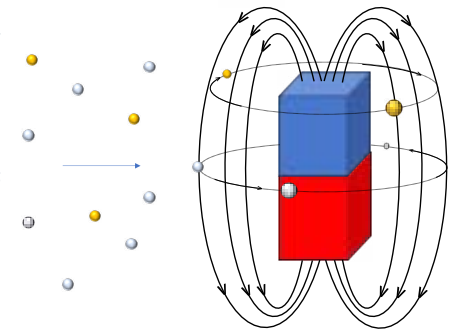
### Passive Shielding

- Passive shielding relies on static materials as a barrier, able to absorb and/or attenuate both charged and uncharged radiation that is unaffected by the Coulomb forces.
- Composite materials containing low-Z constituents and enriched with high-hydrogen content have gained recognition through their improved structural and radiation shielding performance, especially against radiation poses charge neutrality.

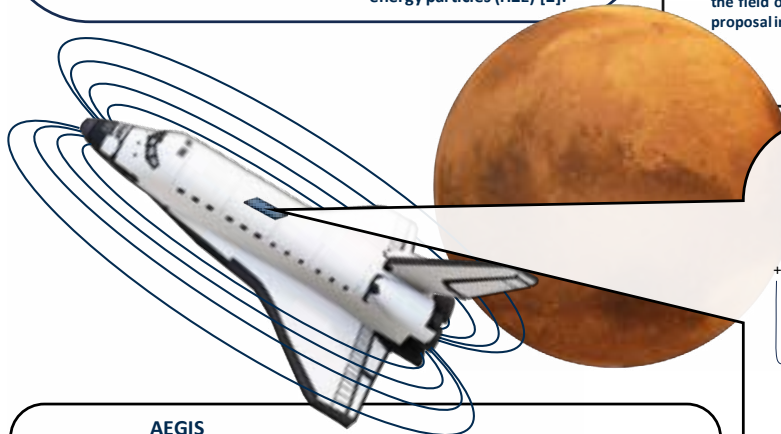


### Active Shielding

- Active shielding utilises an external energy source to create an electromagnetic field around the habitable zone of the spacecraft, deflecting incoming charged particles.
- Following the discovery of the superconductivity phenomenon in 1911 [3], the application of superconducting magnets, which, through their unique ability to generate strong magnetic fields and exhibit zero electrical resistance, has emerged as a transformative approach in the field of active shielding, with the first proposal in the 1960s [4]

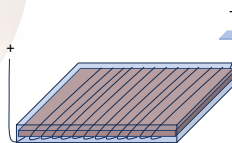


● proton ● electron ● neutron ● He ion ● HZE ● gamma-ray

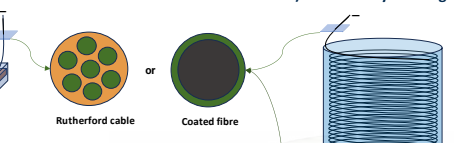


## Types of Superconductor Composite Structure

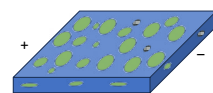
### 1) Composite panel winding



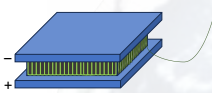
### 2) Whole-body winding



### 3) Powder in composite



### 4) Forest sandwich



■ superconductor ■ matrix/resin ■ composite panel ■ fiber/tube

## AEGIS

According to Greek mythology, aegis is a device carried by Zeus and Athena as a shield featuring the head of a Gorgon – three female monsters. Inspired by Medusa's hair, a connection between snakes and magnetic lines is built for the logo of the project.

Building upon the combined principles of both shielding methods, this project draws inspiration from the concept of superconductive-enhanced composite materials. This innovative approach integrates active shielding, leveraging superconducting additives, with passive shielding using matrix constituents within a family of well-characterised polybenzoxazine resins [5][6].

## References

- [1] Durante, M., & Cucinotta, F. A. (2008). Heavy ion carcinogenesis and human space exploration. *Nature Reviews Cancer*, 8(6), 465-472.
- [2] Simpson, J. A. (1983). Elemental and isotopic composition of the galactic cosmic rays. *Annual Review of Nuclear and Particle Science*, 33(1), 323-382.
- [3] Van Delft, D., & Kes, P. (2010). The discovery of superconductivity. *Physics today*, 63(9), 38-43.
- [4] Evans, B. R., Lian, J., & Ji, W. (2018). Evaluation of shielding performance for newly developed composite materials. *Annals of Nuclear Energy*, 116, 1-9.
- [5] Kong, K., Gargiuli, J., Worden, G., Lu, L., Brown, K. R., & Hamerton, I. (2023). Non-destructive evaluation of the curing of a polybenzoxazine nanocomposite blend for space applications using fluorescence spectroscopy and predictive mechanical modelling. *Polymer Testing*, 129, 108291.
- [6] He, Y., Suliga, A., Brinkmeyer, A., Schenk, M., & Hamerton, I. (2024). Effect of atomic oxygen exposure on polybenzoxazine/POSS nanocomposites for space applications. *Composites Part A: Applied Science and Manufacturing*, 177, 107898.

Background picture credit: NASA

# Damage Tolerance of 3D Woven Composites

Christian Stewart\*, Bassam El Said, Stephen Hallett  
\*christian.stewart@bristol.ac.uk

There is a growing use of 3D woven composites across several industries due to their increased damage tolerance. These materials are especially beneficial in components that are susceptible to barely visible impact damage (BVID). In this project, we aim to investigate how the presence of BVID affects the static and fatigue performance of 3D woven carbon-epoxy composites. In the work presented here, we experimentally investigate the development of damage under quasi-static indentation, which is analogous to low-velocity impact. Through the characterisation of damage, we then identify the BVID level suitable for subsequent static and fatigue testing.

## Quasi-static indentation tests

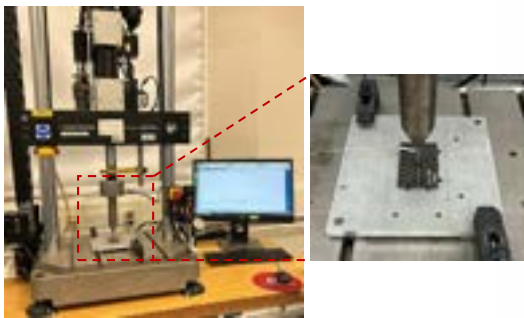


Figure 1: Quasi-static indentation test set-up

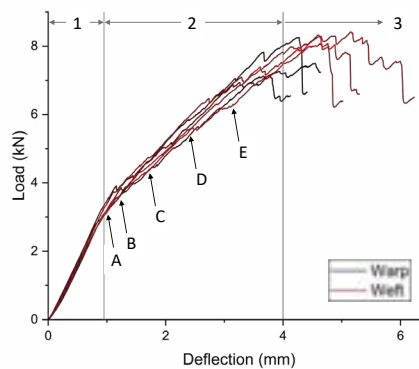


Figure 2: Load-deflection results

- Quasi-static indentation tests carried out on specimen oriented in both warp and weft directions (Figure 1).
- Three clear stages identified (Figure 2):
  1. Linear stage up to damage initiation (knee point).
  2. Nonlinear damage propagation up to catastrophic failure (load drop).
  3. After load drop.
- Subsequent tests were interrupted at different levels (labels A to E in Figure 2) to characterise the evolution of damage.

## Damage characterisation

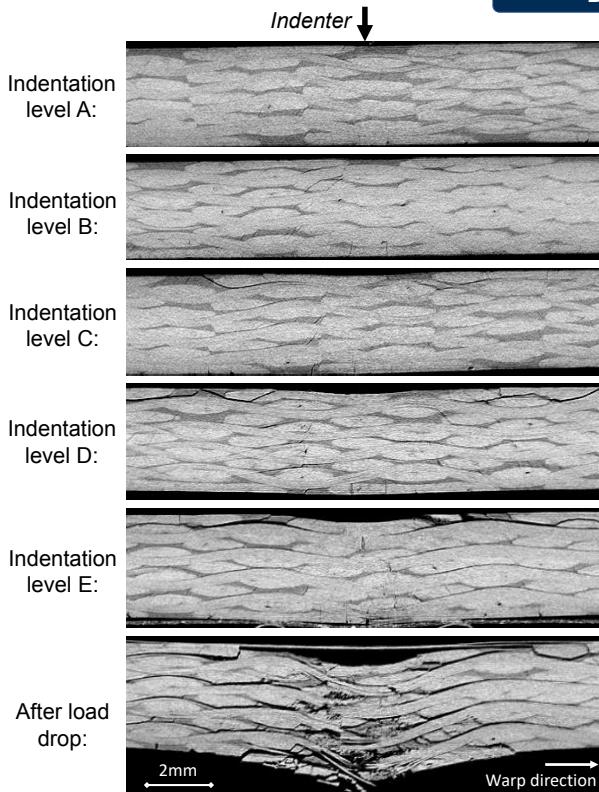


Figure 4: CT scans of indented specimen at different indentation levels. 2D slices taken through indentation point

- Extent of damage was first characterised by ultrasonic C-scanning (Figure 3). No information about actual damage mechanisms.
- Actual damage mechanisms were characterised using X-ray CT scanning (Figure 4), namely matrix cracks, intra-yarn transverse cracks, yarn debonding, yarn tensile failure and yarn fibre kinking.
- The damage is diffused before indentation level C, whereas severe damage with significant features are present beyond indentation level D.
- Therefore, indentation level C is selected to introduce BVID before subsequent static/fatigue testing.

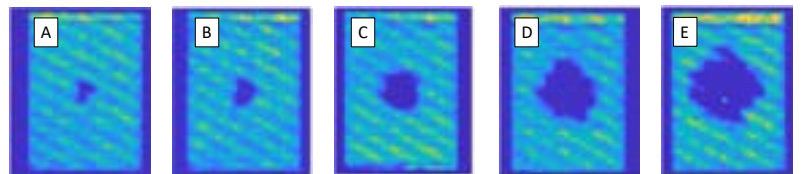


Figure 3: C-scans of indented specimen at different indentation levels. Dark regions show the projected areas of damage.

## Future work

- This work has identified the indentation level to be used for subsequent post-BVID tests. Such tests will investigate the effect of BVID on tensile and fatigue performance.
- These tests will then be used to develop models that are able to predict the post-impact fatigue behaviour of 3D woven composites.





## Aims and Objectives

Many of the methods for producing manufacture materials with reclaimed carbon fibres (rCF) specify a permissible fibre length range. At stages of the recycling process for end-of-life composite waste, the fibre length can be altered and not necessarily in a uniform manner. The aim is to develop a robust method for chopping and measuring fibre length distribution (FLD) of rCF samples that can be scaled for industry. The High Performance Discontinuous Fibre (HiPerDiF) process can be used with fibre lengths of between 3 and 12mm to produce partially impregnated aligned fibre material [1]. The next aim is to understand the impact of FLD on the HiPerDiF 3G based at NCC and characterise the relationship between FLD and composite tensile performance.

## Methodology

- Cylinder produced using Toho Tenax-E HTS45 carbon fibre yarn and Prime 37 epoxy
- Fibres reclaimed at B&M Longworth using a steam-based thermal process (Fig. 1)
- Virgin and reclaimed carbon fibres chopped using a pneumatic powered tool to set target lengths: 3mm, 4.5mm, and 6mm

Fibre length distribution (FLD) measured using the FASEP 3E Eco system and image analysis software [2]:

1. Disperse fibre sample in water and dilute to concentration level of 20 to 40 mg per litre.
2. Pour fibre solution in petri dish and scan image at 4800dpi.
3. Define fibre objects in the image by setting a pixel grayscale range (Fig. 2).
4. Define the area of interest in the image (Fig. 3) with fibres excluded if they interact with boundary edge.
5. Objects categorised as: dust, fibre, or cluster. Dust eliminated using a minimum width criteria, clusters processed using Hough transform to define as individual fibre lengths.
6. FLD measured from fibre objects and presented as volume weighted histograms (Fig. 4-5).



Figure 1: Cylinder component after fibre reclamation



Figure 3: Defining area of interest in the sample

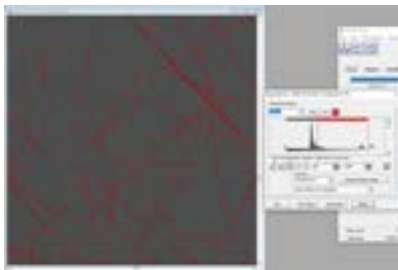


Figure 2: Defining fibre objects using pixel segmentation

## Key Findings

### Virgin

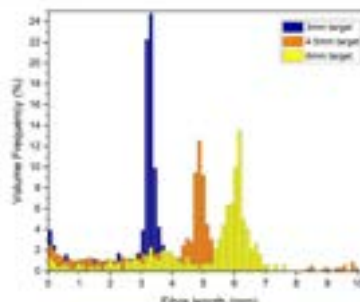


Figure 4: Fibre length distribution of unimodal virgin carbon fibre samples

### Reclaimed

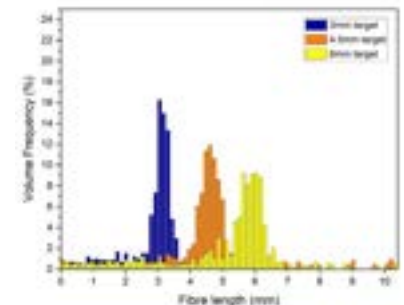


Figure 5: Fibre length distribution of unimodal reclaimed carbon fibre samples

- Chopping reclaimed fibres has a higher tail toward shorter fibres, but reduced dust likely due to fraying from lack of sizing
- Welch's method T-test [3] showed no significant difference between the virgin and reclaimed samples with the cylinder geometry when excluding fibres < 2mm

- All mode values slightly longer than target length, positive offset from pneumatic tool
- Greater standard deviation with increase in length, consistent for both virgin and reclaimed fibres
- Chopping methodology with cylinder geometry largely successful and retaining fibre length at >2m before chopping deemed critical

## Next Steps

- Fibre samples have been processed into material using the HiPerDiF 3G machine (Fig 6-7) and ASTM D3039 tensile specimens manufactured
- Chopped virgin fibres will be unsized in acetone at 75°C to also investigate influence of sizing on the process and performance



Figure 6: Aligned chopped fibre preform midway through HiPerDiF process



Figure 7: Output of HiPerDiF with preform partly impregnated with epoxy resin film

[1] The HiPerDiF method for the remanufacturing of mixed length reclaimed carbon fibres. Longana et al. Proceedings of ICCM21. August 2017.

[2] FASEP ultra-automated analysis of fibre length distribution in glass-fibre-reinforced products. Hartwich et al. Proceedings of SPIE 7389. 17 June 2009.

[3] The significance of the difference between two means when the population variances are unequal. Welch. Biometrika (29), pp 350-362. February 1938.

This work was supported by the EPSRC through the Future Composites Manufacturing Research Hub [EP/P006701/1]



# Explosive Chrysopoeia

Jan Maurycy Uszko, Professor Simon Hall, Doctor Avinash Patil, Professor Steve Eichhorn

Alchemists' fascination with the transmutation of base metals into gold (Chrysopoeia) led to the discovery, in the 15<sup>th</sup> century, of the first high-explosive compound, fulminating gold. Upon its detonation, it produces a characteristic purple smoke. It has been stipulated that dispersed nanoparticles cause its unusual colour. To date, however, there has been no experimental verification of the composition of the smoke on the detonation of fulminating gold. Here, we show for the first time that the explosion of fulminating gold creates gold nanoparticles, ranging in size from 5 to over 300 nm.<sup>1, 2</sup>

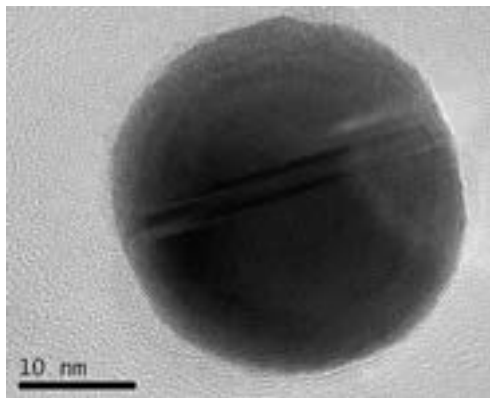


**Figure 1:** TEM image of a nanoparticle, from detonated fulminating gold, with visible lattice fringes.

The sample of fulminating gold was detonated onto a copper grid and investigated using a transmission electron microscope (TEM). **Figure 1** shows a high-resolution TEM image of a single nanoparticle with visible lattice fringes. With spacing of 0.24 nm, consistent with the (111) crystal planes of gold. The selected area electron diffraction pattern illustrated in **Figure 2** further confirms the presence of gold.

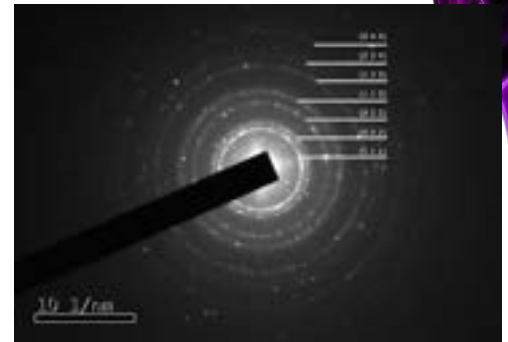


**Figure 2:** Selected area electron diffraction ring pattern from gold nanoparticles. The rings are indexed to gold as per the Joint Committee on Powder Diffraction Standards (JCPDS) card no. 04-0784..

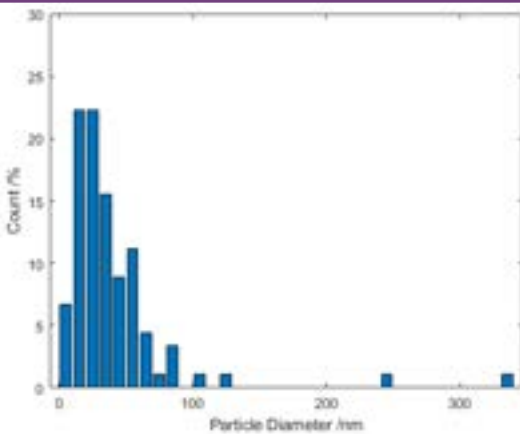


**Figure 3:** Particle size distribution of gold nanoparticles from the detonation of fulminating gold.

TEM images of grids that were exposed to the purple smoke showed clusters of spherical nanoparticles exhibiting a wide size distribution from 5 nm to over 300 nm, with an average particle diameter of 40 nm [ $\sigma = 44$  nm] illustrated in **Figures 3 and 4**. The broad particle size distribution and sphericity are indicative of the extreme rapidity and high temperature of the synthesis, with no possibility of achieving a lower polydispersity via the usual mechanisms.

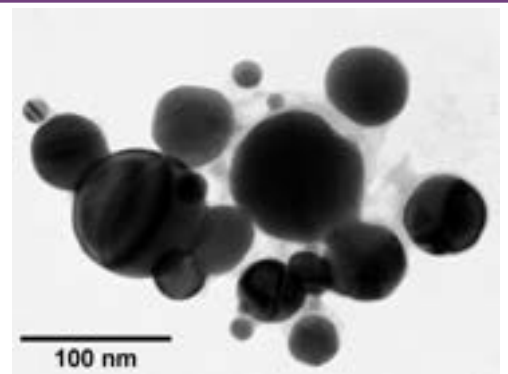


**Figure 4:** TEM image of a cluster of gold nanoparticles captured from detonated fulminating gold. The image demonstrates visually the broad dispersion of particle sizes.



**Figure 5:** Process of collecting nanoparticles on the TEM grid.

**Figure 5** shows the process of collecting nanoparticles where the TEM grid is held in tweezers and fulminating gold is heated on aluminium foil.

The detonation method can be applied to other metals besides gold and can be used to coat materials with a layer of nanoparticles, which is illustrated in **Figure 6**.

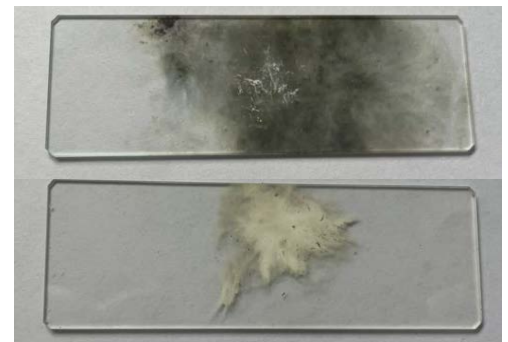


**Figure 6:** Glass slides coated with silver by detonation of silver fulminate.

# Crystallisation Modelling of Thermoplastics for Interfacial Strength Predictions in Composite Over-Moulding Products

Maria Veyrat Cruz-Guzman

Jonathan Belnoue, Steve Eichhorn, James Myers, Adam Chaplin, John Grasmeder, Dmitry Ivanov

## Thermoplastic Crystallisation + Why We Care:

- The most important phase transition to consider when processing thermoplastics.
- An important relationship exists between crystallinity and interfacial strength (& other macroscale properties).
- Crystallisation modelling is essential for process optimisation in 3D printing, over-moulding, press-forming and other processes; resulting in improvements in mechanical properties, processing time and energy consumption.

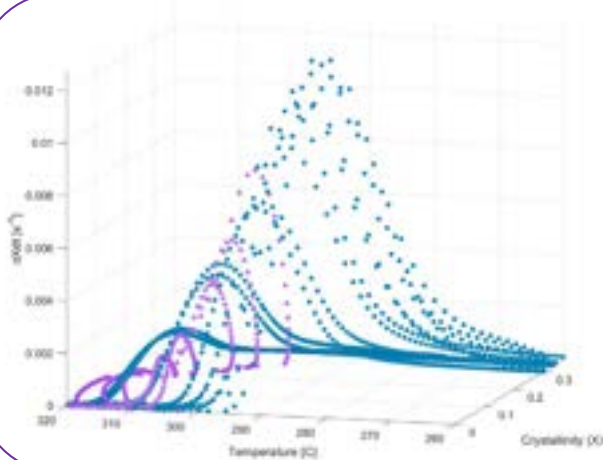


**Fig 1:** Conventional 3D space using the conventional variable crystallinity, temperature and crystallisation rate. Purple: Isothermal data; Blue: Dynamic data.

## State of the art

- Current crystallisation models such as *Avrami* and *Nakamura*, tend to overpredict crystallinity and do not consider thermal history, which makes them unsuitable for complex thermal history.
- Current models exhibit large numbers of parameters and fitting constants.
- The physical meaning of these laws is debated, particularly in the context of secondary crystallisation
- Experimental data shows that models formulated in the conventional state variable space (Crystallisation, Temperature, Rate) cannot reconcile available data. **Fig1.**

## New Model Formulation

- To account for complex thermal history, fractional crystallinity rates are suggested as a new variable:

$$Y = \frac{1}{\Gamma(1-\alpha)} \int_0^t \frac{dXdt}{(t-\tau)^\alpha} d\tau \quad \alpha = 0.92$$

- This new fractional variable space can reconcile dynamic and quasi-isothermal experimental data. **Fig 2.**
- A simple double Weibull fit describes the data given with sensible accuracy. **Fig 2 & 3.**

$$D^m X = k * W_1(T) * W_2(X)$$

- The fit shows that more data around the glass transition region is needed for an improved distribution fit.

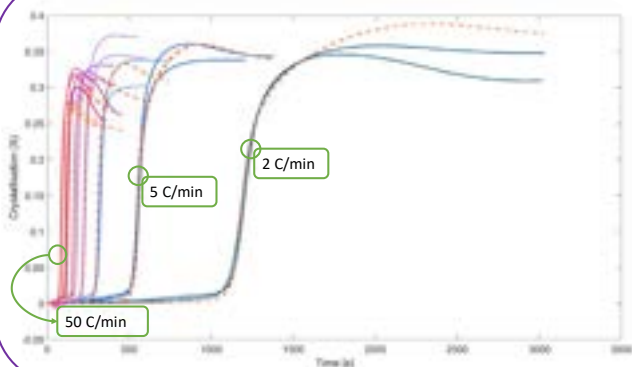


**Fig 3:** Crystallisation (time) comparing dynamic experimental data (Blue to Pink) vs the proposed fractional model (Orange)

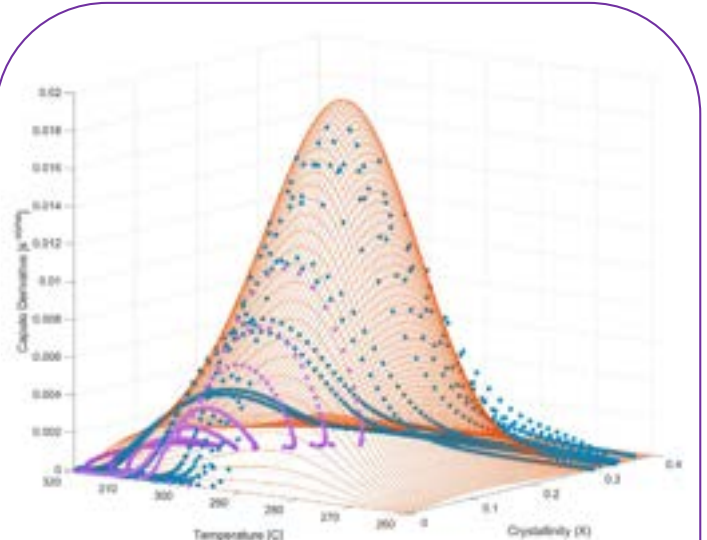


**Fig 2:** A fractional space was created showing the relationship between crystallinity, temperature and history-corrected crystallisation rate. Purple: Isothermal dataset; Blue: Dynamic dataset & Orange: Initial Weibull distribution fit.

## Next steps

- Promising results on the fractional variable space need to be generalised for melting dynamics.
- The physical meaning of the fractional laws and fitting needs to be further considered.



# Interlaminar Fracture Toughness of IM7/8552 at Elevated Temperatures

Anna Williams

As high temperature composites are employed within extreme environmental conditions, it is important to understand how they will react in elevated temperatures. This study has set a baseline standard of quantitative properties and qualitative fracture features using IM7/8552 for performance comparison with newly developed high-temperature polymer matrix composites.

## Testing Methods

A leading aerospace-grade epoxy-based composite material, IM7-8552, was selected for testing as it is readily available, widely used, and is currently employed in high temperature applications. This work characterised and recorded the Mode I fracture toughness properties of IM7-8552 in room temperature conditions, 23°C, and at elevated temperatures, 90°C, representative of heat conditions experienced in aerospace applications.

The test set up for both temperatures is shown in Figure 1, in which unidirectional double cantilever beam specimens were manufactured and tested according to ASTM D5528 [1], including 12µm PTFE film to create the pre-crack. During testing, the load, displacement, time, and crack growth were recorded to calculate fracture toughness properties using the modified beam theory.

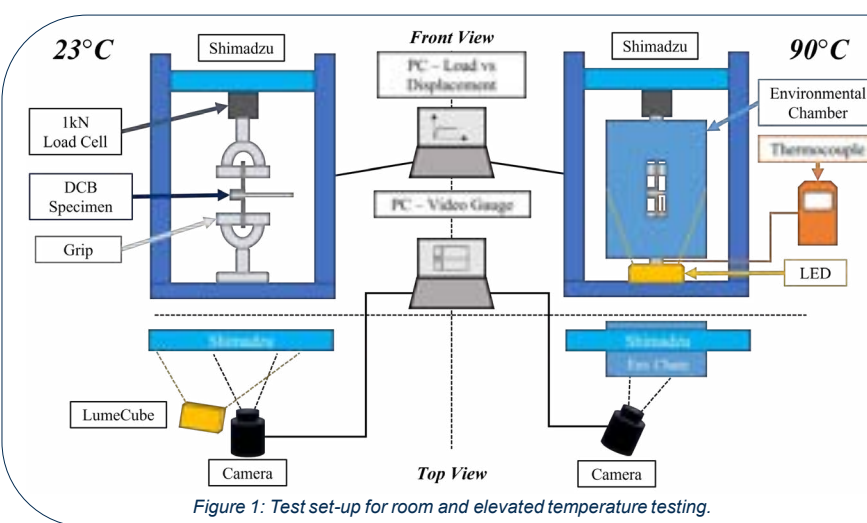


Figure 1: Test set-up for room and elevated temperature testing.

## Fractographic Analysis

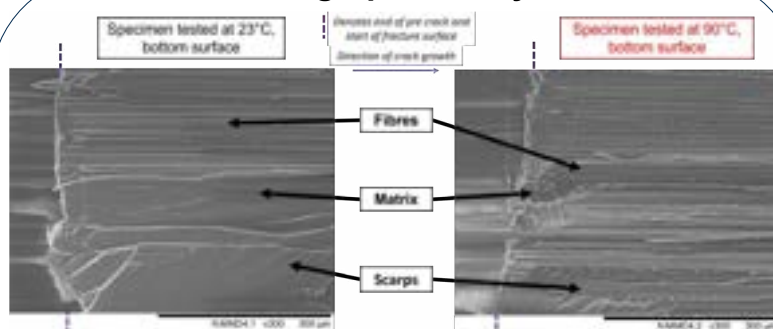


Figure 2: SEM images of fractured surfaces.

The morphology of the tested specimens was studied to compare and contrast the fracture surfaces between the two temperatures, and to give a greater insight as to how damage initiates and propagates within this material. Scarps were observed, with more evidence of fibre bridging and pull-out during high temperature testing.



Figure 3: Fibre bridging after 45mm of crack growth.

## Fracture Properties

The calculated visible and 5% compliance non-pre cracked Mode I fracture toughness,  $G_{IC}$  values were equivalent to literature [2], at  $0.21 \text{ kJ/m}^2$ , and similar at both temperatures with comparable critical forces, suggesting the  $G_{IC}$  values were dominated by the blunt PTFE film insert. However, Figure 4 shows there is a significant increase in  $G_{IP}$  at elevated temperatures as the crack propagates through the specimen. This is due to fibre bridging and increased ductility of the matrix leading to more compliant specimens.

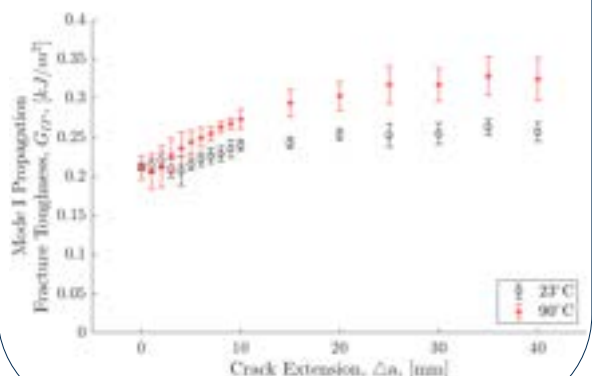


Figure 4: Averaged R-curve plots.

## Future Work

- Moisture conditioning samples
- Mixed Mode I/II Fracture testing
- Fatigue testing to give insight into deterioration during cycling in hot/wet environments material life
- Testing at higher temperatures (>150°C) to observe behaviour close to glass transition temperature



# Compressive Single Fibre Micromechanical Analysis via *in-situ* Raman Spectroscopy

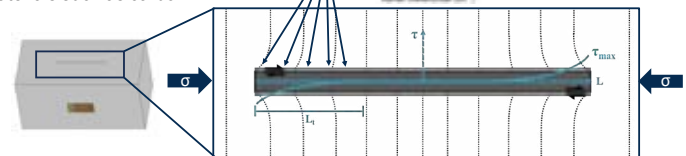
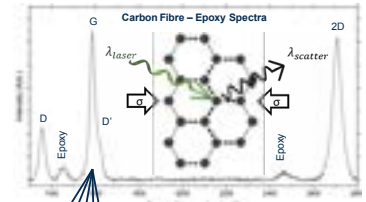
Cameron G Woodgate<sup>a</sup>, Prof. Richard S Trask<sup>a</sup>, Prof. Milo SP Shaffer<sup>b</sup>, Prof. Stephen J Eichhorn<sup>a</sup>

<sup>a</sup> Bristol Composites Institute, School of Civil, Aerospace and Design Engineering, University of Bristol, UK

<sup>b</sup> Department of Materials and Department of Chemistry, Imperial College London, UK  
cameron.woodgate@bristol.ac.uk, s.j.eichhorn@bristol.ac.uk

## Introduction

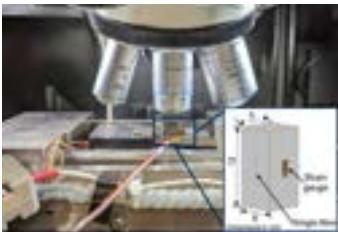
- Unidirectional carbon fibre reinforced polymer composites frequently exhibit compressive strengths approximately 60% lower than their tensile strengths, making compressive performance a critical design consideration.
- Understanding compressive performance and failure mechanisms at the constituent material level, particularly on the fibre scale, is necessary. However, measuring the compressive response of single fibres, particularly their interface, is experimentally demanding via conventional methods.
- Raman spectroscopy can be utilised as a versatile tool to measure local stresses within graphitic materials such as carbon fibres and carbon nanotubes, and is able to measure *in-situ*, during compressive loading.
- By measuring localised variations in stress along a length of single fibre, point-to-point stress maps can be used to investigate interfacial behaviour as well as the propagation and evolution of compressive failure processes.



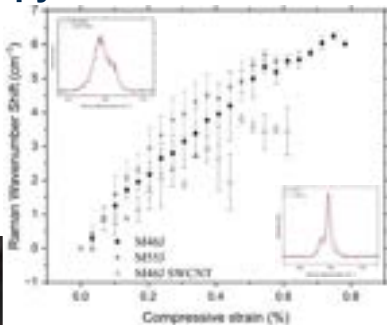
## 1. Raman Spectroscopy

Raman spectroscopy examines the inelastic scattering of monochromatic light to assess atomic bonding in carbon fibre samples.

Spectral peaks correspond to structural features, where the graphitic or 'G' band indicates ordered graphitic planes.



Single fibre epoxy prisms deformed via uniaxial compression in a 5 kN Deben microtester, within a Raman spectrometer for stress mapping.

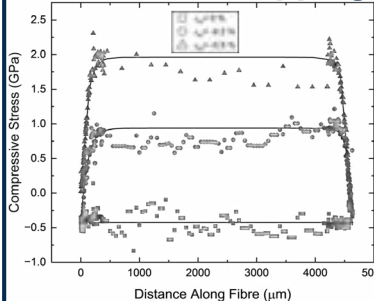


Raman wavenumber shift vs compressive strain calibration curve for the G band shift for high modulus carbon fibres and SWCNT coated fibres, with a visualisation of the spectral shifts.

The position of the G band is sensitive to stress, and its wavenumber shift during deformation is linked to stress within the fibre.

Once a wavenumber shift of the G band is convertible to stress, stress mapping becomes feasible.

## 2. Interfacial Mapping

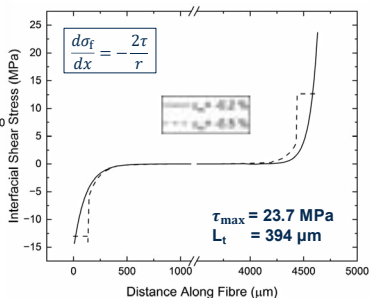


Point-to-point Raman stress map for a M46J carbon fibre in an LV/HYS052 epoxy matrix undergoing uniaxial compressive loading.

Interfacial shear stress can be derived, allowing analysis of local interfacial behaviour in compression.

Parameters such as maximum observed shear stress  $\tau_{max}$  and transfer length  $L_t$  can be extracted and analysed.

Point-to-point stress mapping using *in-situ* Raman spectroscopy enables the examination of the micromechanical behaviour of single fibres under compressive loading.

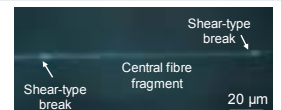


Derived interfacial shear stress of a length of M46J carbon fibre under compressive loading. Derived via a balance of forces approach.

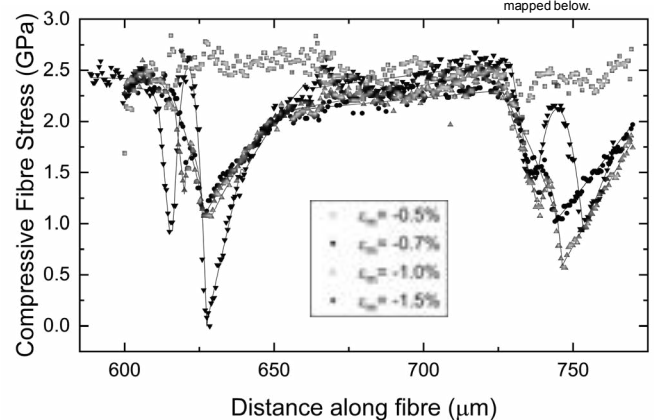
## 3. Failure Mapping

High modulus carbon fibres experience fibre fragmentation as their compressive failure mechanism.

To gain a better understanding of how the failure initiates and propagates, high spatial resolution stress maps are produced.



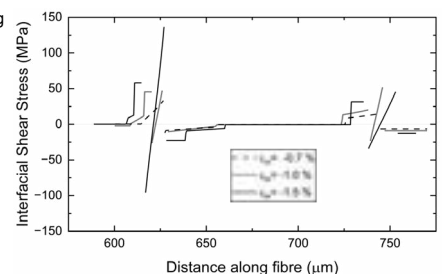
Optical micrograph of the fibre fragment mapped below.



Point-to-point stress map of an M55J undergoing failure via compressive failure. A sampling resolution of 2000 spectra per mm was used. Solid lines represent fitting a micromechanical model, a modified shear lag approach, to the data.

Key features and mechanisms occurring during the compressive failure:

- The lowest strain level shows no large drop in stress when failure first initiates as a microcrack.
- As loading increases, the breaks develop into shear-type breaks as stress drops to a non-zero value at either end of the fragment.
- Stress minima of non-zero indicates the fragment ends are in contact, transferring stress across the break.
- Interfacial debonding at the ends of fragments is characterised by a linearisation of stress.
- Inter-fragment wedges are present between fragment ends, which are thought to be sections of fibre ejected during fragmentation. Wedges may suggest a mixed failure mode of combined shear, bending and compressive stresses<sup>1</sup>.



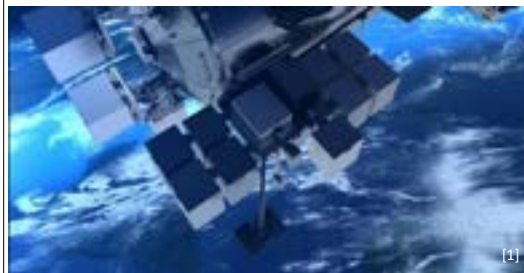
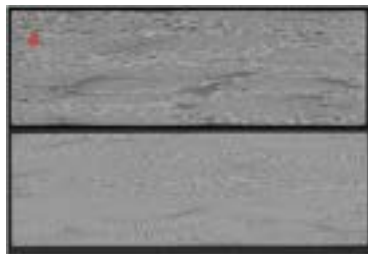
Interfacial shear stress derived for the M55J fibre undergoing compressive failure, mapped above. Interfacial shear stress is calculated via a balance of forces approach.

# Improving the resilience of benzoxazine-based composite materials for space applications

George Worden, Kate Robson Brown, Sebastien Rochat & Ian Hamerton

## Research problem and aim

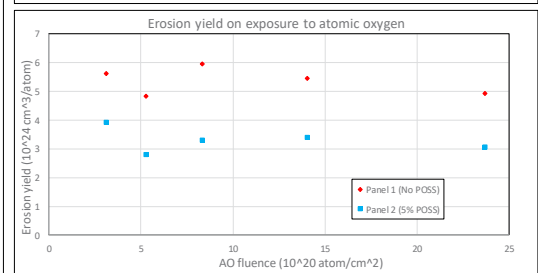
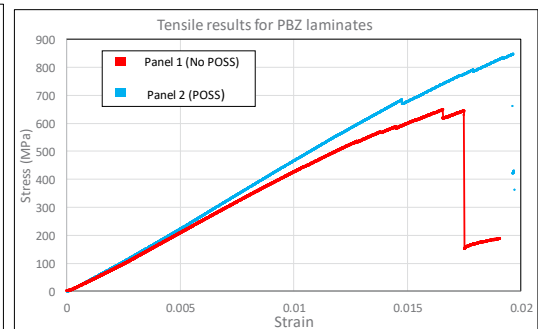
- The environment in low Earth orbit (LEO) is hostile to many materials, due to the presence of atomic oxygen, micrometeoroids and multiple types of radiation. These can damage materials through erosion, impacts, and degradation. In addition, directly testing materials in space is problematic due to the high cost and limited capacity of sending materials into orbit.
- A novel benzoxazine based polymer (PBz) has been developed to be resistant to the LEO environment with the addition of silicon-containing nanoparticles while remaining easily processed into composite laminates. The aim of this project is to further characterise the material through mechanical and thermal testing as well as improve its longevity through the introduction of self-healing functionality and radiation resistance.



X-ray CT scan images of RTM-produced CFRP laminates. a: pre-exposure, b: 0% POSS post exposure, c: 5% POSS post exposure

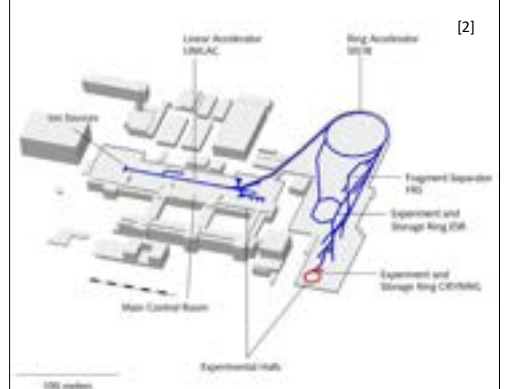
## Current focus

- X-ray CT scans of CFRP panels containing the PBz matrix have been carried out. These clearly show that the newer, RTM manufactured panels do not have the widespread voids and delamination of previous materials. Post atomic oxygen exposure scans also show the depth and extent of AO-induced erosion.
- A campaign of mechanical testing has been performed on samples of this new material to characterise it prior to LEO exposure. The results of this testing suggest that the addition of 5wt% POSS to PBz has a significant positive impact on the strength and stiffness of CFRP materials manufactured using it in addition to reducing oxygen erosion.
- A framework for a finite element model for the mechanical performance of the material using x-ray CT data has been produced and applied to neat resin containing CFRP. This will be applied to further materials containing nanocomposite and vitrimeric fractions.



## Future work

- Addition of vitrimeric components to CFRP to introduce some self-healing functionality to the material. CFRP will be characterised through mechanical and thermal testing and evaluated for self-healing capability (following thermal cycling) and AO resistance. Early testing will include both neat resins and CFRP specimens to ensure the new formulations will work with the current processing methods, while maintaining performance.
- Access to the GSI accelerator facility in Darmstadt has been secured through ESA with UKSA support. This will be used to expose samples of the novel CFRP to high energy/mass particles similar to the galactic cosmic rays found in space. The radiation resilience and shielding properties of the composites will be quantified in order to determine the extent they could contribute to radiation protection on a spacecraft.
- Kong *et al.*, Physical and mechanical properties of nano-modified polybenzoxazine nanocomposite laminates: pre-flight tests before exposure to low Earth orbit, *Composites Part B*, 2024 in the press.





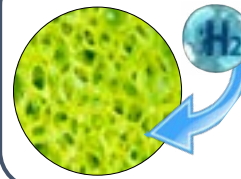
# Enhancing hydrogen storage capacity through tuneable polytriphenylamine conjugated microporous polymers

J. D. Worth, V. P. Ting & C. F. J. Faul

## 1. Hydrogen (H<sub>2</sub>) for renewable energy

- ✓ Clean combustion  
 $2\text{H}_2 + \text{O}_2 \rightarrow 2\text{H}_2\text{O}$
- ✓ Globally abundant
- ✓ High gravimetric energy density
- ✗ Toyota Mirai achieves density of 5.7 wt%
- ✗ High mechanically performing containment materials needed
- ✗ Highly compressed (~70 MPa)
- ✗ The United States Department of Energy (DoE) goal is to achieve a H<sub>2</sub> storage capacity of 0.065 kg H<sub>2</sub> kg<sup>-1</sup> (6.5 wt%) for onboard storage systems<sup>1</sup>

## 2. Conjugated microporous polymers (CMPs) for more efficient H<sub>2</sub> storage



H<sub>2</sub> adsorption in pores combats storage issues  
Engineering micropores (<2 nm) for optimal H<sub>2</sub> storage capacity  
Conjugated microporous polymers (CMPs) offer potential owing to their chemical and thermal stability and established synthetic routes

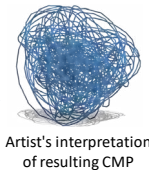
## 3. Material synthesis and confirmation

CMP Name	Bromine	Amine	Yield (%)
PTPA-Br <sub>1</sub> N <sub>1</sub>	1	1	14
PTPA-Br <sub>1.5</sub> N <sub>1</sub>	1.5	1	34
PTPA-Br <sub>2.25</sub> N <sub>1</sub>	2.25	1	40
PTPA-Br <sub>3</sub> N <sub>1</sub>	3	1	37
PTPA-Br <sub>1</sub> N <sub>1.5</sub>	1	1.5	12
PTPA-Br <sub>1</sub> N <sub>2.25</sub>	1	2.25	7
PTPA-Br <sub>1</sub> N <sub>3</sub>	1	3	0

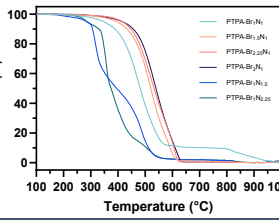
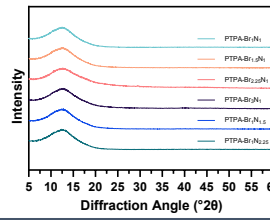
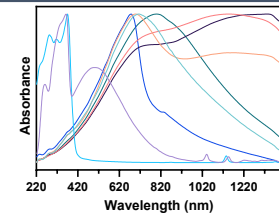
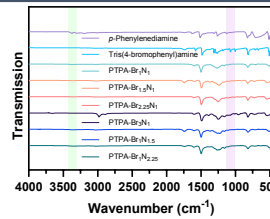
Monomers coupled with Buchwald-Hartwig amination

Stoichiometry of these reactants was systematically adjusted to control the ratio of bromine to amine groups present in the idealised final structure.

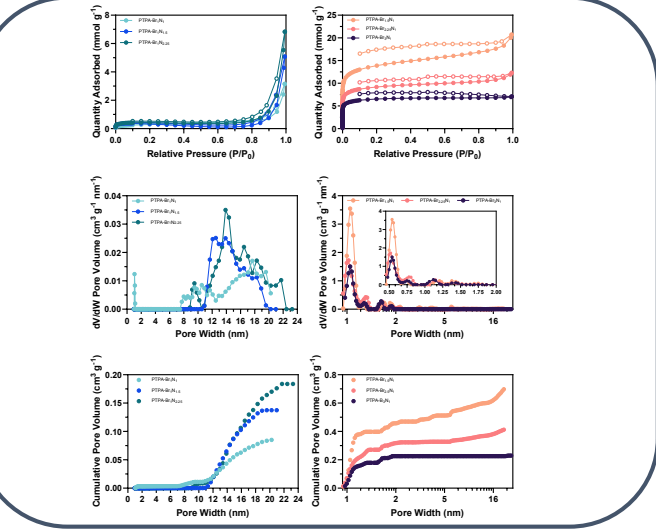
The polymers are named with the convention PTPA-B<sub>x</sub>N<sub>x</sub> where B<sub>x</sub>N<sub>x</sub> is the ratio of bromine atoms to amine functional groups present in the idealised structure of the resulting material.



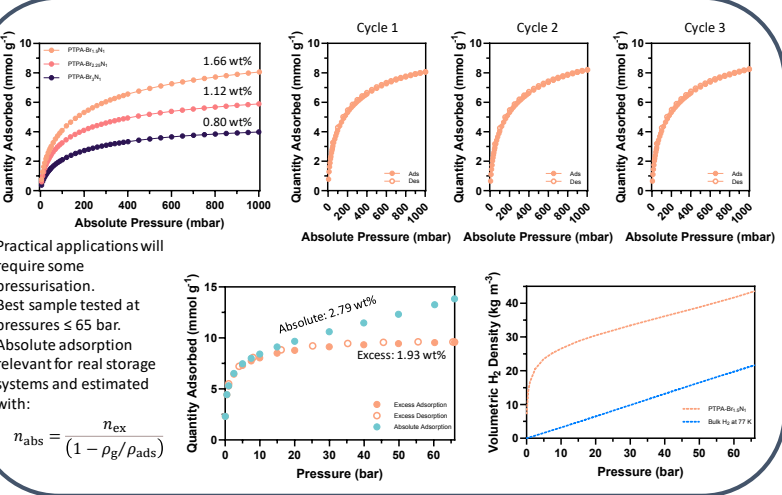
Artist's interpretation of resulting CMP



## 4. Volumetric nitrogen gas sorption analysis

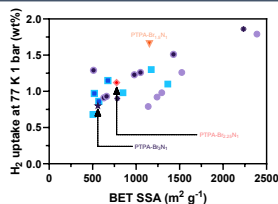


## 5. Excess & absolute H<sub>2</sub> storage capacities and estimated volumetric density



## 6. Conclusion and composite preparation

- Successful synthesis of CMPs of turned to varying levels of porosity.
- Volumetric density of H<sub>2</sub> shown to be greater confined within material than without at certain conditions.
- High performing material within the CMP class at 77 K and 1 bar.



CMPs exist as powders (like most porous materials).

Forming solid composites using other porous polymers (PIM-1) could help with real world applications.

Porous polymer that can be cast as films.

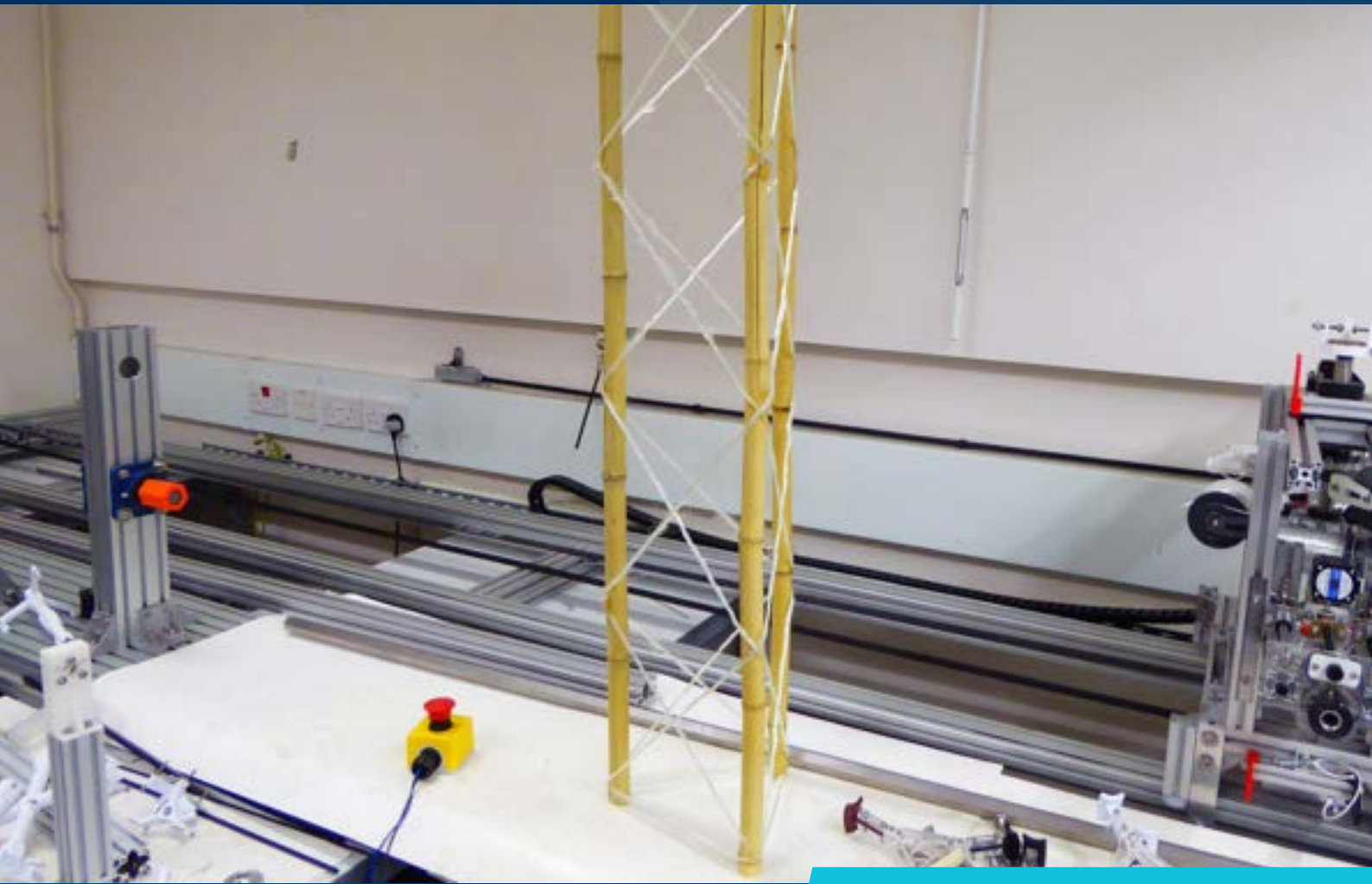


Various wt% loadings prepared:

- 10 wt%
- 15 wt%
- 20 wt%
- 25 wt%
- 30 wt%

Results pending.





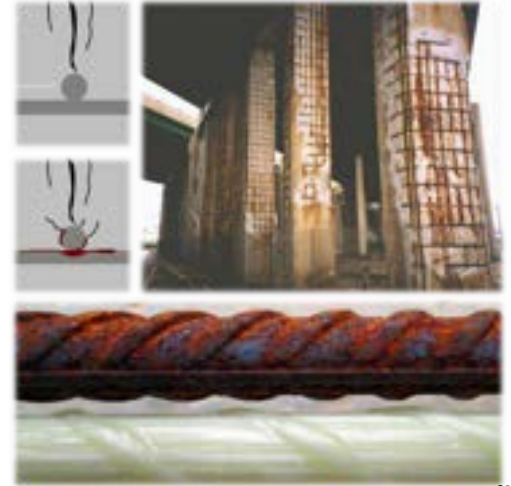
# STRUCTURES

# Durability Assessment of GFRP Bars in Marine Environments

Asaad Biqai, Eleni Toumpanaki, Manjola Caro, Ian Hamerton

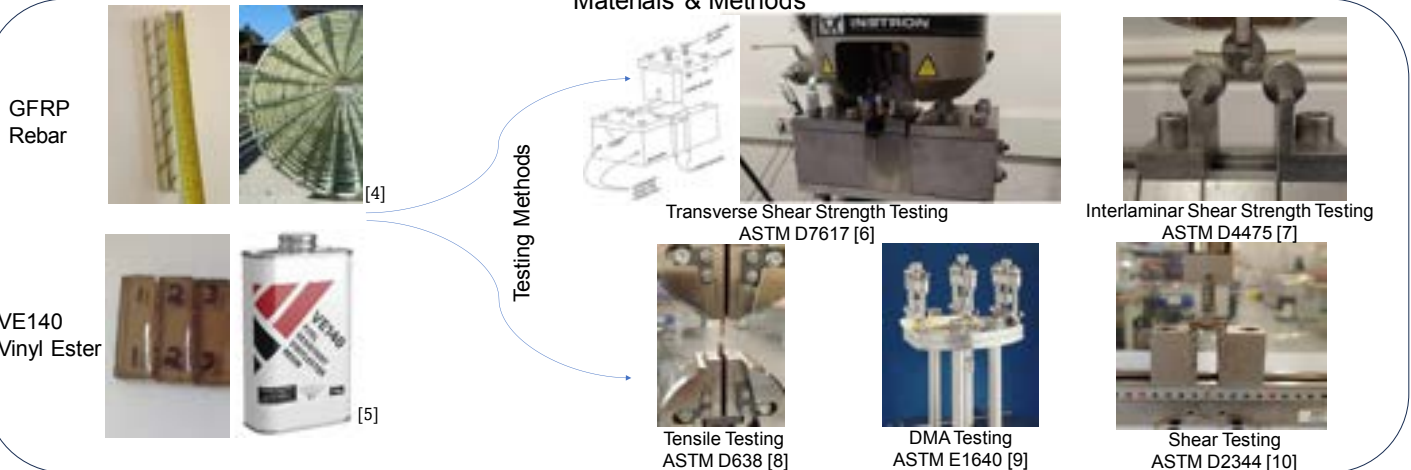
Steel corrosion is the leading cause of degradation for concrete structures near saline environments. It can lead to brittle catastrophic failures and collapses, reducing the structural expected service life. The cost of corrosion for most developed European countries is estimated to be approximately 4-5% of the gross national product [1]. For the UK, the cost of infrastructural repair between April 2015 and March 2021 is about £10.3 billion [2]. What if alternative materials were used to reinforce concrete structures that don't corrode? Why not consider FRP rebars?

This project investigates how glass fiber-reinforced polymer (GFRP) bars used in concrete structures degrade in marine environments. The project examines both the resin and GFRP samples to understand how each component and their composite behaviour deteriorates with exposure time, particularly focusing on interactions at the fiber-matrix interfaces. Accelerated aging is simulated with high temperatures and direct immersion in a saline solution containing sodium chloride and sodium sulfate. Resin samples are tested for tension, shear, and Tg analysis through Dynamic Mechanical Analysis (DMA), and GFRP bars for transverse and interlaminar shear strength after 15 and 30 days of exposure. Moisture uptake is also measured to link it with mechanical degradation. The study finds that resin samples degrade faster in tensile strength initially due to moisture uptake, while transverse shear strength degradation in GFRP bars increases steadily with exposure time. The correlation between resin and GFRP degradation suggests shear testing of resin could assess FRP bar degradation. These results offer insights for developing a durability test protocol for FRP bars in saline environments.

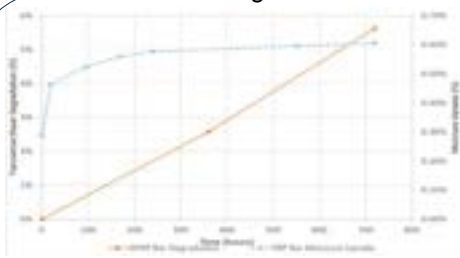


[3]

## Materials & Methods



## FRP Testing Results

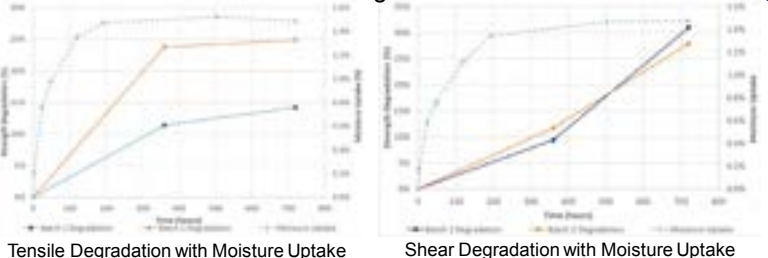


Transverse Shear Degradation with Moisture Uptake



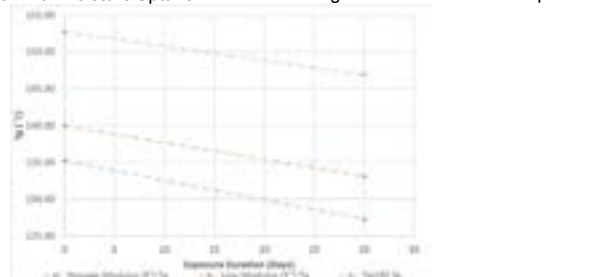
Interlaminar Shear Mode of Failure

## Resin Testing Results



Tensile Degradation with Moisture Uptake

Shear Degradation with Moisture Uptake



Tg Decrease with Saline Exposure

## References:

- [1] Pritchard, O., Hallett, S., & Farewell, T. (2013). Soil corrosivity in the UK – impacts on critical infrastructure. Infrastructure Transitions Research Consortium.
- [2] (2014). Maintaining strategic infrastructure: roads. Department for Transport and Highways Agency.
- [3] Composite TECH. (2024, February 28). Retrieved from <https://composite-tech.com/2023/10/24/world-experience-of-frp-rebar-use-the-new-era-of-construction-reinforcement/>
- [4] GFRP Rebars. (2024, February 28). Retrieved from SIREG. <https://www.sireg-usa.com/gfrp-rebars/>
- [5] VE140 Fuel Resistant Vinyl Ester Resin. (2024, February 28). Retrieved from EasyComposites. <https://www.easycomposites.co.uk/>
- [6] ASTM D7617M – 11 Standard Test Method for Transverse Shear Strength of Fiber-Reinforced Polymer Matrix Composite Bars
- [7] ASTM D4475 – 21 Standard Test Method for Apparent Horizontal Shear Strength of Puttuded Reinforced Plastic Rods By the Short-Beam Method
- [8] ASTM D638 – 22 Standard Test Method for Tensile Properties of Plastics
- [9] ASTM E1640 – 23 Standard Test Method for Assignment of the Glass Transition Temperature By Dynamic Mechanical Analysis
- [10] ASTM D2344M – 22 Standard Test Method for Short-Beam Strength of Polymer Matrix Composite Materials and Their Laminates



# Failure Analysis of Hybrid Laminates under Impact Using 2D Axisymmetric Model

An Chen, Xun Wu, Luiz Kawashita, Michael Wisnom

## Background

- Carbon laminates are vulnerable to through-thickness impact loading due to low strain to failure.
- Hybrid laminates composed of carbon and high strain fibres such as glass have better impact performance.
- However, the underlying mechanism for the improvements are not well understood.
- Here an efficient 2D axisymmetric model is established to simulate the response of hybrid laminates against quasi-static indentation for the aim of understanding the factors controlling the response as well as the detailed damage mechanism under low-velocity impact.
- The preliminary prediction of baseline CFRP laminate using the axisymmetric model is shown below to show the potential of this method.

## Method & Results

The model represents half of the through-thickness cross section of the test

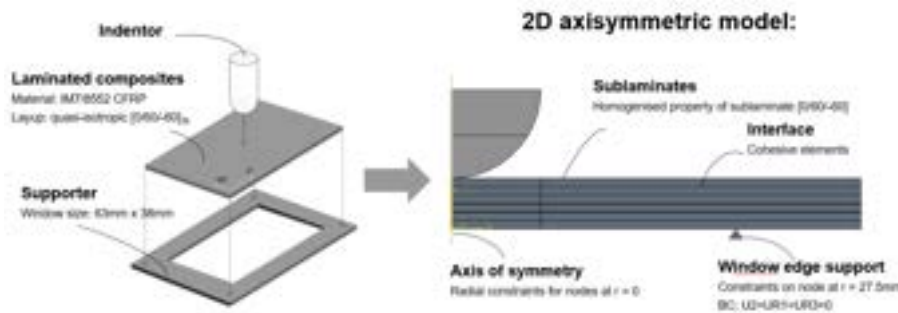


Figure.1 The schematic diagram of quasi-static indentation test (left) and the 2D axisymmetric model (right)

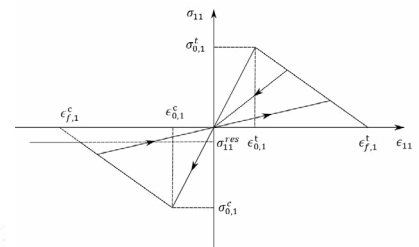


Figure.2 Material longitudinal response

### Accurate global response prediction

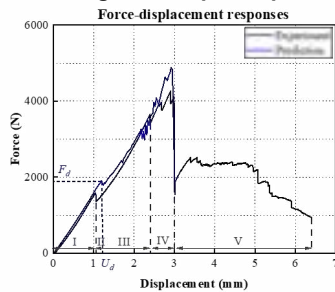


Figure.3 Load-displacement curves of baseline carbon laminate

### The predicted local delamination correlates well with experiment

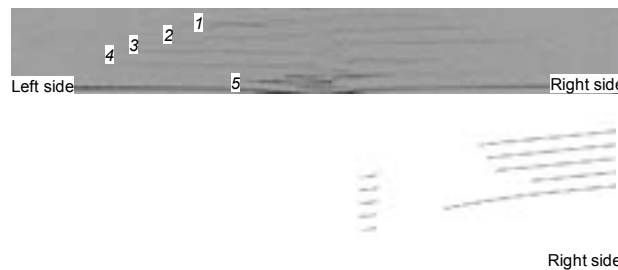


Figure.4 Delamination pattern from experiment (top) and from prediction (bottom) at displacement 2.75mm

Table.1 Delamination length at displacement 2.75mm

Interface No.	Exp avg [mm]	Model [mm]
1	4.7	6.5
2	6.6	6.7
3	8.9	7.1
4	7.2	9.0
5	4.6	3.4

### Delamination influences fibre loading state

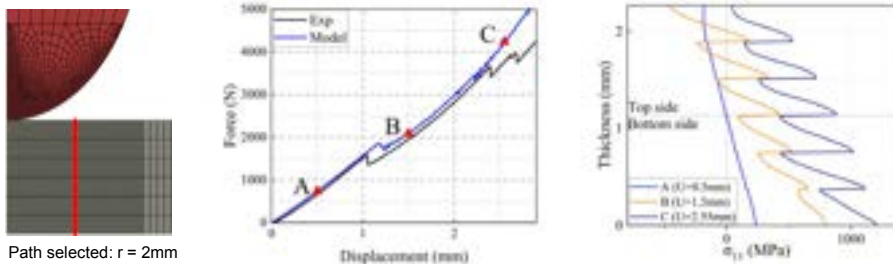


Figure.5 Through-thickness variation of  $\sigma_{11}$  at critical displacements

Along with delamination propagation, the compressive load at some upper plies changed to tensile load at large displacement.

## Conclusions:

- 2D axisymmetric model is particularly efficient in the analysis of local events like penetration and it can reduce the high computational cost presented in the state-of-the-art 3D impact modelling.
- Failure analysis shows one effect of delamination is that at large displacement, the impact force is reacted to a larger extent by membrane rather than shear forces, putting more of the laminate into tension/compression in pure bending.

# Second-order homogenisation of 3D woven composites using shell elements

**Athira Anil Kumar, Aewis K. W. Hii, Bassam El Said, Stephen R. Hallett**

3D woven composites have become increasingly popular due to improved mechanical properties, near net shape and reduced manufacturing costs. However, their internal architecture presents complex challenges in the computational modelling, with multiple length scales. To tackle this problem, users are employing computational homogenisation techniques to address the impracticality of high-fidelity (HF) models. The classical first-order homogenisation framework (1OH), although well-established, fails to properly capture the complex coupling (extension-bending) observed in woven composites. The higher-order deformation modes, such as bending and twisting, along with the effects of strain localisation from the structural model can be accounted for in a second-order homogenisation (2OH) scheme. This work focuses on implementing a second-order thick shell homogenisation framework<sup>[1]</sup> for woven composites and comparing the results with 1OH and high-fidelity models through 4-point bending (4PB) and short beam shear (SBS) tests. The 4PB test demonstrates the effectiveness of the framework in scenarios where bending loads are predominant, while the SBS test highlights its limitations in capturing through-thickness stress variations.

## Homogenisation Frameworks

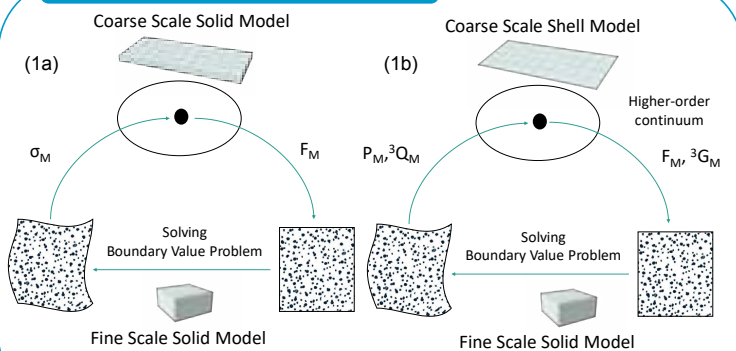


Figure 1: (a) First-order, and (b) second-order computational homogenisation framework

## Weave Models

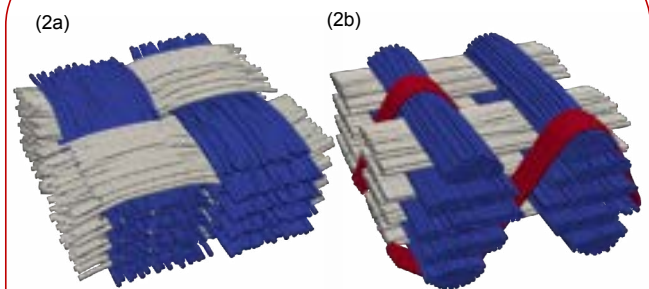


Figure 2: (a) Multi-layer plain weave and (b) 3D orthogonal weave configuration built in SimTex

## 4-Point Bending (4PB) Test

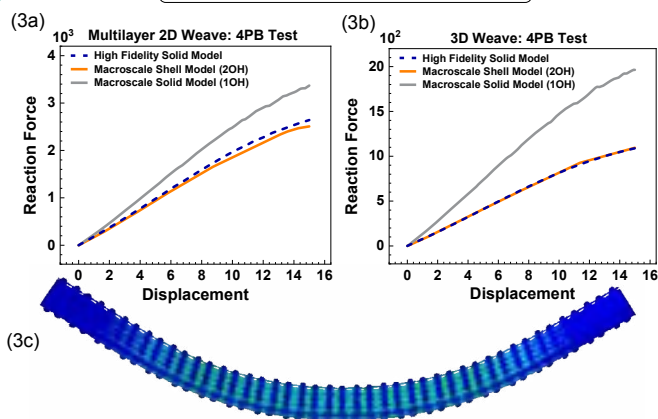


Figure 3: 1OH, 2OH and high-fidelity force-displacement responses for (a) a multi-layer plain weave model and (b) a 3D orthogonal weave model undergoing 4PB test (c) 4PB response of a high-fidelity 3D orthogonal weave model (yarn elements) is also shown.

## Short Beam Shear (SBS) Test

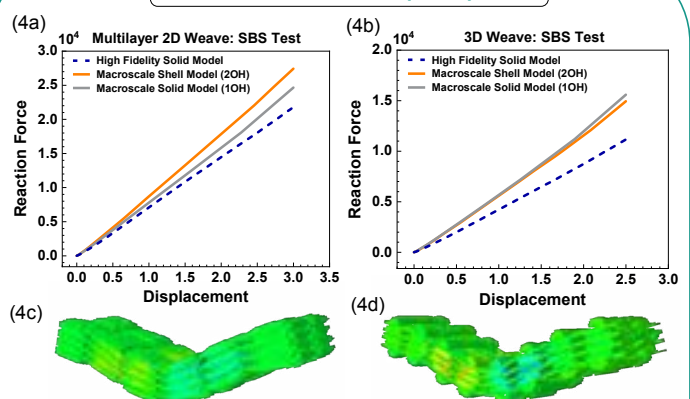


Figure 4: 1OH, 2OH and high-fidelity force-displacement responses for (a) a multi-layer plain weave model and (b) a 3D orthogonal weave model undergoing SBS test.

The through-thickness variability of transverse shear stress captured in the (c) multi-layer 2D and (d) 3D weave yarn elements are also shown.

## Future Work

- Development of a second-order homogenisation framework using solid elements.
- Explore the use of machine learning (ML) techniques to replace the fine-scale analysis with an ML model.

[1] Aewis K.W. Hii, Bassam El Said, A kinematically consistent second-order computational homogenisation framework for thick shell models, Computer Methods in Applied Mechanics and Engineering, Volume 398, 2022.



# Natural Material WrapToR Trusses for Sustainable Structural Solutions

Matthew Lillywhite

Trusses are incredibly efficient structures which exploit structural scaling laws to maximise the performance of small amounts of material. The Wrapped Tow Reinforced (WrapToR) truss manufacturing method creates highly efficient truss beams rapidly on low cost machinery. This project seeks to use this process to create truss structures from natural materials, for example bamboo longitudinal members wrapped with natural fibres to create a new class of sustainable solutions for civil engineering and infrastructure applications.

## Natural Materials

Materials sourced from the natural world that require little to no human intervention to make them usable.

Lower Material Cost

Lower Environmental Impact

Worse Mechanical Properties

Shape and Property Variation

## WrapToR

Manufacturing process for composite trusses that wraps chord members in a wetted composite tow to produce a rigid truss structure once cured.

Produces Highly Structurally Efficient Trusses

Low Input Energy Manufacture Method

Requires Adaption For Natural Material Variable Geometry

## Modelling, Structural Analysis and Optimisation

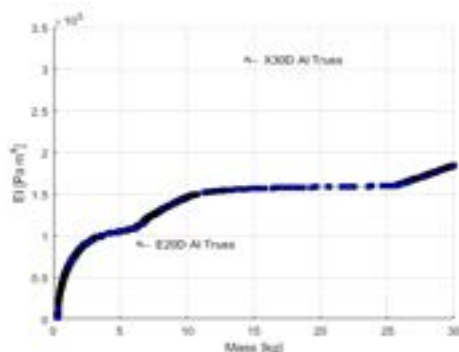
Design space exploration and optimisation to determine influential truss parameters; behaviour unique to natural materials in WrapToR; and the trade-offs between performance, environmental impact and cost.

### Mass vs Bending Rigidity (EI)

Pareto Optimal Configurations

4m span - bamboo/glass fibre truss.

Commercial Aluminium Truss Values Included



## Production of Natural Material WrapToR Trusses



Manufacture and testing prototype trusses to validate models and determine areas of improvement in manufacture process.

## Adaption of WrapToR Process for Natural Materials

Updating the WrapToR auto-winder to account for variable surface geometry of chord members.



New Mandrel Design



Finding effective methods of adhesive surface preparation for bamboo culms

## Local Reinforcement

Locally reinforcing weak adhesive joints at WrapToR nodes to help address bonding difficulties with bamboo and improve performance whilst limiting mass increase.



# Modelling of GATOR Panels as a Fairing for Folding Wingtip Joints

Student: Nuhaadh Mahid

Supervisors: Dr Benjamin Woods, Dr Mark Schenk, Dr Branislav Titurus

## 1. Background

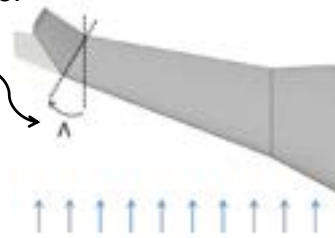
### Semi-Aeroelastic Hinge

Extended wingspan in flight, folded wingtip when approaching airport gate.

Flare angle helps to alleviate gust load. [1]

A morphing fairing needed to cover the hinge joint.

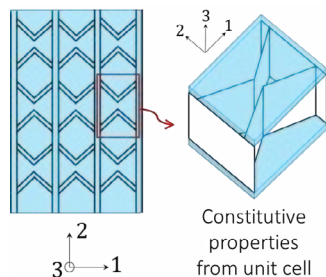
The objective is to design a fairing with low torsional stiffness and low cross-section warping as the wingtip folds.



## 2. Modelling Fairing

Morphing sandwich panel with cellular core and elastomeric facesheets for fairing. [2]

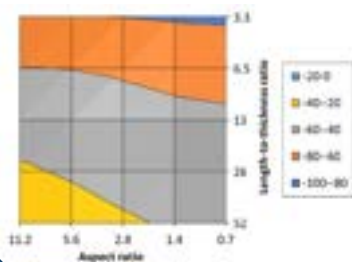
Homogenisation of panel elastic properties to equivalent shell stiffness matrix.



## 3. Equivalent Core Properties

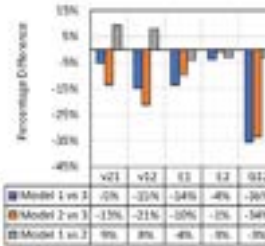
**Analytical homogenisation:** Cell walls modelled as shear deformable beams.

**FE homogenisation:** Unit cell modelled with periodic boundary conditions.



Error increases as wall geometry deviates from beam assumptions.

## 4. Chevron-Facesheet Interaction



Comparison of three models:  
1. Analytical homogenised core + Laminate theory  
2. FE homogenised core + Laminate theory  
3. FE homogenised panel

### Model 1 vs 2:

Reduced error relative to isolated core. Facesheet contribution to stiffness more significant.

### Model 2 vs 3:

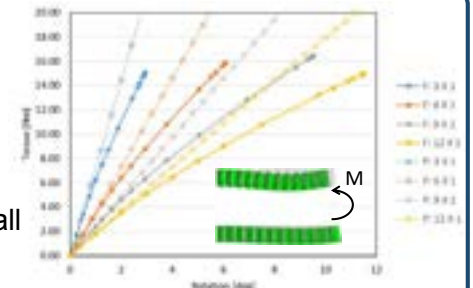
Higher stiffness in FE approach due to non-uniform strain on facesheet. This is not captured in the analytical approach.

## 5. Shell Model vs Full-Scale Model

Initial shell response match well with full-scale models.

Shell model is valid only for small rotation angles.

Shell stiffness needs to be updated based on the strain state of the element (e.g., FE<sup>2</sup> method).



## 6. Conclusions

Significant error in the analytical equivalent stiffness of the core as the walls deviate from beam assumptions.

Effects of chevron-facesheet interaction significant in the stiffness of the panel.

Shell models with equivalent elastic properties of the plate is only valid for small deformations.

Equivalent stiffness of the shell elements need to be updated as the plate deforms.

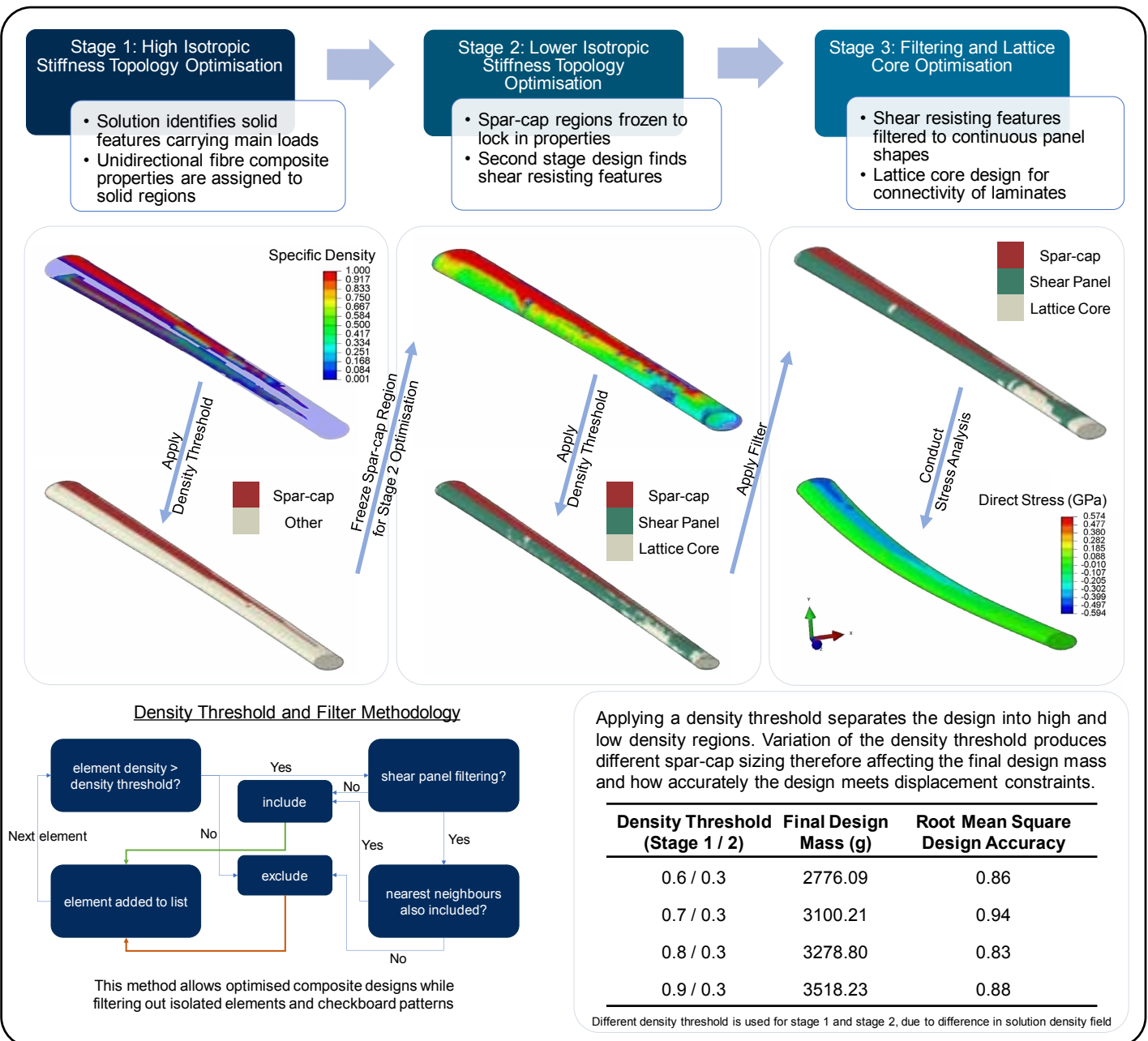
[1] A. Castrichini, V. H. Siddaramaiah, D. E. Calderon, J. E. Cooper, T. Wilson, and Y. Lemmens, "Preliminary investigation of use of flexible folding wing tips for static and dynamic load alleviation," *The Aeronautical Journal*, vol. 121, Art. no. 1235, Nov. 2016.  
[2] B. K. S. Woods and R. M. Heeb, "Design principles for geometrically anisotropic thermoplastic rubber morphing aircraft skins," *Journal of Intelligent Material Systems and Structures*, vol. 34, pp. 29-46, May 2023.



# Don't Overthink It: Intuitive Composite Design Utilising Isotropic Topology Optimisation

Alex Moss, Ajit Panesar, Terence Macquart, Peter Greaves, Mark Forrest, Alberto Pirrera

Topology optimisation is a useful tool for generating structural designs. Using Solid Isotropic Material & Penalisation (SIMP) topology optimisation, a density-based method, composite designs can readily be produced without the significant computation time usually required for anisotropic solvers. For aircraft wing or wind blade structures, the solutions often feature spar-cap type structures to resist the bending loads, indicating an optimal location for primary reinforcement. Similarly, shear resisting features can be found through an additional topology optimisation stage, by freezing the spar-cap regions with unidirectional fibre properties assigned. This methodology allows optimised and importantly, manufacturable composite laminate design.







# Optimisation of multi-rotor wind turbines for reduced cost of energy and environmental impact

Abdirahman Sheik Hassan, Dr Neha Chandarana, Dr Rainer Groh, Dr Terence Macquart

The scaling trends for the current design paradigm of single-rotor wind turbines has led to an increase in composite materials heading to landfill, as well as diminishing returns on levelised cost of energy (LCoE). Multi-rotor wind turbines (MRWTs) show a great deal of promise in reducing LCoE through their advantageous scaling laws, while facilitating the use of more sustainable materials. **This work aims to evaluate the economic viability and environmental impact (EI) of MRWTs against existing baselines – generating designs through bi-objective optimisation and utilising aeroelastic modelling software to comprehensively assess performance.**

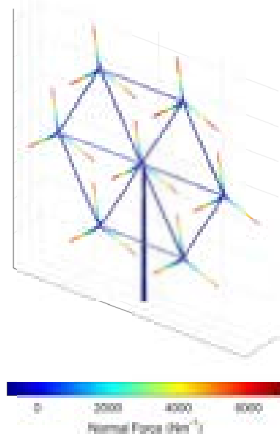
## BACKGROUND

- MRWT designs have existed since the 1930s
- Early models faced vibration and control issues [1]
- Resurfaced in the early 2010s through the INNWIND project
- Commercialisation underway by several start-up companies
- Existing MRWT literature hints at beneficial scaling laws but lacks comprehensive design studies and reliable quantification of MRWT's economic and environmental benefits**

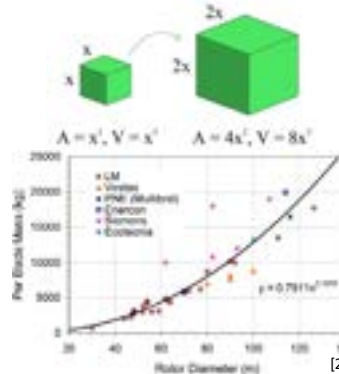
## MODELLING APPROACH

An updated version of our in-house software (**ATOM**) will serve as the foundation for the planned design and optimisation studies, providing **coupled aero-servo-elastic analysis** capabilities.

- Current work focusses on developing and validating the updated aeroelastic software
- Existing code is being restructured to allow for the **rapid exploration of the design space**
- Fully realised, the software will optimise for LCoE and EI on both the local (blade and frame cross-section) and global (rotor number and configuration) levels

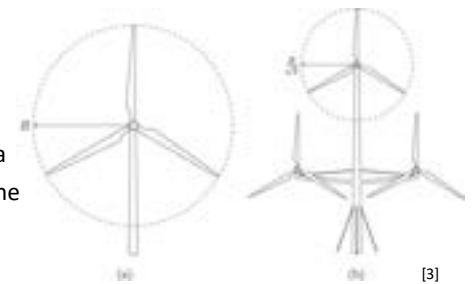


## MOTIVATION 1 – REDUCED COST OF ENERGY



- Single rotors reduce LCoE by lengthening blades to increase power
- This is constrained by the **square-cube law**
  - $Power \propto R^2$
  - $Cost \propto Mass \propto R^{2.1-3}$
  - $LCoE \sim \frac{Cost}{Power}$
- Causes disproportionate mass increase, and diminishing returns on LCoE

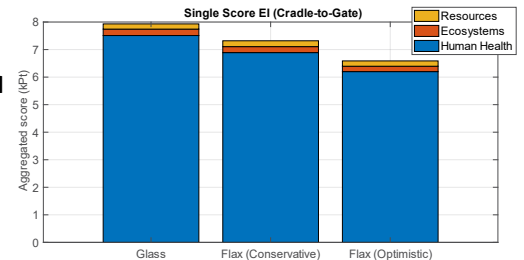
MRWTs arrange several smaller rotors on one structure, **reducing the mass** over a single rotor of equivalent swept area **by up to  $\frac{1}{\sqrt{n}}$**  where n is the number of rotors – thus **saving on LCoE**



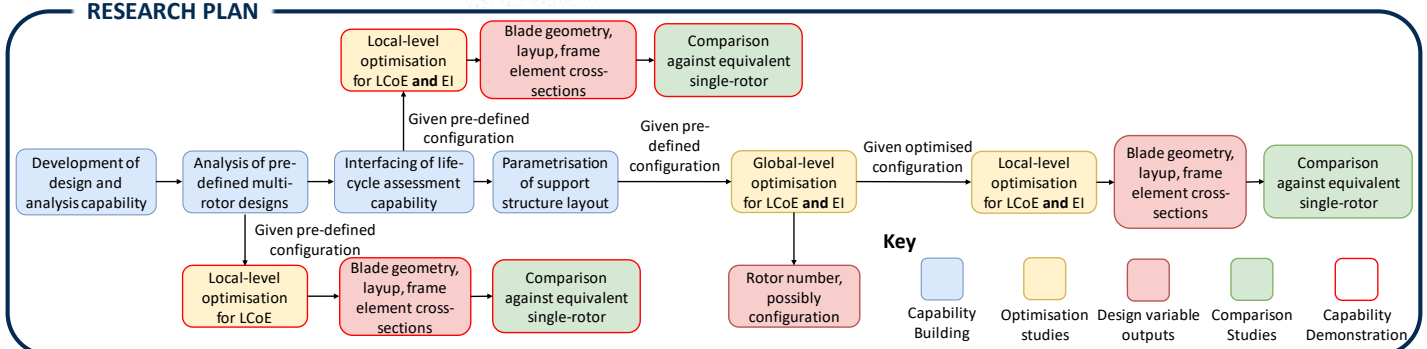
## MOTIVATION 2 – REDUCED ENVIRONMENTAL IMPACT

- Bio-composites** may be implemented in wind turbine blades to reduce the life cycle environmental impact (EI)
- The loads incurred by the size of modern blades result in a greater mass of required bio-composite material, giving **comparable impacts to standard glass fibre blades**
- The below figure illustrates this effect in flax-fibre blades

MRWTs use smaller blades which experience **reduced individual blade loads** – improving the potential to apply sustainable materials



## RESEARCH PLAN



## References:

- Brandon N Owens. The Wind Power Story: A Century of Innovation that Reshaped the Global Energy Landscape, First Edition. 2019.
- Crawford, C. A. (2011). "The Path from Functional to Detailed Design of a coning rotor wind turbine concept". In: Proceedings of the Canadian Engineering Education Association (CEEA). <https://doi.org/10.24908/pceea.v010.3768>
- Oliver Tiederad Filsoof et al. (Aug. 2021). "On critical aeroelastic modes of a tri-rotor wind turbine". In: International Journal of Mechanical Sciences 204. doi: 10.1016/j.ijmecsci.2021.106525.

# A study of factors controlling the compressive behaviour of hybrid composites

Aree Tongloet, Xun Wu and Michael R. Wisnom

## Introduction

- Hybrid composites have been studied to improve the mechanical properties of the composites.
- The compressive failure mechanism of the hybrid composites is not well understood.

## Aim of the study

- To investigate the failure characteristics of the selected hybrid composites.
- To investigate the possible factors controlling the failure characteristics of hybrid composites.

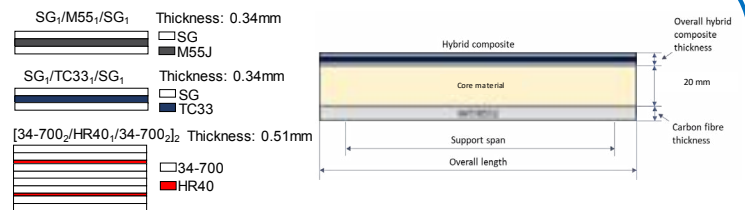
## Experiment

- Perform static 4-point flexural test on 3 different hybrid configurations on sandwich beam
  - High modulus M55 carbon fibre/S-glass
  - High strength TC33 carbon fibre/S-glass
  - HR40 carbon fibre/34-700 carbon fibre
- Observe the failures on each configuration



4-point flexural test

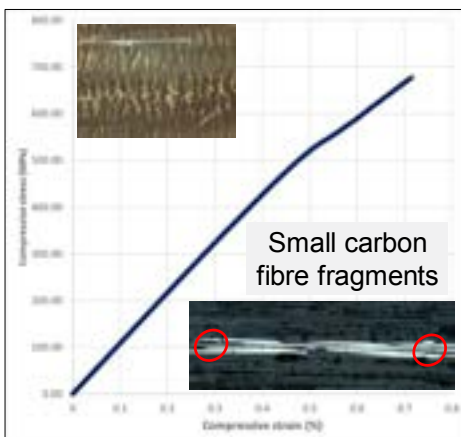
## Specimen configuration



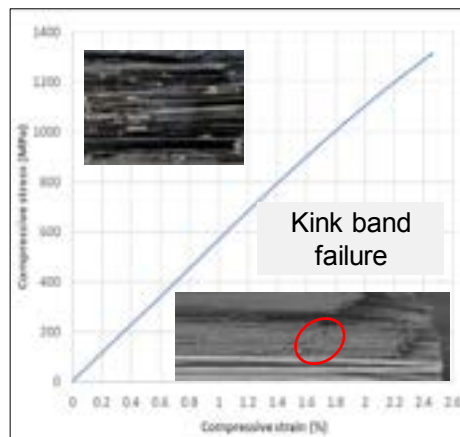
Fibre	Fibre modulus (GPa)	Failure strain (%)	Ply thickness (mm)
M55J	540	0.318	0.03
TC33	230	1.500	0.03
34-700	234	1.427	0.06
HR40	390	0.584	0.015
S-glass	88	3.870	0.155

## Results

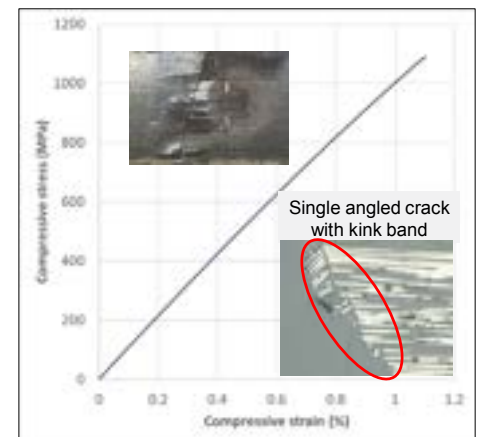
### SG<sub>1</sub>/M55<sub>1</sub>/SG<sub>1</sub>



### SG<sub>1</sub>/TC33<sub>1</sub>/SG<sub>1</sub>



### [34-700<sub>2</sub>/HR40<sub>1</sub>/34-700<sub>2</sub>]<sub>2</sub>



## Experiment summary

- Each hybrid system in this study created different failure characteristics; the M55/S-glass hybrid composite resulted in small fibre fragments in the carbon fibre layer, but kink band failure occurred for TC33/S-glass and HR40/34-700 hybrid composites.
- The failure compressive strain of lower-strain material was improved with the hybridisation concept.

## Future work

- Study another hybrid system to observe the failure characteristics of the material under compressive loading (HR40/S-glass).



# Modal Nudging and Elastic Tailoring for Blade-Stiffened Wing Structures

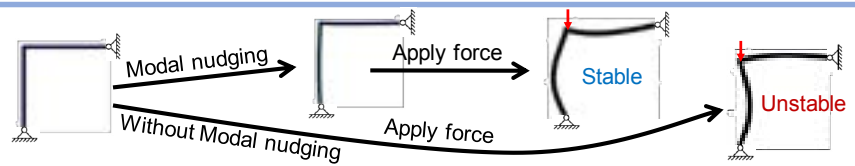
Lichang Zhu, Rainer Groh, Mark Schenk, Jiajia Shen and Alberto Pirrera

## Abstract

Modal nudging is a structural design technique [1] which can improve the post-buckling response of slender or thin-wall structures without any significant increase in mass. It enhances control over the post-buckling behaviour to increase load-carrying capacity or reduce imperfection sensitivity. Modal nudging changes the geometry of all surfaces of a structure. This work generalises the concept for application to thin-wall structures with geometry constraints and investigates its robustness to the presence of random imperfection.

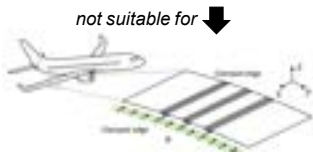
## What is modal nudging?

Modal nudging exploits stable post-buckled solutions to alter the baseline geometry of the structure, thereby favouring the seeded post-buckling response over potential alternatives.



## Current Work

Modal nudging changes both upper and lower surfaces (exaggerated nudge: actual nudge imperceptible).  
not suitable for

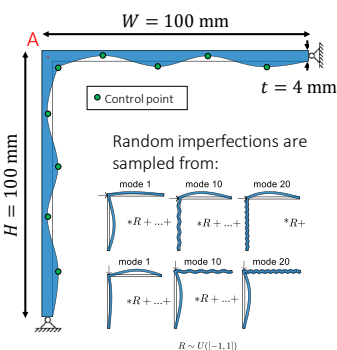


The outer geometry is constrained by aerodynamics.

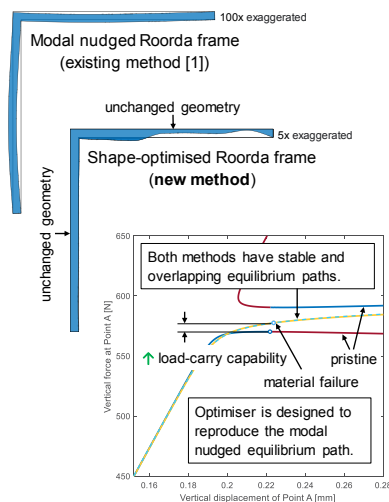
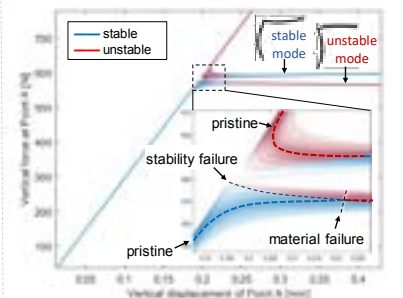
**New method:** use shape optimisation to achieve modal nudging under a constrained outer geometry.

First study a 2D *Roorda frame* which captures the essence of a nonlinear structure with two post-buckling modes to establish efficacy and robustness.

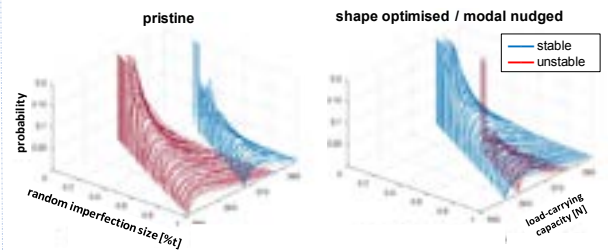
Inner surface is defined by control points.



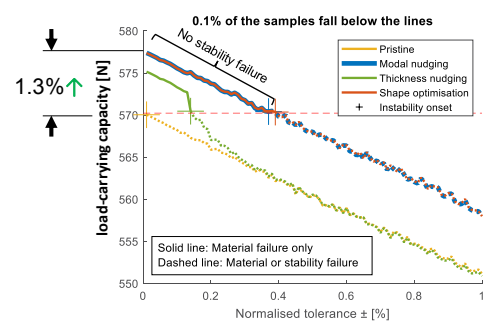
## Equilibrium paths with imperfections.



## Imperfection sensitivity analysis.



Pristine Roorda frames' load-carrying capacity show bimodal distribution where **unstable mode** dominates **stable mode**; shape optimisation and modal nudging allow **stable mode** to dominate and delay **instability**.



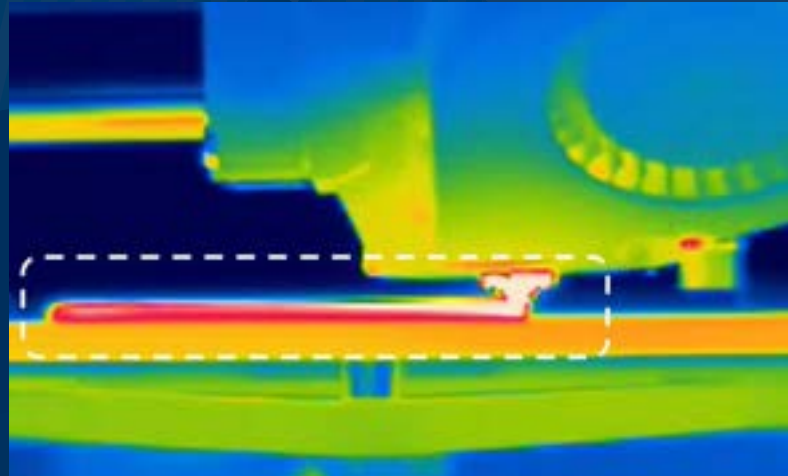
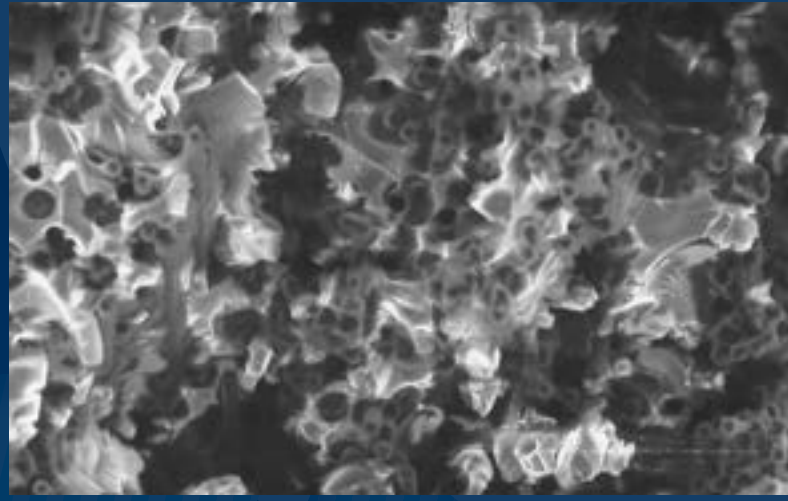
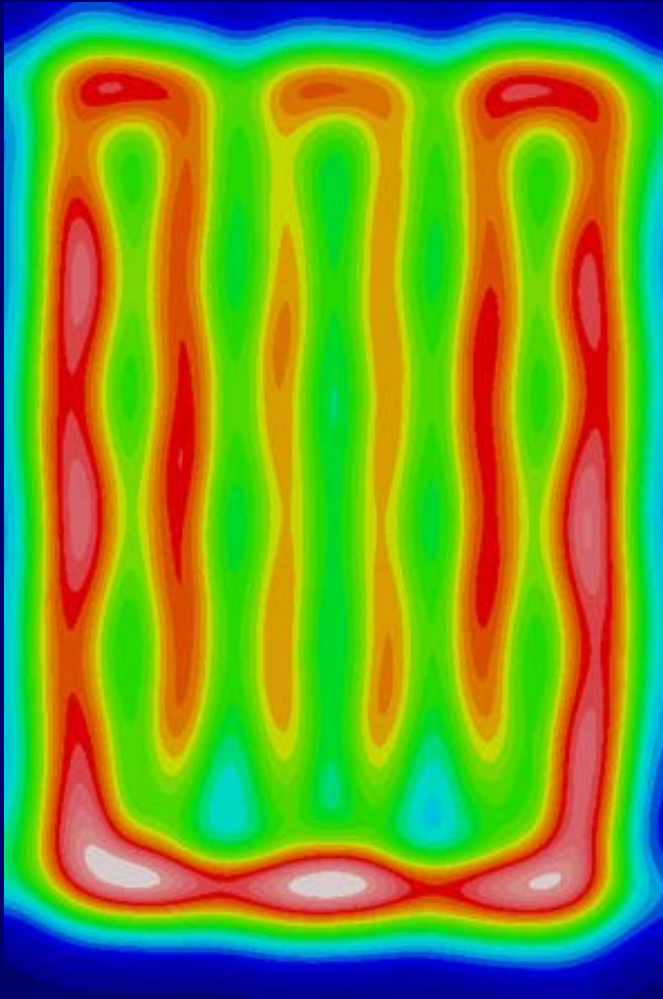
**Conclusions:** Successfully increased the load-carrying capacity and eliminated the risk of instability on design with geometric constraints. The method is robust, provided that specific manufacturing tolerances can be achieved.

## Future Work

Future work involves applying the shape optimisation method to blade-stiffened panels and verifying its effectiveness through imperfection sensitivity analysis.

## Bibliography

- [1] Cox, B. S., Groh, R. M. J., Avitabile, D., & Pirrera, A. (2018). Modal nudging in nonlinear elasticity: Tailoring the elastic post-buckling behaviour of engineering structures. *Journal of the Mechanics and Physics of Solids*, 116, 135–149.
- [2] Cox, B. S., Groh, R. M. J., & Pirrera, A. (2019). Nudging Axially Compressed Cylindrical Panels Toward Imperfection Insensitivity. *Journal of Applied Mechanics, Transactions ASME*, 86(7).



# MANUFACTURING AND DESIGN



# Generation and Characterisation of Wrinkles in an AFP Representative Experiment Setup

Ege Arabul, Vincent Maes, Rob Hughes, James Kratz

## Summary:

A novel experiment was developed to establish a relation between tension and wrinkling, where realistic wrinkles of varying fibre orientations, amplitudes and wavelengths were achieved. The wrinkled layers were combined to form a quasi-isotropic laminate containing multiple defects and the wrinkle's evolution to post-cure waviness was analysed.

## Experiment Setup

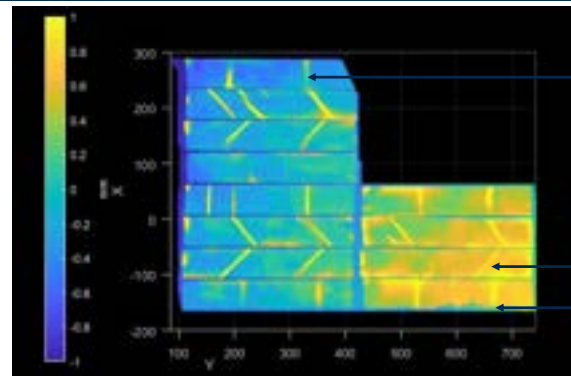
Longer, tensioned composite ply  
Shorter, applied composite ply



Tensile testing clamps

Backplate with tactile sensor

Experiment setup where tension is applied to the initial layer and released, causing wrinkling

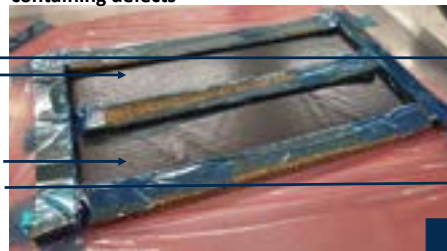


Laser scan of wrinkles before combining individual layers to form the quasi-isotropic laminate containing defects

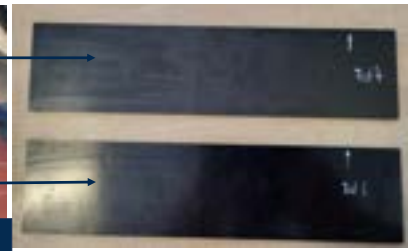
## Generating the wrinkles:

The experiment involved applying tension to a ply of composite prepreg, representative of its state during AFP deposition. While the first ply was under tension, a secondary ply was applied to the initial layer using a backplate and roller. The initial tension was then released, where the excess material length caused wrinkling within the scale of 0.1-0.5 mm.

Control Laminate (No defects)  
Sample containing multiple defects



Quasi-isotropic laminates after debulking, before autoclaving

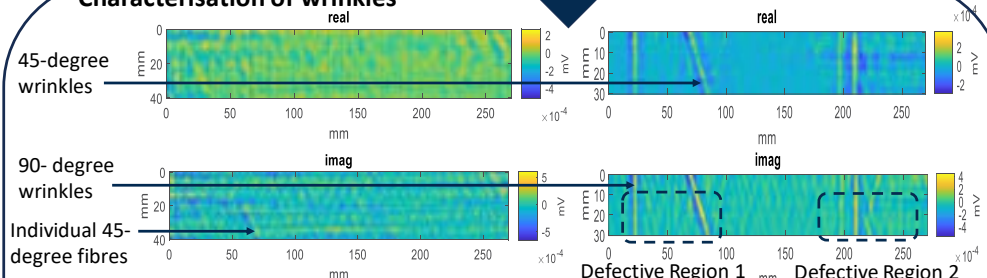


Composite laminates after autoclaving and trimming

## Characterising the Wrinkles:

The wrinkled layers were combined into a quasi-isotropic laminate and cured using an autoclave, and the post-cure waviness was characterised using eddy current sensors and section analysis. Both evaluation techniques could detect the waviness within the material, verifying the experimental methodology.

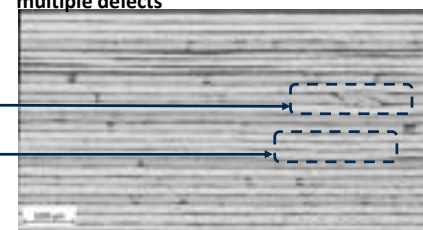
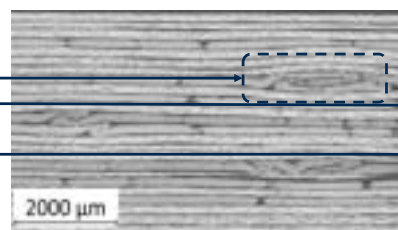
## Characterisation of wrinkles



Eddy-current scan of the control sample

Eddy-current scan of the sample containing multiple defects

45-degree wrinkle  
90-degree wrinkle  
0-degree in-plane waviness



Side-profile micrograph of defective region 1 Side-profile micrograph of defective region 2

## Future Work:

Subsequent studies will focus on implementing the theory to AFP deposition scenarios, in-line characterisation of defects, and control approaches for defect rectification.





# Digital twinning for faster, higher quality manufacture of composites

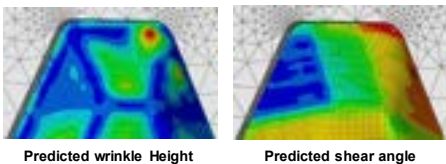
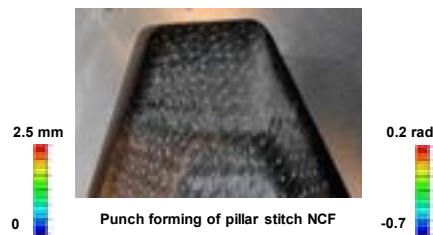
Siyuan Chen, Adam Thompson, Tim Dodwell (Exeter University), Stephen Hallett and Jonathan Belnoue

The utilisation of dry non-crimp fabric (NCF) and liquid composite moulding (LCM) processes is gaining prominence. Despite being a cost-effective and environmentally friendly alternative to conventional prepreg/autoclave methods, this technique poses unique challenges. One significant obstacle is the handling of NCF materials during the preforming stage, where the dry fabric is shaped to fit the 3D mould. Severe fabric defects like wrinkling could happen in this stage, highly affecting part strength and compromising design tolerances. Furthermore, material variability of the preform affects the wrinkling by altering the stress distribution.

The project aims at developing a digital twin for the fabric forming, that conducts real-time measurement, optimisation and adjustment to achieve zero-wrinkle forming process irrespective of the material variability. At the proposed framework the core is a Gaussian process (GP) emulator trained by finite element (FE) simulations, which makes real-time predictions and optimisation once trained.

## 1. FE simulator

- Abaqus VUMAT subroutine: Hypodrape.
- Accurately describe the behaviour of **textile material** by isolating in-plane shear and out-of-plane bending.
- Capture the **wrinkles** generated during forming.
- Accurate but CPU-intensive.

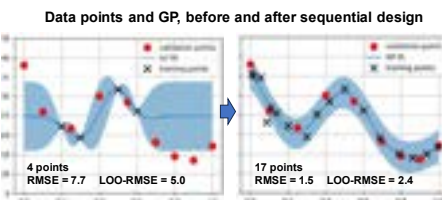


## 2. Gaussian Process (GP) emulator

- A **machine learning method** (surrogate model) that is mathematically tractable.
- Trained based on the data from the simulator.
- Suitable to small dataset. Natural ability for **uncertainty quantification**.
- **Input:** position and magnitude of tensioners.  
**Output:** overall wrinkle magnitude.

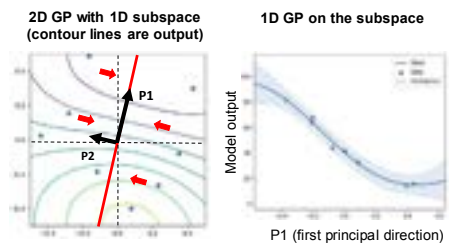
### Sequential design (active learning)

- Iterative addition of data points, to improve model predictive capabilities efficiently.
- More efficient than one-shot sample design.



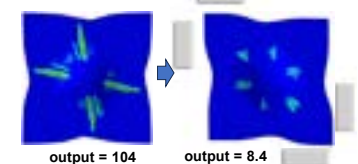
## Dimension reduction

- How can we optimise large problems that contain many **inputs** with only a **small dataset**?
- Method: active subspace.



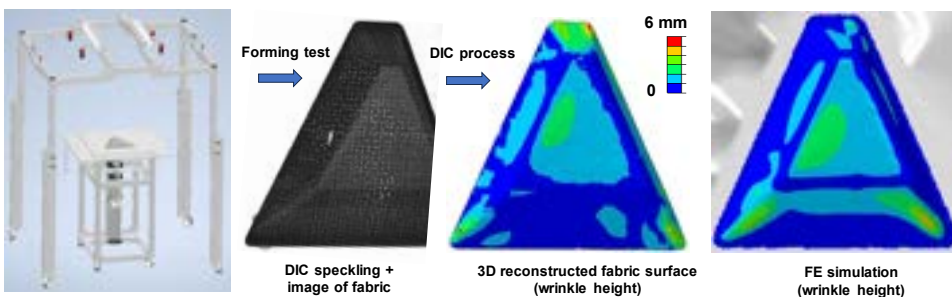
### Real-time optimisation: wrinkle eliminated

- 8 input parameters, only 100 data points used.



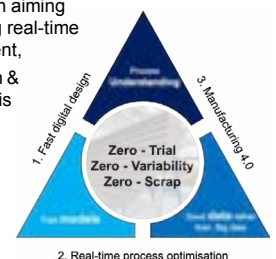
## 3. Forming cell, wrinkle monitoring and quantification in real world

- A forming rig instrumented with **four-camera DIC system**.
- Open-source DIC code DuoDIC used to **reconstruct the 3D surface** and the shear strain field on the fabric.
- Metrics developed to **quantify wrinkles**' severity.
- Measures **material variability** and quantify its effect on wrinkling.
- **Helps to understand the mechanism of wrinkling behaviour (macro and meso scale).**



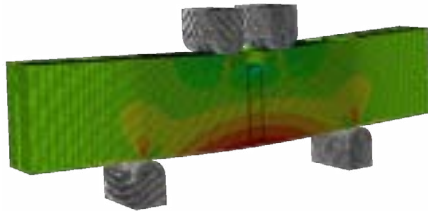
## Conclusions and future plans

- A GP emulator for the forming process was built, based on data generated from large physics-based computer models.
- Real-time optimisation realized using the GP emulator.
- A forming cell that monitors and quantifies real-world wrinkles was built.
- A digital twin aiming at achieving real-time measurement, optimisation & adjustment is on-going.



# Four point bend test of pultruded composite, investigation on the limits of the test method

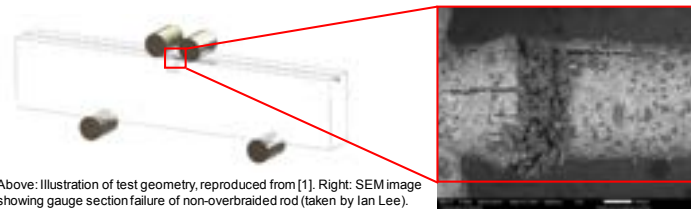
Nicolas Darras, Laura R. Pickard, Ian Lee, Dimitrios Bikos, Bohao Zhang, Gustavo Quino, David B. Anthony, Charlie Sharp, Curtis Wong, Tony Fan, Lucas Lu, Giuliano Allegri, Michael R. Wisnom, and Richard S. Trask



Science is based on facts, observation and analysis of data obtained during experiments in labs. It is, however, expensive to perform many tests by following a trial-and-error approach. Modelling those tests therefore becomes useful as it allows the users to get a first estimation of the possible output of an experiment.

These models are even more crucial when they tend to represent the complex behaviour of a system, as is the case with compression of Fibre Reinforced Polymers (FRP): the shear instability, the buckling, twisting and rotations resulting from compression loads are not trivial to predict. The present poster aims to investigate the behaviour of hierarchical pultruded rods in bending as well as the limits of the test performed.

## Single Rod Test



Above: Illustration of test geometry, reproduced from [1]. Right: SEM image showing gauge section failure of non-overbraided rod (taken by Ian Lee).

Prior work has shown that PMMA material was good enough for the cradle beam, supporting the load during a four point bend test, and transmitting the strain to the rod.

Material	Diameter	Volume fraction	Average strain	Average force (kN)
Carbon fibre - Epoxy resin rod*	0.8 mm	~55 %	-1.42 (± 0.2)	-5.0 (± 1.0)

\* EasyComposite, CFROD-08-1

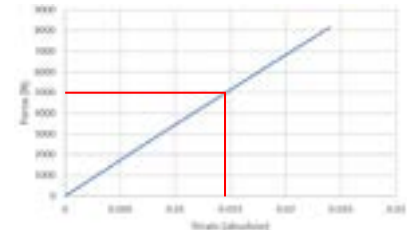
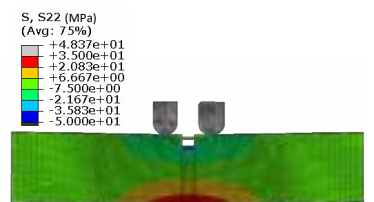
Preliminary tests showed that the specimens failed within the notch section.

## Single Rod Model

A finite element (FE) model has been made with two objectives:

- Check the strain in the rod
- Check the integrity of the beam structure

- Example: A load of 5 kN has a resultant strain of 1.42% for a carbon fibre – epoxy rod, experimental results matches modelling



Strain in the rod as a function of the load applied to the beam. All data have been gathered from the Finite Element model in Abaqus.

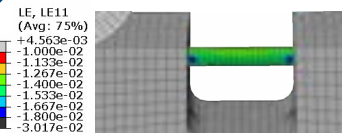
## Four Point Bend Test



Photograph: Four point bend test setup modified from ASTM2002 [1].

Applied load results in compression of the upper part of the beam and the rod.

A composite rod is bonded to PMMA beam and a digital image correlation (DIC) system is used to collect strain data.



Finite Element model showing the concentration of strain on the rod.



A cross-section of the overbraided rod after cure.

## Conclusions

After validation, the FE model shows:

- A strain concentration on the rod at the extremity of the notch.
- A tension at the base of the beam

Post cure analysis using computer tomography scanning indicates an improvement of the manufacture process is also required.

V2 beam design using an updated finite element model to predict the stress in the structure is in progress

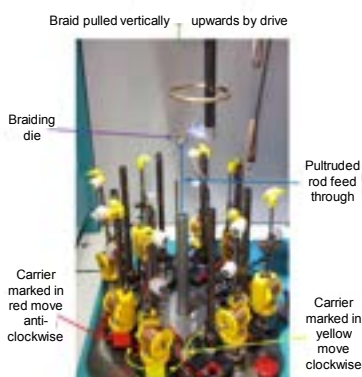


3D reconstruction of the sample scanned.

## Future Work

The overbraided fibres can be from a choice of fibres:

- Aramid, carbon, glass, Zylon™
- Or a combination of two (or more)



Photograph: Braider setup with tow overbraided rods.

Current design of the four point bend test's beam is not suitable for overbraided rods. A new beam design will be informed from FE analysis.

Overbraiding the rod might:

- Improve compressive strength
- Act like a spring and absorb energy
- Improve the interface rod/matrix
- Provide a hybrid effect



Photograph: A broken beam with an overbraided rod (post test).



# Quantifying Preform Defects in Large-Scale Aerostructures from Shopfloor Photographs

Umeir Khan, Vincent K Maes, Robert Hughes, James Kratz

Industrial Sponsors: Petar Zivkovic, Jon Wright, Turlough McMahon, Airbus

## THE PREFORMING BOTTLENECK

Resin Infusion of **Non-Crimp Fabrics (NCF's)** has demonstrated **rate-enabling capability** for delivering the next-generation of aircraft.



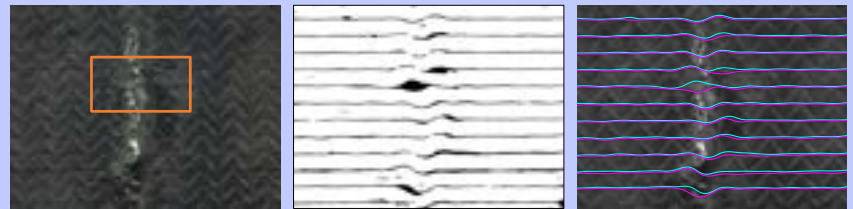
Image from Airbus

**Preforming** remains integral but can be subject to material and process variabilities – leading to **ply defects** (e.g. **waviness, wrinkling**).

## DEFECT ANALYSIS

**Aim: Assess part quality** of NCF preforms

Shopfloor photography is a **fast** and **cost-effective** inspection solution. Yet, current photo-based assessment remains **mostly qualitative**. **Applying Deep Learning** can enable **rapid waviness quantification**.



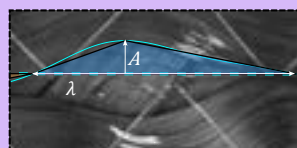
DSLR Photo-Capture

Tow / Gap Segmentation

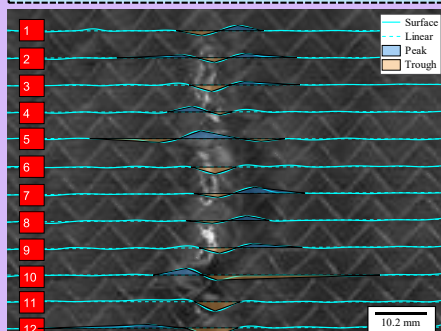
Waviness

## MAIN RESULTS – WAVINESS METRICS

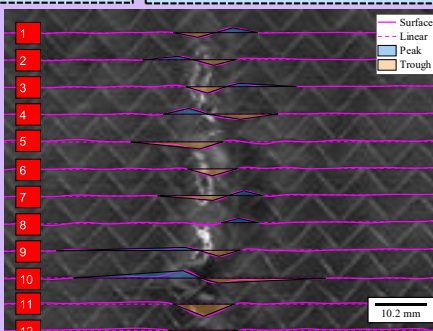
**The challenge:** Waviness along the upper and lower tow edges are not necessarily equal (e.g. intra-tow splitting). Therefore, characterisation (for each edge type) is needed. Both plots show peak / trough regions which flag as waviness (according to where the amplitude,  $A$ , exceeds a critical value,  $A_{crit}$ ).



Waviness if  $|A| \geq A_{crit}$   
( $A_{crit} = 0.5 \text{ mm}$ )



Desc: The **lower** edge waviness with highest amplitude occurs as a: **trough** in Tow 12 with  $A_{max} = 1.88 \text{ mm}$  ( $\lambda = 10.50 \text{ mm}$ )



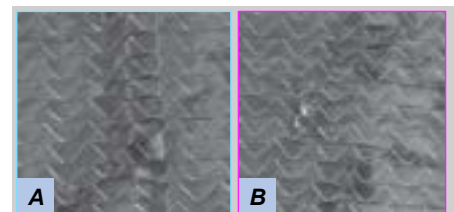
Desc: The **upper** edge waviness with highest amplitude occurs as a: **trough** in Tow 11 with  $A_{max} = 2.38 \text{ mm}$  ( $\lambda = 12.09 \text{ mm}$ )

## SUMMARY

Quantifying in-plane waviness by analysing shopfloor photographs was demonstrated, using a Deep-Learning based workflow.

This enabled preform defects in complex and industrially-relevant aerostructures to be reported on (at rates of up to 45s per photo).

## OUTLOOK: 2 PHOTOGRAPHS



Which shows higher defect severity?

# An investigation into the performance of aligned discontinuous carbon fibre reinforced composites (ADFRC) produced with the HiPerDiF 3G

Chantal Lewis<sup>1\*</sup>, Jonathan Meegan<sup>2</sup>, Mark Harriman<sup>2</sup>, Karthik Ram Ramakrishnan, Marco Longana<sup>3</sup>, Carwyn Ward<sup>4</sup> and Ian Hamerton<sup>1</sup>

<sup>1</sup>Bristol Composites Institute, University of Bristol

<sup>2</sup>Syensqo, Wrexham, UK

\*Chantal.Lewis@bristol.ac.uk

<sup>3</sup>"Giulio Natta" Department, Politecnico di Milano


<sup>4</sup>School of Engineering, UWE Bristol

## Introduction

Discontinuous fibre composites generally exhibit lower tensile properties when compared with their continuous counterparts. However, if the fibres are well aligned and longer than their critical length it is possible to maximise their mechanical properties while retaining the formability advantages short fibres already possess. This poster outlines how we have explored varying the parameters of the HiPerDiF 3G alignment process to manufacture composites with improved performance. The tensile performance of unidirectional ADFRC samples were compared with unidirectional continuous composite samples of similar constituent materials manufactured using the same manufacturing methods.

## Manufacture & testing


**1 HiPerDiF 3G machine**



Key process parameters:

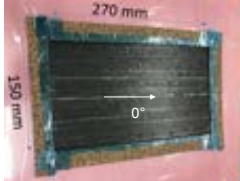
- Belt speed
- Fibre concentration
- Fibre Length (longer than critical length = improved stiffness)

**2 Impregnated roll**



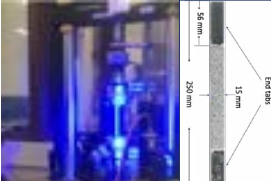
- CYCOM® resin, 36gsm
- Tenax® A HT C124 short fibres
- 30mm width, 50m length
- Resin impregnation process automated using HiPerDiF 3G

**3 Test panel manufacture**



- [C<sub>g</sub>] Unidirectional
- Prepreg tapes 30mm wide placed together during manual layup whilst minimising gaps and overlaps
- Autoclave cure for 120 mins @180°C

**4 Mechanical testing**

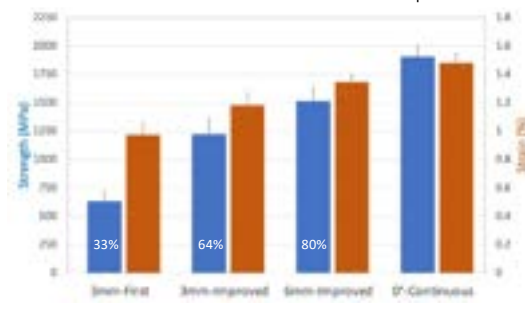
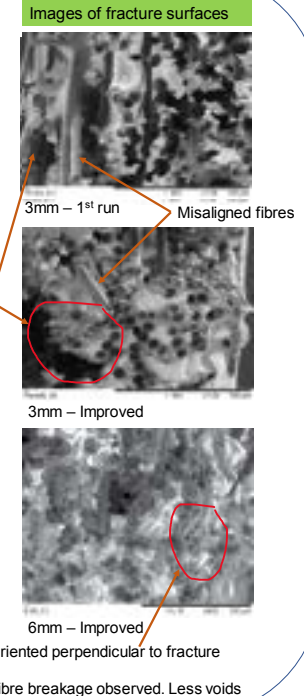
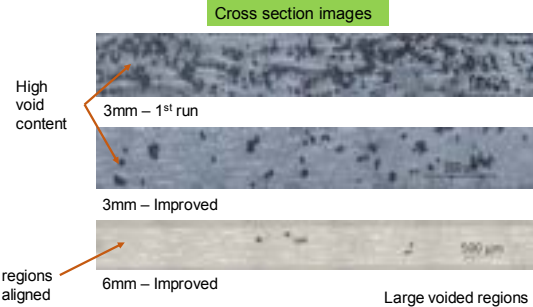
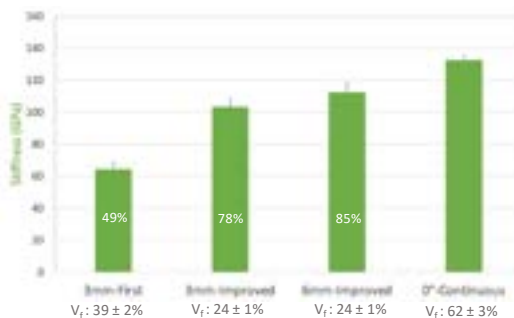


- 0° unidirectional tensile test using test method ASTM D3039/3039M
- Strain measured by Digital Image Correlation

## Results

Batch	HiPerDiF 3G input (key parameters)			Output
	Fibre Length (mm)	Fibre concentration (% w/v)	Belt speed	
1	3	0.006	Low	36
2	3	0.004	Med	21
3	6	0.004	Med	21

### Tensile test results



- Mechanical properties of ADFRC compared against unidirectional (UD) continuous samples of similar constituent materials.
- Stiffness and strength for all specimens normalised to 55% V<sub>f</sub>, highest achievable demonstrated previously by the HiPerDiF technology. [1]

## Conclusions

- Reducing fibre concentration and increasing fibre length produced a more consistent quality of material with higher alignment
- ADFRC with 6mm fibres and improved machine settings achieved 85% in stiffness and 80% in strength when compared to UD continuous composites at a normalised fibre volume fraction (V<sub>f</sub>) of 55%
- Next steps will be to manufacture and test other layup configurations of ADFRC using HiPerDiF 3G prepreg material

[1] H. Yu, K. D. Potter, M. R. Wisnom, A novel manufacturing method for aligned discontinuous fibre composites (High Performance-Discontinuous Fibre method), Composites Part A: Applied Science and Manufacturing 65 (2014) 175–185. doi:10.1016/j.compositesa.2014.06.005.-1.



# Liquid Composite Moulding of High Performance-Discontinuous Fibre (HiPerDiF) Preforms.

William Mahoney, Karthik Ram Ramakrishnan, Neha Chandarana and Ian Hamerton.

The purpose of this work was to investigate the feasibility of manufacturing vacuum-assisted resin transfer moulding (VARTM) HiPerDiF preforms. Expanding the scope of manufacturing methods of HiPerDiF to include out-of-autoclave (OOA) processes such as VARTM and HPRM will greatly increase the scope of potential applications and research for HiPerDiF. With this novel form of HiPerDiF, several new challenges and unknowns related to its handleability and ability to withstand fibre washout during infusion. Fibre washout occurs when an excessively high injection resin flow rate causes the displacement and misalignment of a preforms' fibres. Due to the topology and purpose of HiPerDiF, this could be a seriously detrimental and limiting manufacturing flaw. Initial manufacturing trials using a double vacuum bag VARTM method were done to better understand the behaviour, manufacturability and potential flaws of this novel form of HiPerDiF.

## Materials

6mm long carbon fibres were used to create the HiPerDiF preform, shown in Figure 1. A Gurit PRIME™ 37 resin with the Ampreg™ 3X slow hardener was used to VARTM infuse the specimens. The specimens were double bagged, shown in Figure 2, and cured at 67°C for 7.5 hours. Cured specimens were then debagged and prepped for optical analysis, Figure 3.

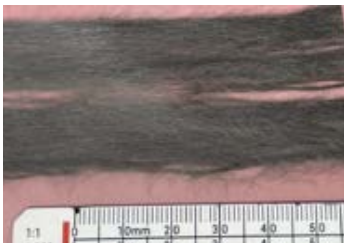


Figure 1: HiPerDiF Preform.



Figure 2: Double bagging method.



Figure 3: Cured plies for VARTM HiPerDiF.

## Preform Defects

When manufacturing the VARTM HiPerDiF specimens, it became clear that the more the preform was susceptible to introducing flaws into the preform during handling. The flaws seen included changes in fibre alignment, areas of lower fibre overlap/ $V_f$  and fibre/tow displacement, shown in Figures 4, 5 and 6, respectively.

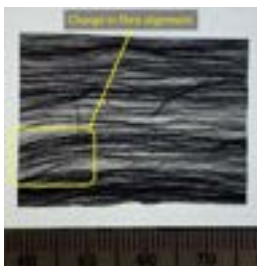


Figure 4: Changes in fibre alignment.

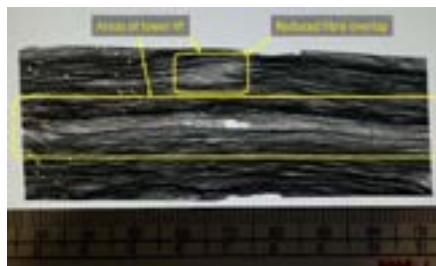


Figure 5: Areas of lower fibre overlap/ $V_f$ .

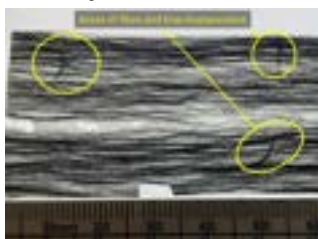
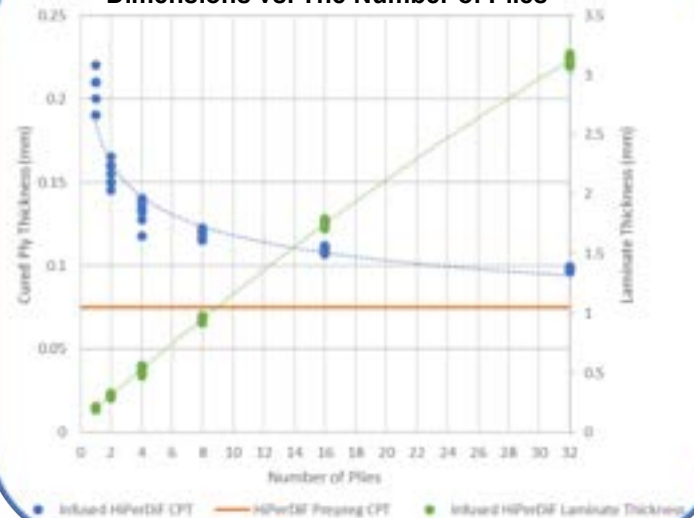


Figure 6: Fibre/tow displacement.



Figure 7: Cross-section of specimens.

## Infused HiPerDiF Laminate Dimensions vs. The Number of Plies



## Future Work

No fibre washout was found during these trials. HPRM will be investigated to determine at what flow rate this occurs for HiPerDiF. Figure 7 shows the  $V_f$  of the specimens was around 12%. Work has been done to change the form of the HiPerDiF preform before infusion to increase the  $V_f$ . This work increased  $V_f$  to 40-50% and will continue further.



# Origami-inspired Design for Manufacture of Curved Composite Structures

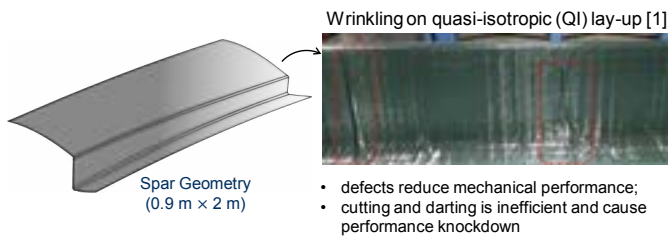
Sutharsanan Navaratnarajah, James Kratz, Mark Schenk

The growing interest in dry fibre manufacturing processes is driven by their potential to achieve increased production rates at reduced cost. As the complexity of the geometry increases, forming becomes more challenging, leading to a higher likelihood of defects such as wrinkles. This study adopts a novel approach to manufacturing composite structures by employing origami techniques. The aim is to achieve design for manufacture, by exploring curved geometries with inherently fewer defects. A feasibility study is conducted to assess the forming capability of Biaxial NCF over a curved crease origami-based geometry.

## Background & Aims

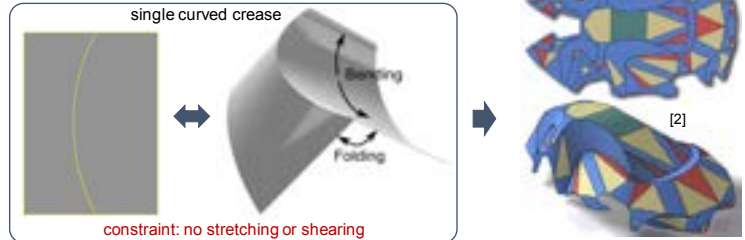
### challenge in dry fibre processing

#### geometric complexity and defects during preforming

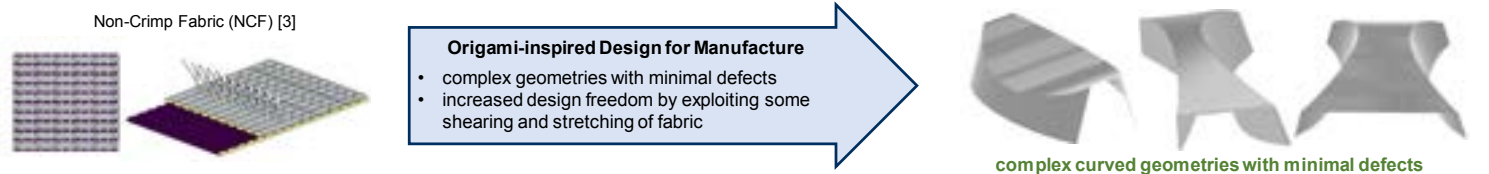


### curved crease origami

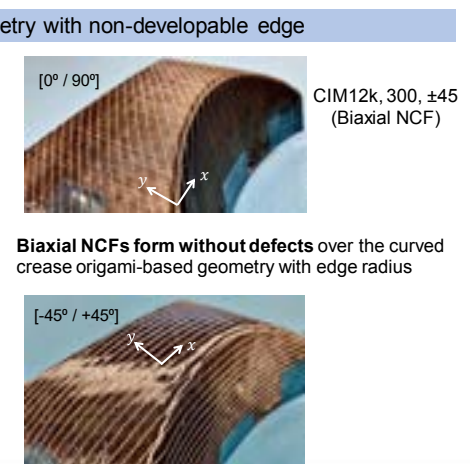
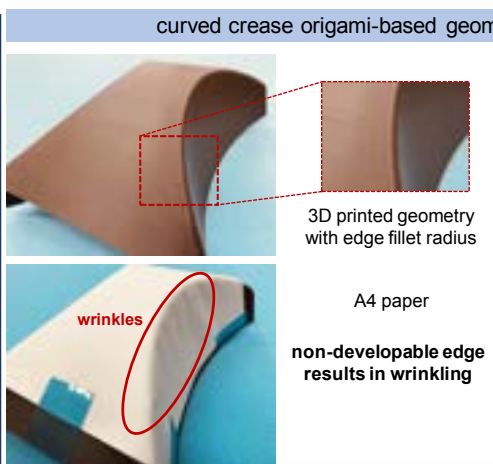
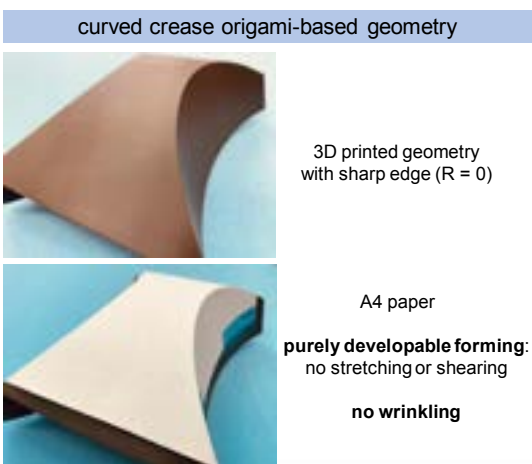
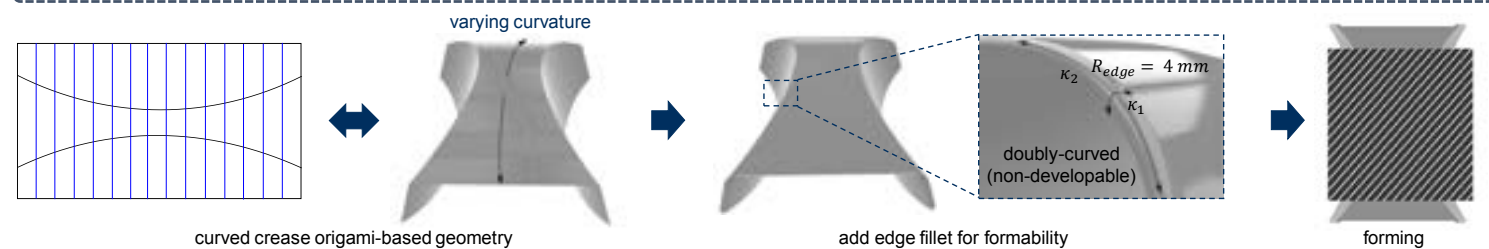
#### ability to create complex geometries from flat sheets



design for manufacture using curved crease origami – explore achievable geometries when allowing stretching and shearing within material allowables



## Methodology & Results



### References

- [1] Martin, C. J., Maes, V., McMahon, T., & Kratz, J. (2022). Large Scale Forming of Non-Crimp Fabrics for Aerostructures. *Key Engineering Materials*, 926 KEM, 1387–1398.
- [2] Killian, M., Flory, S., Chen, Z., Mitra, N. J., Sheffer, A., & Pottmann, H. (2008). Curved folding. *ACM transactions on graphics (TOG)*, 27(3), 1-9.
- [3] Chen, S., & Harper, L. (2023). Two-dimensional to three-dimensional dry fibre preforming. In *Design and Manufacture of Structural Composites* (pp. 101–123).



# Novel cellular coil geometry to improve the temperature uniformity of inductive heating in carbon fibre composites

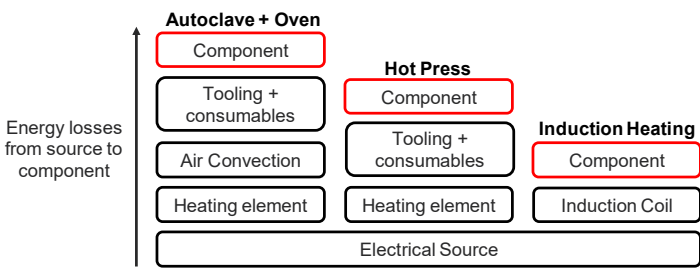
J. Uzzell, L. R. Pickard, I. Hamerton, D.S. Ivanov

Conventional manufacturing processes, such as autoclaves and ovens are very inefficient as time and energy are wasted heating surrounding air, bagging consumables and tooling with high thermal mass. Heating rate is also limited due to convective heat transfer from the air and conduction through thickness.

Electromagnetic (EM) induction provides rapid, volumetric and localised heating with minimal energy lost. Heat is produced directly within electrically conductive carbon fibres reducing losses to tooling and allowing good temperature control and high heating rates. Non-uniformity of temperature distribution in-plane limits the potential applications of induction in composite processing.

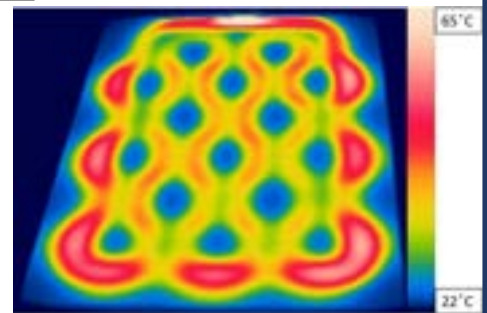
A novel cellular coil geometry designed to address the issue of heating uniformity is presented. The design demonstrates good potential with significantly improved uniformity of temperature field compared to traditional commercially available coils.

## Motivation:



## Experimental results:

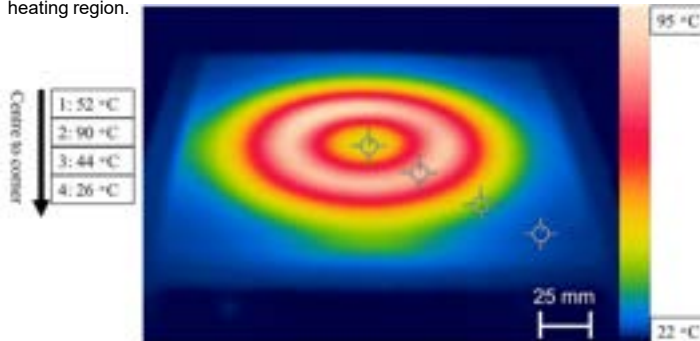
**Right:** Experimental temperature variation on surface of QI CFRP panel heated using cellular coil. Heating matches coil geometry but demonstrates central cell cancelling effect and dominant edge heating.



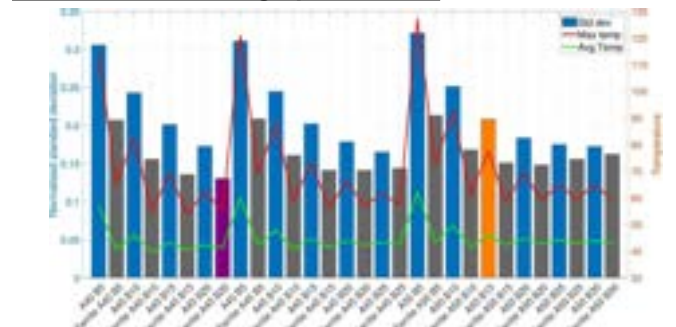
Numerical modelling in Abaqus used to optimise the geometry based on cell size and spacing.

## Challenge:

**Below:** Experimental temperature variation on surface of QI CFRP laminate using standard pancake coil. Temperature distribution is highly non uniform. Low thermal conductivity both in plane and through thickness reduces heat spread from localised heating region.



## Parametric modelling optimisation:

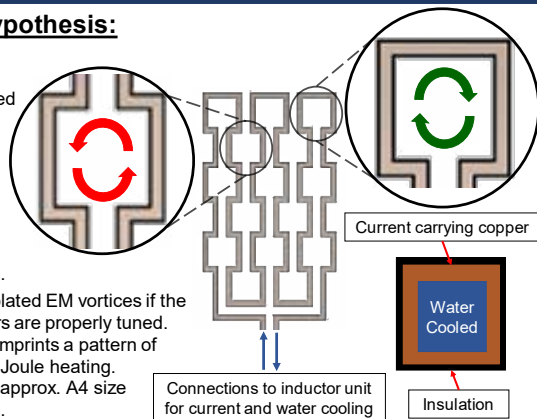


**Above:** Results of parametric design analysis. Focusing on reducing standard deviation to improve inplane temperature uniformity and maximising average temperature for heating efficiency. Orange bar shows experimentally tested geometry and purple is the optimised design.

## Research Hypothesis:

**Right:** Diagram of novel cellular coil. This design is based on the hypothesis that improved temperature uniformity can be achieved by reducing the characteristic heat propagation length.

Each cell forms isolated EM vortices if the process parameters are properly tuned. Each EM vortices imprints a pattern of Eddy currents and Joule heating. Coil manufactured approx. A4 size (350mm x 200mm).

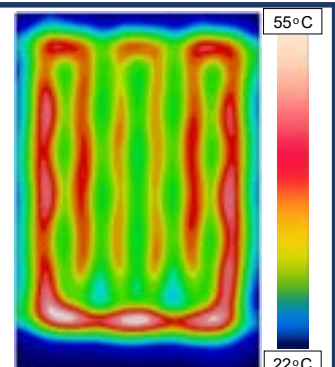


## Modelling result:

**Right:** Modelling of heat produced by optimised cellular coil geometry based on the parametric design analysis.

Calibration of cell size and spacing reduces cancellation between each cell and pronounced edge effects. Design demonstrates clear potential improvements on conventional coil designs.

Future work involves practical application of this cellular coil to demonstrate the energy efficiency advantages of induction compared to oven curing.





# Composite Structural Housing with Integrated Thermal Management via Embedded Microchannels

Toby Wilcox<sup>a</sup>, Richard Trask<sup>a</sup>, Julian Booker<sup>b</sup>

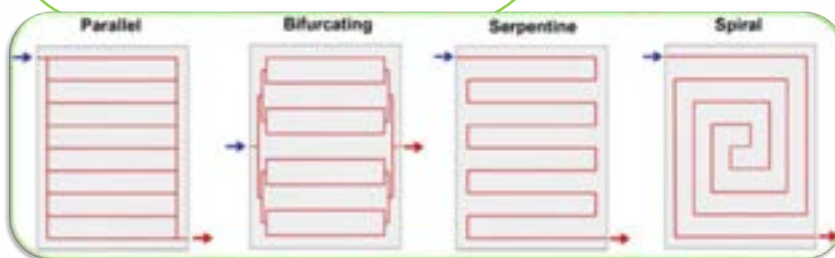
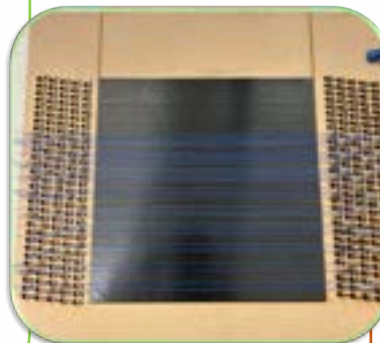
<sup>a</sup>Bristol Composites Institute, Queens Building, Bristol, BS8 1TR <sup>b</sup>Electrical Energy Management Group, Queens Building, Bristol, BS8 1TR \*Author (toby.wilcox@bristol.ac.uk)

## Overview

As rotorcraft move gradually away from conventional drives and mechanisms and more towards electronic components and hybridisation, the need for effective regulation of heat has never been higher. Fibre Reinforced Polymers (FRPs) already have widespread applications in the aerospace industry for both primary and secondary structures. They are however poor thermal conductors and have relatively low working temperatures, making them unsuitable for use in areas of elevated temperature or where significant heat removal is required. If these thermal properties could be improved, the potential applications could be numerous. This project explores this possibility through the use of embedded microchannels within the composite structure to actively cool the housing of heat emitting electric motors and mechanical transmissions. Investigated within this is the fabrication method of the microchannels to prioritise ease of manufacture and complexity, and channel architecture including size, geometry and volume fraction to maximise thermal dissipation per unit mass. The corresponding reduction in mechanical performance due to the presence of the microchannels will also be characterised, with optimisation of thermal-mechanical-vibration performance against the specific requirements of the target applications.

## Channel Fabrication

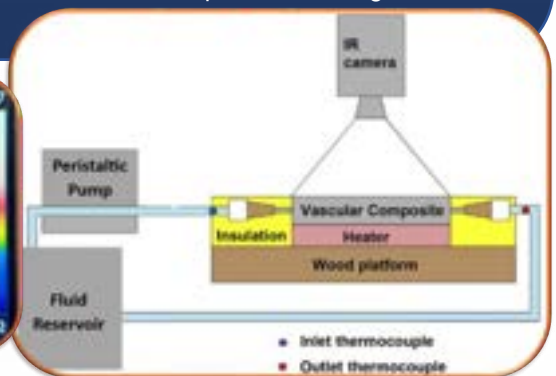
- Several methods of fabrication have been trailed previously in literature, including **manual wire extraction** solder melt, hollow fibres, and **vapourisation of sacrificial components (VaSC)**
- The **Manual wire extraction** method involves embedding strong, low-friction metallic or nylon wires within the layup of the composite which are then pulled out by hand post-cure
- This has been achieved using a bespoke setup to manufacture samples with straight, flat channels at various spacings and diameters
- **VaSC** involves embedding chemically-treated PLA within the layup, which is then vapourised and removed in a post-cure heat treatment
- This will be used to manufacture samples with complex, "2D" geometries which can improve efficiency and target specific hot spots



\* Images courtesy of Stephen J. Pety, Ph.D.

## Thermal Performance

- Assessed via a **conduction setup** using a heater mat to apply a target heat flux to the sample undergoing cooling at a target flow rate, controlled by a peristaltic pump
- Both flow rate and applied heat flux are varied to characterise thermal performance over a range of conditions
- Target heat flux is informed by the typical thermal loads associated with mechanical transmissions
- Channel diameter and pitch, and laminate thickness have been varied to create a range of channel volume fractions (0.4-4%)
- With this wide range of parameters, the optimum conditions can be identified to limit the sample to a temperature below 90°C – the typical working temperatures in mechanical transmission components



# Void analysis of ply-by-ply compacted Out-Of-Autoclave prepregs

Axel Wowogno, Iryna Tretiak, Stephen R. Hallett and James Kratz

This work aims to assess the behaviour of thermoset based prepregs in an Automated Fibre Placement (AFP) process context, where the added material is being heated while being laid. After having analysed the effect of the process parameters (time, temperature, pressure) on thickness evolution, attention is brought on voids, and on how to detect and avoid them.

## Materials

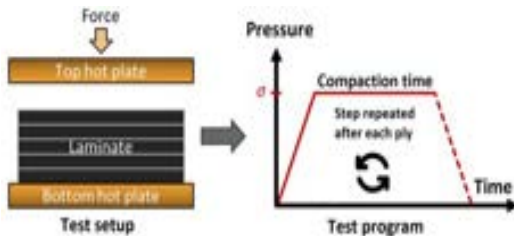
➤ **Out of Autoclave prepreg (OOA):** Hexcel M56/IM7 and **Snap Cure Resin prepreg (SCR):** Hexcel M78.1

## Methods

➤ **Material Characterisation :** Ply-by-ply compaction tests and **Porosity analysis :** CT-scan

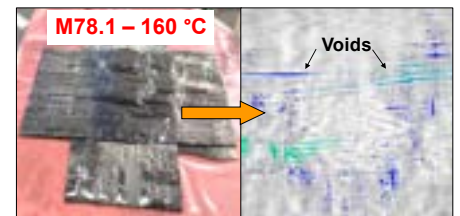
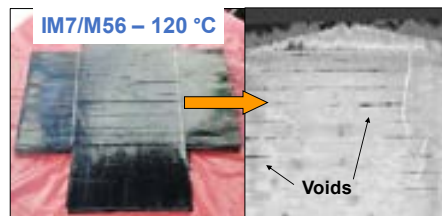
## Goal

Ply-by-ply compaction, to represent the Layer-by-layer manufacturing seen in AFP



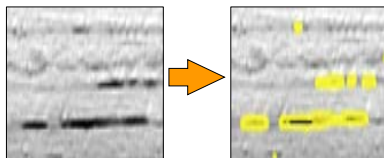
## Challenges

- **IM7/M56 :** Tow gaps appear during heating = creation of a network of voids
- **M78.1 :** Higher process  $T^\circ$  = Faster curing = More defects = Inter-ply voids
- **What are the best temperature ranges and how to properly analyse voids?**



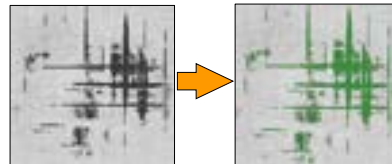
## Void analysis and its software

- **VG Studio:** Surface determination tool. Does not capture the whole defect. Only finds the contour of the void.



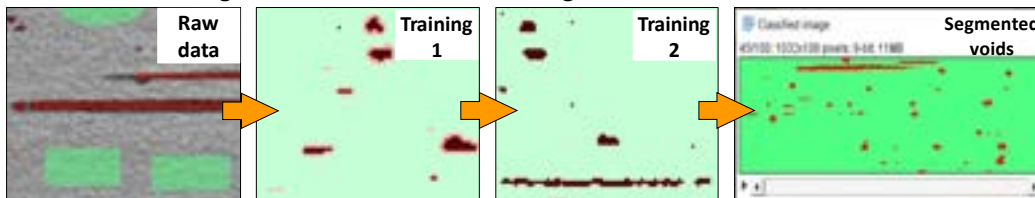
- **Dragonfly:** Thresholding & segmentation tool. Captures the whole void. But sometimes needs manual intervention to adjust the threshold.

*Void seen at low  $T^\circ$  processing on IM7/M56*



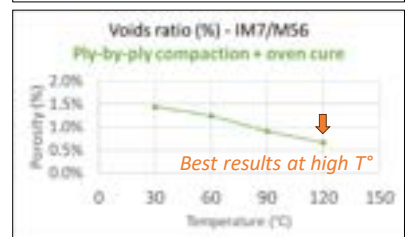
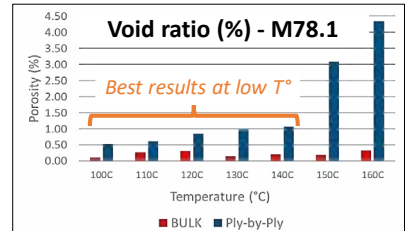
- **Fiji :** WEKA segmentation tool

Tool allowing to train the software to recognize areas such as void or material



## Porosity Results

- **SCR prepreg :** Low  $T^\circ$  needed
- **OOA prepreg :** High  $T^\circ$  needed



## Conclusions

- **The best material is...**

- **M78.1** → Opportunity for on-line consolidation of parts, with shorter consolidation processes at **lower temperatures**
- **IM7/M56** → Suitable for AFP with **higher temperatures**, to enable high-quality **preform** production (still a 2-step process)

- **The best void analysis method is...**

- **Fiji:** Easy segmentation and training tool
- **Dragonfly :** Good tool for void analysis, but manual steps
- **VG Studio :** Porosity plugin unavailable = Inadequate tool
- **Next steps :** Investigate pre-processing / Combine methods



# Modelling the tensile behaviour of PLA-aligned short carbon fibre (HiPerDiF) under processing conditions

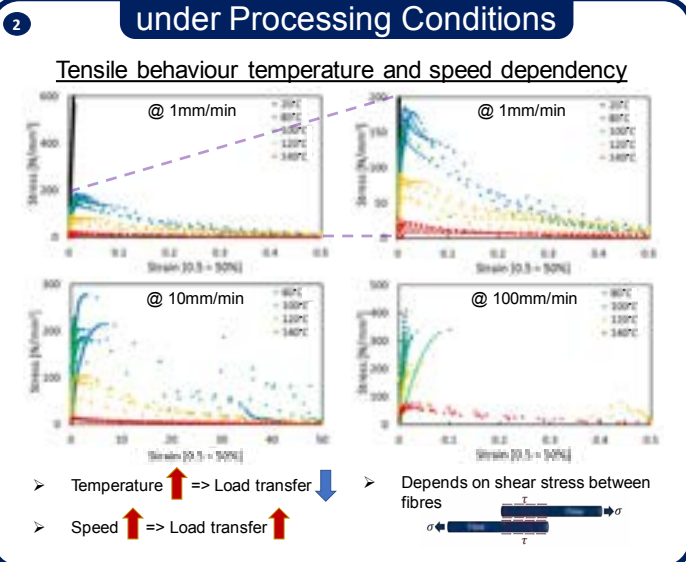
Burak Ogun Yavuz, Ian Hamerton, Marco L. Longana and Jonathan P.-H. Belnoue

Aim: Material characterisation for forming simulations of aligned discontinuous fibre thermoplastic (HiPerDiF) prepreg by using micromechanical model

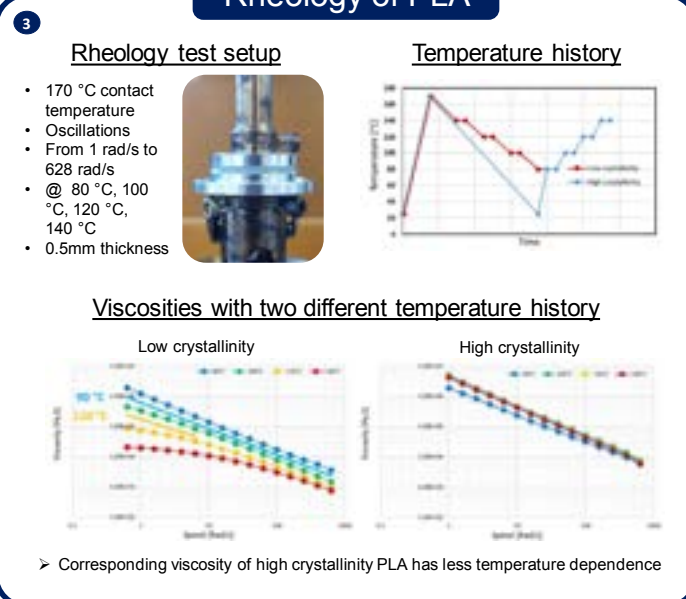
## Manufacturing Method



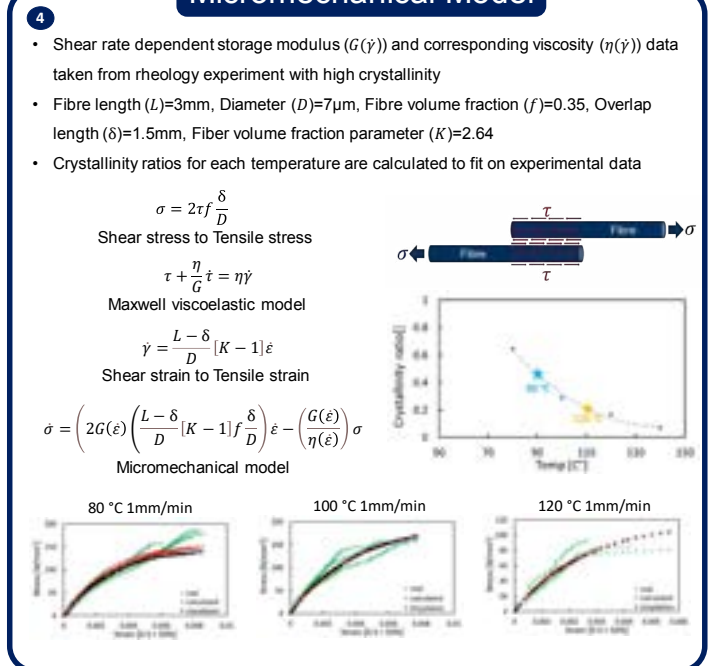
## Tensile Characterisation under Processing Conditions



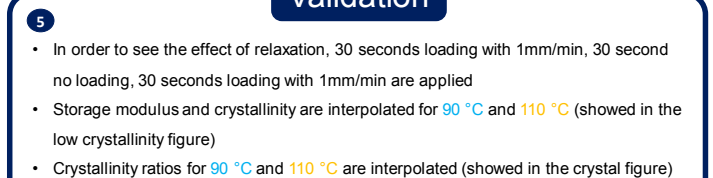
## Rheology of PLA



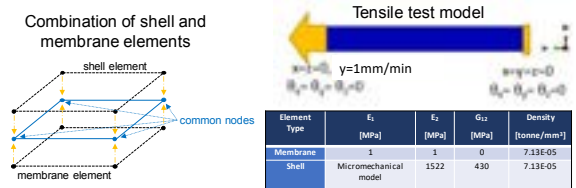
## Micromechanical Model



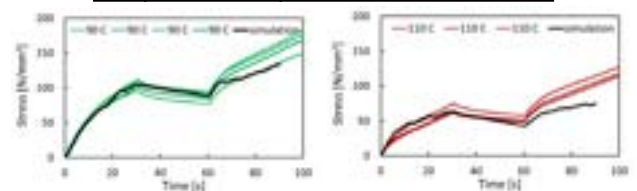
## Validation



## Simulation model and properties



## Comparison of experiments and simulations



Future work: Implementing shear and bending properties into forming simulations → Forming defect free parts experimentally

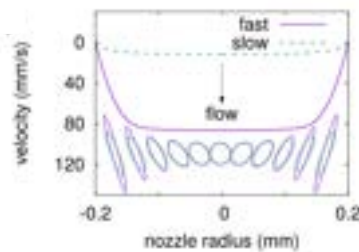
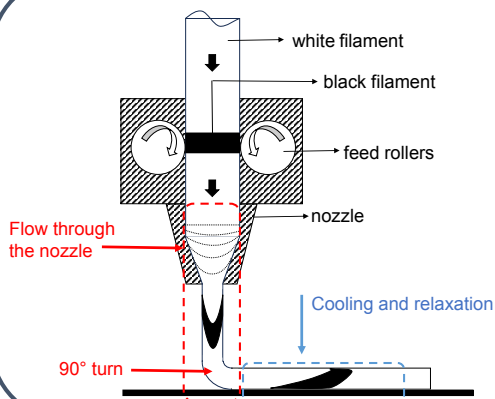
# 4D Printing of Morphing Single Layer Thermoplastic

Erdem Yildiz, Byung Chul Kim, Richard Trask

## Abstract

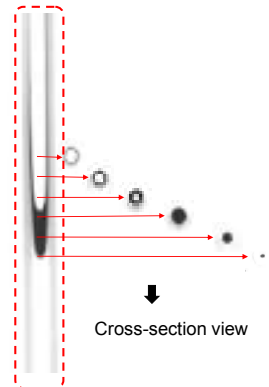
Four-dimensional (4D) printing is a new manufacturing process with unique attributes that emerged from the additive manufacture (3D printing) of smart materials. Morphing of the desired shape occurs over a period of time under a range of potential external stimuli such as light, thermal, chemical, etc. In this project, we consider the potential of 4D printing active layers with highly controllable thermally activated large self-morphing deformations, through the control of the thermal shrinkage rates and manipulation of the Poisson's ratio of the polymer structure. The morphing mechanism are governed by two main factors; the higher initial alignment during flow through the printing nozzles; and the printing deposition rate. The latter triggers faster cooling rates, which leads to rapid quenching through the glass transition temperature, contributing molecular chain anisotropy throughout the printed architecture. The anisotropy is a function of the asymmetric cooling in the deposited filament due to the complex thermal boundary condition. If the reorientation of the molecular chains is arrested by passing through the glass transition, an internal strain field occurs between the printed surface and the tooling.

## Manufacturing

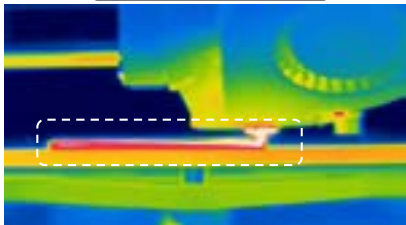


Shear flow visualization of polymer as a deformed sphere. A velocity profile  $w(r)$  and an ellipsoidal representation of polymer deformation across the nozzle radius are shown for fast and slow printing [1]

Extruded filament (before deposition)



## Thermal Mapping



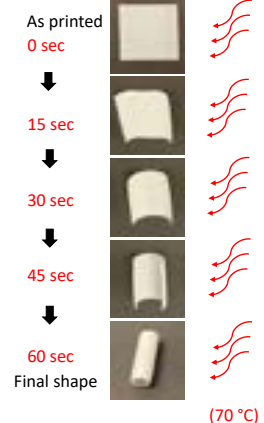
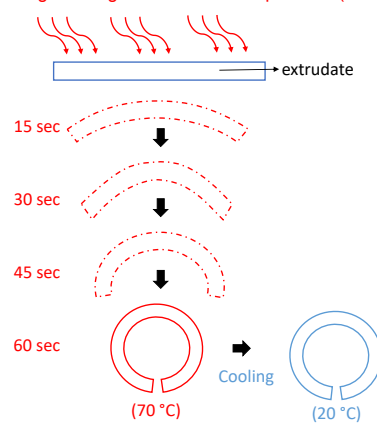
The thermoplastic deposited on the bottom surface cooled dramatically compared to the top due to the boundary conditions, which prevented reorientation of the highly stretched molecular chain to relax by passing through the  $T_g$ , causing it to be trapped owing to fast cooling rate.

A filament's top cools slowly until it reaches room temperature, giving the chain enough time to relax before passing through the  $T_g$ .

Consequently, an internal strain field occurs between the printed surface and the tooling.

## Morphing Mechanism

Heating above glass transition temperature (70 °C)



## Conclusions and Future Work

- On the degree of the thermally activated morphing, as well as the macroscopic properties and structural performance of the final part, was experimentally investigated. It was found that the shape transformation, as a function of internal strain storage and release mechanisms, could be controlled through specific printing parameters, such as the deposition process and the degree of anisotropy between layers.
- Achieving more complex geometries. Implement a wide range of potential applications in the industry. High modulus and stiffness materials (fibre reinforced lightweight composite structures). Quick, cheap and sustainable moldless composite manufacturing

## References

[1] C. McIlroy, P.D. Olmsted, Deformation of an amorphous polymer during the fused-filament-fabrication method for additive manufacturing, J. Rheol., 61 (2) (2017), pp. 379-397, <https://doi.org/10.1122/1.4976839>





## DESIGN, BUILD AND TEST

## CDT23- Design, Build and Test

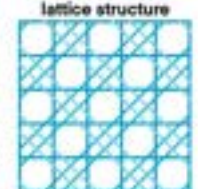
# Sea sponge-inspired structure for aerospace application

Aya Abdo, Cameron Abercromby, Nontanasorn (Boss) Budnincech, Jordan Forbes-Thomas, Jakub Jakimow, Lucas Lu, Tierney McArdle, Ronald Mwesigwa, Robert Oxford Pope, Jula Schroeder, Mary Sintim Donkor, Cyril Varghese Thankachen

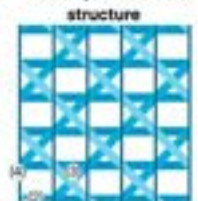
The use of lattice structures in aerospace has been prevalent due to their ability to have high strength and stiffness at a reduced weight over conventional stressed skinned structures [1]. For composite materials, this is increasingly prevalent within the space sector to stiffen skin structures, allowing reduced structural mass. In nature, hierarchical lattice structures have evolved within marine organisms, permitting high strength and material efficiency. This project aims to apply bio-inspired lattice structures within a rocket interstage fairing to demonstrate the potential mass and performance benefits posed by bio-inspired structures [2]. Multi-scale finite element modelling, experimental manufacture and testing with full-field strain-capturing techniques will be used to assess structural and compressive behaviours. These results will be compared against conventional shell structures.



Simplified sea-sponge lattice structure



Bio-inspired lattice structure



- (1) Top and bottom horizontal uni-directional (UD) tape (12 mm width)
- (2) Diagonal lattice structure (12 mm width UD tape)
- (3) Horizontal UD tape (12 mm width)
- (4) Carbon fibre over-braided rods
- (5) Top and bottom horizontal UD tape (12 mm width) (2nd layer)
- (6) UD prepreg skin

Bio-inspired lattice cone



### Design



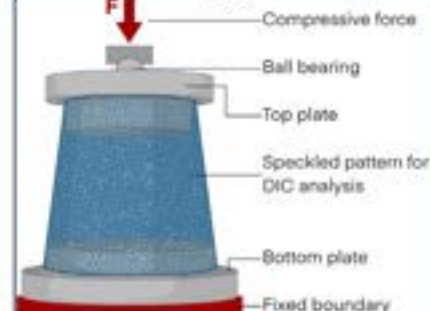
Non-linear finite element analysis of the lattice structure was carried out to assess the elastic stability and strength of the bio-inspired structure [6]. Due to the shear load constraints, the twin diagonal members of the idealised sea-sponge lattice were fused to a continuous wide tape. High fidelity unit cell modelling will be undertaken to quantify the effect of manufacturing defects on the structure to allow design knock down factors to be created.

### Manufacture



The mould will be made from polystyrene cut to the cone's dimensions. The part will then be constructed by laying up UD prepreg tapes over the mould in, Lattice structure (specified above), followed by 12 evenly-spaced over-braided rods and a final UD prepreg skin to aid with analysis. Following layup, the part is bagged and cured in a SE70 oven at 70°C for 16 hours. Once cured, the mould is removed from the structure by dissolution in acetone.

### Test



The conical structure will be compressed axially with a load of 1.13 kN to investigate instability during the launch acceleration of the rocket. A top plate with a ball-bearing design will be implemented to level the structure and ensure pre-set boundary conditions are met. The full-field deformation will be captured using stereo Digital Image Correlation (DIC), allowing analysis of the structure's buckling response under the applied loads.



#### References

- [1] Madsen, H., Bayazit, I.A., and Pook, D.P., 2012. Inspired composite lattice structures: Development and analysis verification. *Composites structures*, 94(5), pp.1177-1187.
- [2] Wilson, A., Bayazit, I.A., and Pook, D.P., 2013. The structural efficiency of the sea sponge: Experimental design and analysis for a conical structure. *Journal of the Royal Society Interface*, 10(244), p.201210.
- [3] Bayazit, I., 2015. *From sponges to space: The art of generating a structure and lattice (with Prof. David Hinton)*. Bristol: University of Bristol.
- [4] Bayazit, I., 2015. *The Conical Structure of a Sea Sponge*. Bristol: University of Bristol.
- [5] Bayazit, I., 2015. *How to make a sea sponge lattice structure*. Bristol: University of Bristol.
- [6] Bayazit, I., 2015. *How to make a sea sponge lattice structure*. Bristol: University of Bristol.
- [7] Bayazit, I., 2015. *How to make a sea sponge lattice structure*. Bristol: University of Bristol.

This work was supported by the Engineering and Physical Sciences Research Council through the EPSRC Centre for Doctoral Training in Composites Science, Engineering and Manufacturing [grant number EP/S021726/1].



composites-institute@bristol.ac.uk  
X @UoBrisComposite

Queens Building,  
University Walk,  
Bristol, BS1 8TR

